

THE STABILITY OF LAMINAR INCOMPRESSIBLE BOUNDARY LAYERS
IN THE PRESENCE OF COMPLIANT BOUNDARIES

by

RICHARD E. KAPLAN

S.B., Massachusetts Institute of Technology (1961)

S.M., Massachusetts Institute of Technology (1961)

SUBMITTED IN PARTIAL FULFILLMENT OF THE
REQUIREMENTS FOR THE DEGREE OF
DOCTOR OF SCIENCE

at the

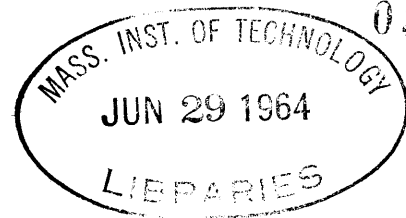
MASSACHUSETTS INSTITUTE OF TECHNOLOGY

June 1964

Signature of Author Richard E. Kaplan
Department of Aeronautics and Astronautics, May 1964

Certified by _____
Thesis Supervisor

Accepted by _____
Chairman, Departmental Graduate Committee



THE STABILITY OF LAMINAR INCOMPRESSIBLE BOUNDARY LAYERS
IN THE PRESENCE OF COMPLIANT BOUNDARIES

by

Richard E. Kaplan

Submitted to the Department of Aeronautics and Astronautics
on May 15, 1964 in partial fulfillment of the requirements for
the degree of Doctor of Science.

ABSTRACT

A numerical technique has been developed for the solution of the Orr-Sommerfeld equation for a boundary layer flowing over a general class of compliant boundaries. Sample calculations are worked out in detail for several types of models of compliant boundaries. It is shown that a compliant boundary can have a significant influence on the stability of the laminar boundary layer, both by delaying the appearance of unstable disturbances until higher values of the Reynolds number and by reducing the total spatial amplification of any frequency band.

The general requirements for materials of the boundary are that the equivalent shear modulus should be of the order of the dynamic pressure, the density of the order of the density of the fluid in the boundary layer, the thickness should be large compared to that of the boundary layer, and there should be as little dissipation as possible in the boundary. These parameters also influence types of instabilities other than those that appear for a boundary layer over a rigid surface, but examples are shown of significant stabilization without the introduction of new instabilities.

The methods are described in detail, including an outline of a technique to reduce the parasitic errors that occur in the numerical integration of certain types of differential equations. The results are favorably compared with those of other authors and experiments, and the generality of the technique is demonstrated by a sample computation of the stability of a two-dimensional jet and an adverse pressure gradient profile. Detailed spatial amplification rates are worked out for all cases.

Thesis Supervisor: Marten T. Landahl

Title: Professor of Aeronautics and
Astronautics

ACKNOWLEDGMENTS

The author wishes to express his appreciation to Professor Marten Landahl, who suggested this topic, offered helpful advice and criticism throughout the course of this investigation, and served as thesis supervisor. Thanks are also due to Professors Erik Mollo-Christensen and David Benney who served on the thesis committee, Professors L. N. Howard and A. E. Gill for suggesting and criticizing the jet stability results, and to Mrs. Gertrude Hubbard, who typed the manuscript.

This work was supported by the Office of Naval Research under contract number Nonr-1841(89), ONR Project No. RR 009 01 01 administered by the Aeroelastic and Structures Research Laboratory, Massachusetts Institute of Technology. The computations were performed at the M.I.T. Computation Center as Problems M1952, M2283.

Finally, the author wishes to express his appreciation for the aid and comfort given him by his wife, without whose patience and understanding this work would never have been brought to completion.

TABLE OF CONTENTS

<u>Chapter</u>		<u>Page</u>
1	INTRODUCTION	1
	1.1 History of the Problem	1
	1.2 Purpose of this Investigation	3
2	SMALL PERTURBATIONS ON A PARALLEL SHEAR FLOW	6
	2.1 The Orr-Sommerfeld Equation	6
	2.2 Dimensionless Variables	8
	2.3 Boundary Conditions	12
	2.4 The Characteristic Value Problem	17
	2.5 Oblique Disturbances in the Boundary Layer	18
	2.6 Spatial Amplification of Disturbances	21
3	DYNAMICS OF THE COMPLIANT BOUNDARY	27
	3.1 Admittance of a Compliant Boundary	27
	3.2 Admittance of a Spring Supported Membrane	28
	3.3 Admittance of a Rubber Surface	30
	3.4 Matching of Surface Shear Stresses	35
	3.5 Inviscid Liquid with Zero Mean Motion	36
	3.6 Coupled Helmholtz Resonators	37
4	COMPUTATION OF THE BOUNDARY LAYER ADMITTANCE	42
	4.1 Solutions of the Orr-Sommerfeld Equation Far from a Boundary	42
	4.2 Numerical Integration of the Orr-Sommerfeld Equation	44
	4.3 Parasitic Growth of Truncation Errors	46
	4.4 Parasitic Error Purification Scheme	50
	4.5 Numerical Determination of the Boundary Layer Admittance	55
	4.6 Determination of the Eigenfunction	56
5	DETERMINATION OF THE EIGENVALUES	58
	5.1 Selection of the Eigenvalue Criterion	58

TABLE OF CONTENTS Continued

<u>Chapter</u>		<u>Page</u>
	5.2 The Inverse of the Eigenvalue Criterion	60
	5.3 Interpolation of the Eigenvalues	63
	5.4 Prediction of the Eigenvalues	66
6	STABILITY OF THE BOUNDARY LAYER OVER A RIGID SURFACE	68
	6.1 Eigenvalues for the Blasius Boundary Layer	68
	6.2 Comparisons of the Stability of the Blasius Boundary Layer with Experiments and other Theories	71
	6.3 Calculation of Spatial Amplification	74
	6.4 Stability of the Laminar Boundary Layer in an Adverse Pressure Gradient	76
7	STABILITY OF THE LAMINAR BOUNDARY LAYER OVER SELECTED COMPLIANT BOUNDARIES	78
	7.1 The Three Classes of Disturbances	78
	7.2 Effect of a Membrane on Boundary Stability - Class A Waves	80
	7.3 Modifying the Membrane to Improve its Performance	84
	7.4 Class B Waves in a Membrane	85
	7.5 Oblique Disturbances	87
	7.6 Effect of a Rubber Surface on Boundary Layer Stability	88
8	JETS, WAKES, AND SHEAR FLOWS	92
	8.1 Compliant Boundary Model for the Stability of Jets, Wakes, and Shear Flows	92
	8.2 Stability of Symmetric and Antisymmetric Profiles	93
	8.3 Asymmetric, Unbounded Shear Flows	94
	8.4 Stability of the Two-Dimensional Jet	96

TABLE OF CONTENTS Continued

<u>Chapter</u>		<u>Page</u>
9	BOUNDARIES EXHIBITING A SPATIAL VARIATION OF PROPERTIES	98
	9.1 Occurrence of Spatial Variation of Boundary Parameters	98
	9.2 Membrane Supported by a Spring of Varying Stiffness	99
	9.3 Parametric Resonant Conditions	104
	9.4 The Altered Stability Problem	108
10	CONCLUSIONS	111
	10.1 Boundary Layer Stabilization with Compliant Boundaries	111
	10.2 The Mechanisms Causing Instability	114
	10.3 Suggestions for Future Investigation	116
	REFERENCES	118
	ILLUSTRATIONS	123
<u>Appendix</u>		
A	ASYMPTOTIC SOLUTION OF THE ORR-SOMMERFELD EQUATION	148
B	NUMERICAL TECHNIQUES	156
C	COMPUTER PROGRAMS	162
	C.1 Use of the Computer Programs	162
	C.2 Description of Computer Programs	165
	C.3 Listing of the Important Computer Programs	169

TABLE OF CONTENTS Continued

ILLUSTRATIONS

<u>Figure</u>		<u>Page</u>
1	Boundary Layer over a Compliant Boundary	123
2	Examples of Flexible Surfaces	123
3	Two-Dimensional Array of Loosely Coupled Helmholtz Resonators	123
4	Integration of the Orr-Sommerfeld Equation	124
5	Growth of Parasitic Solutions (Schematic)	124
6	Illustration of Eigenvalue Problem	125
7	Topology of Eigenvalue Criterion - Membrane Surface	125
8	Eigenvalues c_r , c_i for the Blasius Boundary Layer over a Rigid Surface	126
9	Spatial Amplification Rates for the Blasius Boundary Layer over a Rigid Surface	127
10	Comparisons of the Neutral Curves for the Blasius Boundary Layer over a Rigid Surface	128
11	Comparisons with Experiment for the Blasius Boundary Layer over a Rigid Surface	128
12	Comparison with Experiment - Temporal Amplification Rates	129
13	Comparison with Experiment - Spatial Amplification	130
14	u Perturbation Amplitude Distribution	131
15	Falkner-Skan Profile $\bar{U} = cx^m$ -- $m = -0.05$	131
16	Eigenvalues c_r , c_i for the Falkner-Skan Flow over a Rigid Surface	132
17	Spatial Amplification Rates for the Falkner-Skan Boundary Layer over a Rigid Surface	132
18	Effect of the Propagation Speed c_0 on the Stability of a Membrane	133
19	Effect of the Damping Coefficient d on the Stability of a Membrane	133

TABLE OF CONTENTS Concluded

<u>Figure</u>		<u>Page</u>
20	Effect of Membrane on Spatial Amplification Class A Waves	134
21	Eigenvalues for a Membrane Surface - Class A Waves	135
22	Effect of Boundary Layer Thickening on the Effective Mass of a Membrane	136
23	Effect of Variations of Damping on the Sta- bility of a "Tailored" Membrane	136
24	Eigenvalues for a Tailored Membrane Surface - Class A Waves	137
25	Eigenvalues for a Membrane Surface - Class A and B Waves	138
26	Disturbance Amplitude Distributions - Membrane Surface	139
27	Group Velocity of Disturbances	140
28	Neutral Curves for Class A Waves over a Membrane as a Function of the Direction of the Wave	141
29	Critical Reynolds Numbers for Oblique Dis- turbances	141
30	Effect of Thickness of the Rubber Surface	142
31	Eigenvalues for a Rubber Surface	143
32	Eigenvalues for a Rubber Surface	144
33	Eigenvalues for a Rubber Surface	145
34	Disturbance Amplitude Distributions - Rubber Surface	146
35	Stability of a Two-Dimensional Jet	147

Chapter 1

INTRODUCTION

1.1 History of the Problem

There are several methods of influencing the transition of the boundary layer of a fluid flowing over a general solid surface. Engineers learned quite early that a smoothly finished surface, free from large-scale roughness, exhibited a later transition to turbulence than a roughened surface. Careful planning of the pressure distribution on an airfoil affected the location of the transition point as well as the separation point. Suction of the fluid in the boundary layer through the wall was also known as a technique for delaying transition, and is the basis for present studies of laminar flow aircraft.

At the present time, additional techniques for boundary layer control are being investigated. These include the addition or injection of non-Newtonian fluids into the boundary layer, cooling the boundary layer of compressible fluids, and the use of various kinds of compliant surfaces.

The realization that compliant boundaries might have an effect on boundary-layer transition began with a paper by M.O. Kramer (1957).^{*} In a later paper (1960), Kramer presented the results of some provocative experiments that indicated a reduction of drag on bodies towed in water by coating the surfaces of the bodies with a compliant material. Kramer's contention was that the coating delayed the transition of the laminar boundary layer by introducing added dissipation into the combined system by coupling the boundary layer and the dissipative coating.

^{*}References are indicated by the author's name followed by the year of publication.

However, Kramer did not perform the necessary analysis of the situation to support his claim, but based his arguments on an intuitive physical understanding of the role of dissipation on the motion of physical systems. Other investigators did perform analyses and came up with explanations for this phenomenon that did not agree with the reasoning used by Kramer.

Benjamin (1960) undertook an investigation of this phenomenon as an extension of the theory of stability of parallel flow. Benjamin investigated linear disturbances in a boundary layer flowing over a membrane and concluded that one must consider several types of disturbances, which he classified. The disturbances that are found in the boundary layer in the absence of a compliant boundary (Tollmien-Schlichting waves) appear modified by the presence of the flexible surface. These are characterized as Class A. Disturbances in the boundary, modified by the presence of the boundary layer were characterized as Class B, and can be compared to aeroelastic flutter of the material in the boundary. Violent disturbances occurring when restoring forces in the surface were insufficient to maintain the motion (later named Class C) were shown to be analogous to Kelvin-Helmholtz instability.

Benjamin showed that Class B disturbances are stabilized by the addition of dissipation to the system, Class C disturbances are unaffected, while Class A disturbances are actually destabilized by an increase of the dissipation in the boundary. Since the Class A disturbances are those that are thought to precede the transition of the boundary layer, Benjamin's results directly contradicted the explanation Kramer used for his measurements.

The investigations of Landahl (1962) were based along lines similar to the approach taken by Benjamin, and in addition, introduced some concepts from acoustics to help characterize the properties of the flexible surface. By using the traveling wave

admittance of the membrane, Landahl succeeded in finding stability boundaries for several membranes. He found both Class A and Class B disturbances, located stability boundaries for these disturbances, and gave a physical interpretation for the differences in behavior of these two types of disturbances by considering the energy needed to bring the boundary layer and surface up to its state of motion. Landahl found that the Class A disturbances were "energy deficient" in the sense that added dissipation in the system necessitates an increase in the intensity of the disturbance to maintain the reduced energy level. Furthermore, Landahl gave simple examples of the existence of Class A disturbances. Benjamin (1963) later showed that the occurrence of Class A waves is not restricted to this problem but is always an important consideration in the stability of coupled systems.

In view of these criticisms of Kramer's explanation and the potentialities of his discovery, interest in the effect of the compliant boundaries spread, and other authors engaged in determining their effect on the stability of laminar flow. Tokita and Boggs (1962) investigated the requirements for the properties of the surfaces, as did Nonweiler (1961). Linebarger (1961) considered the effect of compressibility of the boundary layer, and Hains (1963) investigated the effect of flexible surfaces on Poiseuille flow. All of these investigations indicate that the Class A disturbances can be favorably influenced by the action of a compliant boundary, but that new instabilities may occur.

1.2 Purpose of this Investigation

The previous computations in this area have been based on asymptotic solutions of the Orr-Sommerfeld equation, which governs the perturbations in the boundary layer. However, these computations are very tedious except in simple limiting cases, and for the range of phase speeds of disturbances that can occur

in the presence of these compliant boundaries, can result in significant inaccuracies. A numerical solution of the Orr-Sommerfeld equation was sought to first remove any of these restrictions. It has the further advantage of performing the tedious calculations involved very rapidly, and does not introduce any approximations into the solution that may be difficult to justify for these new cases.

The applications of this technique to problems that have been already completely treated allows sufficient chances to prove out the new methods, and leads directly to the study of closely related problems that have so far defied analysis. The membranes investigated by Landahl, Benjamin, and others can be replaced by other, more realistic models for a compliant boundary. Classes of problems that are impossible to perform efficiently using the asymptotic analysis, and other types of problems that have defied analysis to date can now be considered by use of this technique, such as the stability of two-dimensional, asymmetrical shear flows at arbitrary values of the Reynolds number.

It is recognized that the determination of stability does not explain the transition of the flow. Theoretical considerations of Benney (1961) and experimental work by Klebanoff et. al. (1962) indicate that three-dimensional phenomena are very important in the breakdown of the laminar flow. While no complete three-dimensional analysis of the situation is attempted, three-dimensional effects such as those considered by Criminale and Kovasznay (1962) are of interest and must be carefully investigated.

A very instructive approach to determining the effect of compliant boundaries on the stability problem is offered by considering the spatial growth of disturbances. Calculations of the spatial amplification rates can be made to determine typical length scales that govern the growth of dis-

turbances. In the same vein, a discussion of the requirements of the dimensionless form of the stability equation relative to the determination of spatial amplifications is given. This type of calculation is needed before a general discussion of spatial growth can be undertaken. Furthermore, new knowledge about the group velocity of the disturbances is presented to aid in spatial amplification criteria. The effect of the compliant boundary on these aspects of the stability problem needs to be made for completeness.

Numerical results for a variety of compliant boundaries are presented, including a detailed study of the appropriate loci of eigenvalues for those boundaries that are in some sense optimum. Calculations are also made of some related problems in the stability of parallel flow and on a simple model that introduces a linear coupling between modes of instability. The calculations are compared to existing experiments as a final test of their validity.

The general formulation used in this paper provides a useful technique for solving a greater range of parallel flow stability problems than more specialized methods. Once the similarity of the flow of a boundary layer over a compliant boundary and more general unbounded shear flows is recognized, then this formulation can be used to great advantage in their solution. The same techniques can be as useful for the solutions of related problems that are based on modifications of the Orr-Sommerfeld equation, and for unrelated problems that cause the same kind of analytical difficulties.

Chapter 2

SMALL PERTURBATIONS ON A PARALLEL SHEAR FLOW

2.1 The Orr-Sommerfeld Equation

Small disturbances on a parallel shear flow must satisfy the basic dynamic equations, the Navier-Stokes equations. For reasons that will be discussed more fully later, it is sufficient to consider two-dimensional motion. For a two-dimensional, viscous flow, the Navier-Stokes equations are equivalent to the vorticity equation which can be written (* denotes dimensional quantities)

$$\frac{\partial \zeta_*}{\partial t_*} + \frac{\partial \Psi_*}{\partial y_*} \frac{\partial \zeta_*}{\partial x_*} - \frac{\partial \Psi_*}{\partial x_*} \frac{\partial \zeta_*}{\partial y_*} = \nu \Delta \zeta_* \quad (2.1)$$

where ζ_* is the vorticity and Ψ_* the stream function

$$\zeta_* = -\Delta \Psi_* = -\frac{\partial^2 \Psi_*}{\partial x_*^2} - \frac{\partial^2 \Psi_*}{\partial y_*^2} \quad (2.2)$$

For the purposes of linearization, assume that

$$\Psi_*(x_*, y_*, t_*) = \int_0^{y_*} \bar{U}(y_*) dy_* + \psi_*(x_*, y_*, t_*) \quad (2.3)$$

where ψ_* is small and satisfies the inequality

$$|\psi_*| \ll U_0 \delta \quad (2.4)$$

for some δ which is a measure of a typical length in the

shear flow (for instance, the boundary-layer thickness). The function $\bar{U}_*(y_*)$ represents the steady parallel shear flow directed along the x-axis of coordinates (Figure 1) and (2.3) yields velocity components

$$\begin{aligned} u_*(x_*, y_*, t_*) &= \bar{U}_*(y_*) + \frac{\partial \psi_*}{\partial y_*} \\ v_*(x_*, y_*, t_*) &= - \frac{\partial \psi_*}{\partial x_*} \end{aligned} \quad (2.5)$$

Equation (2.1) can be regarded as written in dimensionless form by normalizing all velocities with respect to the reference velocity U_0 , all lengths with respect to the reference length δ , and all times by the reference time δ/U_0 . Further aspects of this nondimensionalization will be discussed in Section 2.2. The direct result of this procedure is to replace the kinematic viscosity ν by the dimensionless ratio $\nu/U_0 \delta$, the inverse of the Reynolds number R .

Inserting (2.3) into (2.1), dropping the *, and linearizing, one finds

$$\left\{ \frac{\partial}{\partial t} + \bar{U} \frac{\partial}{\partial x} - \frac{1}{R} \left(\frac{\partial^2}{\partial x^2} + \frac{\partial^2}{\partial y^2} \right) \right\} \left(\frac{\partial^2 \psi}{\partial x^2} + \frac{\partial^2 \psi}{\partial y^2} \right) = \frac{d^2 \bar{U}}{dy^2} \frac{\partial \psi}{\partial x} \quad (2.6)$$

Assuming that the Reynolds number R is a constant, solutions to (2.6) can be found of the form

$$\psi(x, y, t) = \phi(y) e^{i\alpha(x-ct)} \quad (2.7)$$

Equation (2.7) represents traveling wave disturbances of wave number α and phase speed c . Substi-

tuting (2.7) into (2.6) yields the familiar Orr-Sommerfeld equation

$$\frac{d^4 \phi}{dy^4} - 2\alpha^2 \frac{d^2 \phi}{dy^2} + \alpha^4 \phi - i\alpha R \left\{ (\bar{u} - c) \left(\frac{d^2 \phi}{dy^2} - \alpha^2 \phi \right) - \frac{d^2 \bar{u}}{dy^2} \phi \right\} = 0 \quad (2.8)$$

A full justification of the terms retained in (2.8) requires that the oscillatory solution ψ represents a more rapid variation in the x-direction than that caused by the growth of the boundary layer. This is equivalent to the assumption that the Reynolds number is a constant (i.e., nearly-parallel flow). For further discussions on this point, the reader is referred to Lin (1955) and Dunn (1953).

Equation (2.8) is a linear, fourth order ordinary differential equation with variable coefficients $\bar{u}(y)$, $d^2 \bar{u}(y)/dy^2$. It refers to one physical parameter, the Reynolds number, and to two parameters characterizing the wave under investigation, α and c . A general initial value problem may be solved by considering a superposition of all modes by a Fourier integral when appropriate initial and boundary values are specified. Boundary conditions for ϕ will be discussed in Section 2.4.

The solution to (2.8) is a challenging problem in analysis. A survey of some methods of solution appear in Lin (1955). The approximate analytical solutions of (2.8) make use of the fact that in general, the Reynolds number is a large parameter in problems of the kind under consideration. Thus solutions for large values of R may be sought. An example of an analytic solution appears in Appendix A.

2.2 Dimensionless Variables

The dimensionless Reynolds number characterizes the nature of the fluid dynamics in (2.8), namely that of a nearly inviscid flow for large values of R . As stated in the text

$$R = \frac{U_0 \delta}{\nu} \quad (2.9)$$

and was assumed to be a constant in x . However, it is necessary to consider how the Reynolds number may vary. Hains (1963) engages in a similar discussion for the Poiseuille flow. Inspection of (2.9) indicates four practical methods for changing the Reynolds number

- (a) Vary U_0 for fixed δ/ν
- (b) Vary δ for fixed U_0/ν
- (c) Vary ν for fixed $U_0 \delta$
- (d) Vary $U_0 \delta$ for fixed ν

For the boundary layer over a semi-infinite flat plate, both U_0 and ν are fixed and the boundary-layer thickness δ varies with the square root of the distance from the leading edge of the plate as shown by (2.10)

$$\delta = K \sqrt{\frac{\nu x}{U_0}} = K \times R_x^{-1/2} \quad (2.10)$$

Selecting δ as the point at which the velocity in the boundary layer is 99.9% of the free-stream velocity yields a value for K of 6.02. The Reynolds number based on the distance from the leading edge of the plate is related to the Reynolds number based on δ by

$$R = K \sqrt{\frac{U_0 x}{\nu}} = K R_x^{1/2} \quad (2.11)$$

Thus for the simplest boundary-layer flow, the condition that R be independent of x is not met. However, (2.8) is still valid if

$$\alpha_* \delta \gg \frac{d\delta}{dx} = \frac{1}{2} K R_*^{-1/2} = \frac{1}{2} \frac{K}{R} \quad (2.12)$$

namely, for sufficiently large R .

The total problem that is under consideration involves more than reference to the boundary layer. A correct characterization of the dynamics of the compliant boundary requires that appropriate dimensionless coordinates be available. Since the Reynolds number is to be varied by changing δ , and since δ is the only length scale available for the boundary layer, some care must be taken to insure that the dimensionless parameters of the surface do not reflect the growth of the boundary layer. It is for this reason that the dimensionless parameters describing the surface must vary with the Reynolds number.

If the surface has a typical y dimension H , this scheme requires that

$$H = \frac{H_*}{\delta} = \frac{H_* U_0}{\nu} \cdot \frac{1}{R} \quad (2.13)$$

where $H_* U_0 / \nu$ is the proper non-dimensional representation of this length that is independent of the boundary-layer growth. A convenient scheme for determining H is to set $H = H_0$ at $R = R_0$, so that

$$H = H_0 R_0 / R \quad (2.14)$$

Any dissipation in the compliant boundary which is represented by a dynamic term of the form

$$-d_* \frac{\partial}{\partial t_*}$$

has an operational representation of

$i \alpha c d$

by use of (2.7). Even though $d = d_* U_0^2 / \nu$, the effect of the length scale appearing in $\partial/\partial t$ requires that d vary as

$$d = d_0 R_0 / R \quad (2.15)$$

where the notation is the same as in (2.14).

The appearance of a resonant or cutoff frequency requires a similar variation with Reynolds number, namely

$$\omega = \omega_0 R_0 / R \quad (2.16)$$

Analogous to this, the dimensionless frequency ω_r of the perturbation in the boundary layer is found to be

$$\omega_r = \frac{\omega_* \nu}{U_0^2} = \frac{\alpha c}{R} \quad (2.17)$$

and should be compared to β_r in Lin (1955) and Schlichting (1935).

It must be mentioned that the characteristic velocity of the boundary layer has a well-defined form, and does not have to be modified for the Blasius flow. Of course, when considering the flow in a pressure gradient, the velocity itself changes with position, and any propagation velocity in the boundary must be varied accordingly.

When pressure gradients are considered, both U_0 and δ vary (slowly) in space and the preceding arguments must be modified. No general statement can be made about the best technique for selecting the most suitable dimensionless variables, for of course there is none. In complicated situations that might arise, the technique used by Landahl (1962) is recommended wherein the parameters of the surface are re-

garded as constants. This simplifies the handling of the parameters but has the unfortunate result that the actual surface under consideration may vary with the Reynolds number. As Hains points out, Landahl's technique corresponds to choice (c) above, and the difficulty is shifted to the interpretation of the final results, for they represent a variety of physical situations.

2.3 Boundary Conditions

The solution of (2.8) is determined by the specification of appropriate boundary conditions. These boundary conditions are typical for perturbations in a viscous fluid. Two of the necessary four conditions require that the velocity perturbations vanish far from the surface, while the other two express compatibility of the motion in the boundary layer with the motion of the surface. This compatibility condition requires that the fluid adhere to the surface.

The first of these conditions can be stated mathematically as

$$\phi, \phi' \rightarrow 0 \text{ as } y \rightarrow \infty \quad (2.18)$$

Since the coefficients of the Orr-Sommerfeld equation approach constant values far from the boundary, the limiting solutions of (2.8) exhibit an exponential decay for large values of y (see Section 4.1). The determination of this limiting form is discussed fully later.

The compatibility of the flow with the boundary can be dealt with by considering the response of the compliant boundary to traveling wave pressure disturbances, of the same general form as specified by (2.7). The present investigation shall be limited to models of compliant boundaries for which the stress tensor is determined by the in-

stantaneous strains and strain rates in the boundary. In view of the linearization, this is not a severe restriction although materials that exhibit a pronounced hysteresis are excluded from consideration. If U_s, V_s, p_s are the tangential and normal velocity and pressure perturbations, respectively, at the surface of the compliant boundary, they may be expressed in the following forms for traveling wave solutions

$$\begin{aligned} U_s &= \hat{U}_s e^{i\alpha(x-ct)} \\ V_s &= \hat{V}_s e^{i\alpha(x-ct)} \\ p_s &= \hat{p}_s e^{i\alpha(x-ct)} \end{aligned} \quad (2.19)$$

The velocities are related to the strains on the surface uniquely since only this special type of traveling wave disturbance is being considered, so the functions

$$\begin{aligned} Y_{11} &= Y_{11}(\alpha, c) = -\hat{V}_s / \hat{p}_s \\ Y_{12} &= Y_{12}(\alpha, c) = \hat{U}_s / \hat{p}_s \end{aligned} \quad (2.20)$$

are determined by the wave number α , the phase speed c , and the parameters that characterize the dynamics of the surface. The functions are called the normal and tangential traveling wave admittances of the compliant boundary. The admittances in (2.20) are considered to be dimensionless and are related to the dimensional admittances as follows

$$Y_{ij*} = Y_{ij} / \rho U_0$$

where the notation was defined in the preceding section.

Assuming that the pressure perturbation in the boundary layer is the cause of the motion in the compliant

boundary, compatibility between the two systems is insured if the velocity perturbations of the surface match the velocity of the fluid in the boundary layer at the interface.

The shape of the surface is defined to be (see Figure 1)

$$\eta(x,t) = \hat{\eta} e^{i\alpha(x-ct)} \quad (2.21)$$

The normal velocity of the surface is equal to the V velocity perturbation in the boundary layer

$$V_s = \frac{\partial \eta}{\partial t} = -\frac{\partial \psi}{\partial x} \quad \text{at } y = \eta(x,t) \quad (2.22)$$

or in operational notation after linearization

$$\hat{V}_s = -i\alpha c \hat{\eta} = -i\alpha \phi_w \quad (2.23)$$

where the subscript w refers to quantities defined in the boundary layer evaluated at the mean position of the surface $y = 0$.

In the matching of tangential velocities, one must consider the mean value of the \bar{U} velocity in the boundary layer at the displaced position of the surface

$$U_s(x,t) = \bar{U}(\eta) + \frac{\partial \psi}{\partial y} \quad \text{at } y = \eta(x,t) \quad (2.24)$$

Expanding $\bar{U}(\eta)$ around $y = 0$, noting that $\bar{U}(0)$ vanishes, and using (2.23), one finds

$$\hat{U}_s = \bar{U}'_w \hat{\eta} + \phi'_w = \frac{\bar{U}'_w}{c} \phi_w + \phi'_w \quad (2.25)$$

after linearization. Finally, using (2.20) to introduce the tangential admittance and recognizing that the pressure perturbations in boundary layer and surface are identical, one finds

$$\hat{p}_s Y_{12} = \hat{p}_w Y_{12} = \frac{\bar{U}_w'}{c} \phi_w + \phi_w' \quad (2.26)$$

Equation (2.26) is equivalent to matching the tangential admittance of the boundary layer X_0 to the tangential admittance of the surface Y_{12}

$$X_0 = \left(\frac{\bar{U}_w'}{c} \phi_w + \phi_w' \right) / \hat{p}_w = Y_{12} \quad (2.27)$$

Referring to the linearized x momentum equation, \hat{p}_w is shown to be

$$\hat{p}_w = -\frac{i}{\alpha R} (\phi_w''' - \alpha^2 \phi_w') + c \phi_w' + \bar{U}_w' \phi_w \quad (2.28)$$

Inserting (2.28) into (2.26), one arrives at the general condition of compatibility that the perturbation in the boundary layer must satisfy as it disturbs the compliant boundary.

$$(1 - c Y_{12}) \left(\phi_w' + \frac{\bar{U}_w'}{c} \phi_w \right) + \frac{i Y_{12}}{\alpha R} (\phi_w''' - \alpha^2 \phi_w') = 0 \quad (2.29)$$

For some applications, Equation (2.28) is difficult to evaluate, since an estimate of the size of the leading term on the right-hand side might be difficult to make. In these cases, one can apply the y momentum equation which gives the alternative expression

$$\hat{p}_w = \alpha^2 \int_0^{\infty} (\bar{u} - c - \frac{i\alpha}{R}) \phi \, dy - \frac{i\alpha}{R} \phi_w' \quad (2.30)$$

It should be noted that consideration of membranes, for which $Y_{12} = 0$, yields a simpler expression for the pressure

$$\hat{p}_w = \frac{-1}{\alpha R} (\phi_w''' - \alpha^2 \phi_w')$$

by inspection of (2.29) and (2.28). This of course is a special case of the present result.

The application of boundary conditions (2.18) and (2.29) determine the function ϕ to within a (complex) constant multiple. Using this function, one can determine the normal admittance Y_0 of this boundary layer.

$$Y_0(\alpha, c, R) = \frac{-\alpha^2 R \phi_w}{\phi_w''' - \alpha^2 \phi_w' + i\alpha R (c\phi_w' + \bar{u}'_w \phi_w)} \quad (2.31)$$

With this boundary layer admittance Y_0 set equal to the normal admittance of the compliant boundary, the disturbance in the boundary layer is insured to be the cause of the motion of the surface.

For completeness, it must be mentioned that it is usually unnecessary to consider the response of the compliant boundary to shear stress in the boundary layer, but an example of a technique to handle this occurrence is considered in Chapter 3.

2.4 The Characteristic Value Problem

The requirement that the normal admittance of the boundary layer Y_0 match the normal admittance of the compliant boundary Y_{11} can be stated as one of the following equivalent mathematical equations

$$\begin{aligned}\Delta Y &= Y_0 - Y_{11} = 0 \\ \Delta Z &= Y_0^{-1} - Y_{11}^{-1} = 0 \\ E &= 1 - Y_0/Y_{11} = 0\end{aligned}\tag{2.32}$$

All of these take the form

$$E(\alpha, c; R) = 0\tag{2.33}$$

which implicitly states that

$$\begin{aligned}\text{or } \tau &= \tau(\alpha, R) \\ \alpha &= \alpha(\tau, R) \\ \text{or } \frac{\alpha c}{R} &= f(\alpha, R)\end{aligned}\tag{2.34}$$

Thus, Equation (2.32) is the mathematical expression that determines the eigenvalues α , c of the problem. This eigenvalue problem may be solved by the following algorithm

- (i) Select R , α , and c
- (ii) Evaluate $Y_{12}(\alpha, c)$
- (iii) Solve the Orr-Sommerfeld equation and find $Y_0(\alpha, c, R)$

- (iv) Evaluate $Y_{11}(\alpha, c)$ and determine $\mathcal{E}(\alpha, c, R)$
- (v) Vary c so that \mathcal{E} vanishes. The resultant value of c is the desired eigenvalue.

The traditional approach to this problem is to consider α as a real parameter and permit c to take complex values. The reasons for this choice will be discussed more fully in Section 2.6. If c_r, c_i are the real and imaginary parts of the phase speed, then (2.34) can be stated as

$$\begin{aligned} c_r &= c_r(\alpha, R) \\ c_i &= c_i(\alpha, R) \end{aligned} \tag{2.35}$$

where the locus of points $c_i = 0$ is the neutral curve and specifies the only possible values for (α, c, R) for which waves can exist neither amplified nor damped in time. Of course, the eigenvalue relationship (2.33) is a complex function of (α, c, R) .

Thus for fixed (α, R) , the eigenvalue problem reduces to that of determining the zeroes of some complex function \mathcal{E} , where the functional relationship is not known in closed form. A numerical technique for determining these zeroes with a minimum of computation is discussed later.

2.5 Oblique Disturbances in the Boundary Layer

In Section 2.1, discussion was limited to the study of two-dimensional disturbances. The justification for the restriction to two-dimensional disturbances was given by Squire (1933) who demonstrated that any three-dimensional disturbance of the form

$$\begin{aligned}
U(x, y, z, t) &= \tilde{U}(y) e^{i(\tilde{\alpha}x + \tilde{\beta}z - \tilde{\alpha}\tilde{c}t)} \\
V(x, y, z, t) &= \tilde{V}(y) e^{i(\tilde{\alpha}x + \tilde{\beta}z - \tilde{\alpha}\tilde{c}t)} \\
W(x, y, z, t) &= \tilde{W}(y) e^{i(\tilde{\alpha}x + \tilde{\beta}z - \tilde{\alpha}\tilde{c}t)} \\
p(x, y, z, t) &= \tilde{p}(y) e^{i(\tilde{\alpha}x + \tilde{\beta}z - \tilde{\alpha}\tilde{c}t)}
\end{aligned}
\tag{2.36}$$

can be transformed to an equivalent two-dimensional disturbance. Squire's transformation can be written as

$$\begin{aligned}
\alpha \hat{U} &= \tilde{\alpha} \tilde{u} + \tilde{\beta} \tilde{w} & \hat{V} &= \tilde{v} & \hat{p} R &= \tilde{p} \tilde{R} \\
\alpha R &= \tilde{\alpha} \tilde{R} & \tilde{c} &= \tilde{c} & \alpha^2 &= \tilde{\alpha}^2 + \tilde{\beta}^2
\end{aligned}
\tag{2.37}$$

($\tilde{}$ refers to the three-dimensional flow)

Using this transformation, a theorem can be proved which states that the minimum critical Reynolds number occurs for the two-dimensional disturbances. This theorem was first stated by Squire and is valid for incompressible flow over a rigid boundary.

When a compliant surface influences the boundary conditions of the Orr-Sommerfeld equation, a theorem similar to Squire's theorem cannot be proved in general. Squire's transformation can be regarded as a mathematical transformation to recover the two-dimensional equations from the three-dimensional ones, or as a rotation of coordinates to investigate oblique

waves. Since the transformation affects only the velocity, as detailed below, the mathematical and physical interpretations coincide.

When the compliant boundary is present, only the formal aspect of the rotation remains, for it must be recognized that the scaling for the physical properties of the surface vary with the direction of the oblique disturbances. Thus oblique waves must be considered to exist over a series of different but related compliant boundaries.

This rotation of coordinates preserves the length scale δ , the magnitude of the effective wave number α , and $\alpha \geq \tilde{\alpha}$, $R \leq \tilde{R}$, and $p \geq \tilde{p}$. In particular, the effective pressure perturbation for the two-dimensional flow is greater than that for the three-dimensional flow. One can state an equivalent transformation by considering the appropriate scaling variables so that the properties of the compliant boundary can be transformed to measure the response of the boundary to these oblique disturbances.

$$\begin{aligned} U_0 &= \tilde{U}_0 \cos \theta \\ R &= \tilde{R} \cos \theta \end{aligned} \quad (2.38)$$

where

$$\theta = \cos^{-1}(\tilde{\alpha} / \sqrt{\tilde{\alpha}^2 + \tilde{\beta}^2})$$

The equivalent wave speed \tilde{c}^1 can be shown to transform in the same manner, where

$$\tilde{c}^1 = \tilde{c} \tilde{\alpha} / \sqrt{\tilde{\alpha}^2 + \tilde{\beta}^2} = \tilde{c} \cos \theta = c \cos \theta \quad (2.39)$$

It must be recognized that \tilde{c} in (2.36) is not the phase velocity of the three-dimensional waves. The actual phase speed of the waves transforms in the same manner implied by (2.38) for the same effective phase speed of the equivalent

two-dimensional disturbance. This transformation is the same as the inverse of the transformation of the normalizing velocity U_0 .

When computing the dimensionless parameters characterizing the compliant boundary, a new parameter, the angle of the disturbances, must now be considered. Following the results given in Section 2.2, one must have

$$\begin{aligned}
 c_0 &= \tilde{c}_0 / \cos \theta \\
 H &= \tilde{H} \\
 d &= \tilde{d} / \cos^2 \theta \\
 \omega_0 &= \tilde{\omega}_0 / \cos^2 \theta
 \end{aligned}
 \tag{2.40}$$

These transformations of the effective properties of the surface demonstrate that the equivalent surface has greater stiffness and is more highly damped when reacting to the three-dimensional waves, as compared to its reaction for two-dimensional waves.

2.6 Spatial Amplification of Disturbances

In the formulation of the eigenvalue problem (Section 2.4), it was mentioned that one generally considers the disturbances to be amplified (or damped) in time. This was stated in the text preceding Equation (2.35) as considering α to be a real parameter, and accepting complex values of c . This viewpoint of considering temporal amplification of disturbances has produced theoretical predictions that agree very well with experimental observations.

However, it is recognized that the actual physical situation noted by various observers is one of combined spatial

and temporal variation of disturbance amplitudes. For example, Brown's (1963) observations of the breakdown of the laminar flow in a boundary layer, and the sequence of events leading to the transition of the layer to a turbulent state include a series of combined spatial and temporal growth of small, wave-like disturbances. The forced transition experiments of Schubauer and Skramstad (1947), and Klebanoff, Tidstrom, and Sargent (1962) give illustrations of a purely spatial growth of disturbances.

These observations force a closer look into the adequacy of the description of the growth of small disturbances as merely a process of temporal amplification. There are two fundamentally different approaches for bridging the difference in the theoretical and observed description of the phenomenon. The first of these are discussed in detail in a note by Gaster (1962). In this note a relation between the spatial and temporal amplification rates is derived under the assumption that these rates are small. This transformation states that the spatial amplification rate α_i can be determined by knowledge of the temporal amplification rate αc_i by the equation

$$\alpha_i = -\alpha c_i / c_g + O(\alpha^2) \quad (2.41)$$

where

$$c_g = c_r + \alpha \frac{\partial c_r}{\partial \alpha} = \frac{\partial(\alpha c_r)}{\partial \alpha} \quad (2.42)$$

c_g is identified as the group velocity of the disturbances. From comments appearing in his paper, it appears that Schlichting (1935) knew of this result, but presented no proof of his statement.

The interpretation of the group velocity of a dispersive wave system is that it represents the speed at which

the energy of the disturbance is convected. For fixed frequency disturbances, one must recognize that although α_{c_r} is fixed, its variation with wave number does not vanish and energy may still be carried by the disturbance at a velocity different from its phase speed.

The other approach to spatial amplification is a direct attack on Equation (2.33) by regarding α as a complex parameter and considering only real values for c or restricting c to be proportional to the complex conjugate of α so that the frequency ω is real. In this approach, no restriction on the size of α_i need be made as it was in the case of Gaster's transformation.

It must be recognized that complex α introduces amplification terms of the form

$$e^{-\alpha_i X}$$

by virtue of the fact that there is a complex portion of the wave number in (2.7). However, a term of this form causes exponential growth of the disturbances at either $\pm \infty$ for the case of nonzero α_i . Thus, to develop a stability criterion, one must consider separately whether the disturbances grow as they travel in the upstream or downstream direction.

In Table 2.1, criteria for the stability of traveling wave disturbances are formulated for spatial amplification by considering not only the direction in which the wave is amplified, but also the direction in which energy is carried by the disturbance, determined by the sign of the group velocity. In the same table, the temporal criterion for stability is also presented for comparison.

The inclusion of the group velocity in the stability criterion for spatial growth of disturbances is an effective application of a radiation condition. By means of this con-

dition, disturbances are classified as unstable if they con-
 vect energy in the same direction as their spatial growth.
 By means of Gaster's transformation (2.41), it is seen that
 there is agreement of the two criteria from Table 2.1. In the
 neighborhood of the neutral curve determined temporally and
 for the regions of temporal amplification of disturbances,
 the amplification rates c_i are very small and Gaster's trans-
 formation is unquestionably valid. The only question that
 might arise is that of whether there are additional regions,
 far removed from this neutral curve for which the spatial cri-
 terion predicts an instability that is not covered by the tem-
 poral criterion. This constitutes a detailed investigation
 that is beyond the scope of this paper.

Temporal Growth	Spatial Growth	Stability
$c_i > 0$	$\alpha_i < 0 \quad c_g > 0$ $\alpha_i > 0 \quad c_g < 0$	unstable (amplified)
$c_i = 0$	$\alpha_i = 0$	neutral
$c_i < 0$	$\alpha_i > 0 \quad c_g > 0$ $\alpha_i < 0 \quad c_g < 0$	stable (damped)

Table 2.1. Comparison of the Stability Criteria

Both of these criteria, as formulated, deal only with
 the local amplification of the disturbances because of the ap-
 proximations involved in the derivation of the Orr-Sommerfeld
 equation. The interpretation of the Reynolds number of an
 almost parallel flow given in Section 2.2 can entirely invali-
 date the consideration of the Orr-Sommerfeld equation as the
 equation that governs the growth of small disturbances since
 the separation of variables of (2.7) is not valid for $R a$

function of position. However, the interpretation of spatial stability given above implies an investigation of phenomena occurring at long distances (a radiation condition) for which the present analysis should be invalid. Furthermore, important non-linear effects become of interest when the linear disturbances reach a finite size, which occurs rather rapidly in a short spatial range even for the small amplification rates predicted by the temporal stability criterion. Thus any analysis that considers a spatial criterion for stability should unquestionably take the non-linear and three-dimensional phenomena into consideration to be a contribution to existing knowledge of the stability of boundary-layer type flows.

In this paper, only spatial amplification as given by Gaster's transformation will be investigated. As stated above, Gaster's result can be expected to have a high degree of accuracy for amplified disturbances as predicted by the temporal criterion. However, since the eigenvalues α , and c are functions of R , the interpretation of the growth predicted by (2.7) must be made very carefully, in view of the interpretation of R presented in Section 2.2.

One can make a rough estimate of the amount of spatial amplification by using eigenvalues obtained from calculations based on a temporal criterion, applying Gaster's transformation, and interpreting (2.7) to give

$$\ln\left(\frac{A}{A_0}\right) = -\frac{1}{K^2} \int_{R_0}^{R^2} \alpha_i^+ dR^2 + O\left(\frac{dA}{dy} \frac{d\theta}{dx} \Delta x\right) \quad (2.43)$$

where A is some measurable property of the disturbance, such as the magnitude of the u' velocity, and K is defined in (2.10). The first term arises from a generalization of (2.7) applied locally,

$$\int_{x_0}^x \alpha_i^* dx^* = \int_{R_{x_0}}^{R_x} \frac{\alpha_i \nu}{U_0} dR_x = \frac{1}{R_0^2} \int_{R_0^2}^{R^2} \alpha_i^+ dR^2$$

where α_i^+ is made dimensionless in a different manner than α . Henceforth, the superscript + will be omitted and α_i will be considered to be made dimensionless with respect to ν/U_0 .

The second term in (2.43) is an attempt to account for the variation of Reynolds number with x by considering explicitly the growth of the boundary layer with advancing distance downstream. This growth causes the streamlines to slope at a small angle, so that the ordinate y is in reality a similarity variable $y/\delta(x)$. This term is meant to represent the error that exists by consideration of the first term alone. No completely satisfactory estimate of the error can be made, since any model more detailed does not yield the Orr-Sommerfeld equation as a first estimate when boundary-layer growth is considered.

The important consideration, however, is the distinction between two length scales in the physical problem. The first is of the order of the local boundary-layer thickness and is the length over which a small disturbance grows appreciably, or over which the wave number of the disturbance changes significantly. The second and longer length is that for which the boundary-layer thickness changes appreciably. The fact that this second length is much longer than the first is the prime contributor to the accuracy of parallel flow theory for nearly parallel flow.

Chapter 3

DYNAMICS OF THE COMPLIANT BOUNDARY

3.1 Admittance of a Compliant Boundary

The dynamics of a general compliant boundary, in which traveling waves of wave number α and phase speed c exist, can be characterized by normal and tangential admittances. Only materials for which the stress strain laws exhibit a marked hysteresis or non-linear behavior are excluded from this discussion.

The concept of normal and tangential admittance provides a measure of the response of the compliant boundary to a traveling-wave pressure disturbance. The definition of the quantities appear in (2.19) and (2.20). Defining ξ, η as the horizontal (x) and vertical (y) deflections of the material in the compliant boundary, solutions for traveling waves are of the familiar form

$$\begin{aligned}\xi(x, y, t) &= \hat{\xi}(y) e^{i\alpha(x-ct)} \\ \eta(x, y, t) &= \hat{\eta}(y) e^{i\alpha(x-ct)}\end{aligned}\tag{3.1}$$

The deflections are related to the velocities used in (2.19) by the operational relations

$$\begin{aligned}\hat{U}_s &= -i\alpha c \hat{\xi}(0) \\ \hat{V}_s &= -i\alpha c \hat{\eta}(0)\end{aligned}\tag{3.2}$$

The materials that are to be considered have a linear stress-strain law with no hysteresis, so that the stresses are instantaneously related to the local strains and strain rates.

The pressure on the surface, related to the negative of the normal stress σ_{yy} , has a general form

$$\hat{p}_s = -\sigma_{yy}(0) = -\sigma_{yy}(\hat{\xi}(0), \hat{\eta}(0)) \quad (3.3)$$

The following sections are devoted to some sample calculations of the normal and tangential admittances by solving the dynamic equations for some selected examples of compliant boundaries. The examples treated in these sections by no means exhaust the possibilities for models of compliant boundaries, but serve only to illustrate the general technique.

3.2 Admittance of a Spring-Supported Membrane

Consider a membrane of mass/unit length m , damping-unit length d , under a constant tension T , and supported along its length by a spring of constant k . A deflected portion of the membrane is shown in Figure 2(a). The dynamic equation of this simple configuration is

$$-T \frac{\partial^2 \eta}{\partial x^2} + m \frac{\partial^2 \eta}{\partial t^2} + md \frac{\partial \eta}{\partial t} + k\eta = -p \quad (3.4)$$

One defines

$$c_0^2 = T/m \quad \omega_0^2 = k/m \quad (3.5)$$

as the propagation speed of disturbances and cutoff frequency of the membrane. Introducing the complex amplitudes $\hat{\eta}_s$, \hat{p}_s into (3.4), and using (2.19) and (2.20), one finds

$$Y_{11} = -ic/m(c_0^2 - c^2 - icd/\alpha + \omega_0^2/\alpha^2) \quad (3.6)$$

$$Y_{12} = 0$$

The parameters appearing in (3.6) shall be considered dimensionless as described in Section 2.2. In particular, d and ω_0^2 must be varied with Reynolds number as described in (2.15) and (2.16) to model a semi-infinite geometry. In addition, the mass/unit length m is made dimensionless with respect to $\rho\delta$ of the boundary layer, so that for a uniform membrane

$$m = m_0 R_0 / R \quad (3.7)$$

showing that the surface appears to become heavier as the boundary layer gets thinner. The cutoff frequency and damping also appear proportionally greater as the Reynolds number decreases, showing an implicit variation of the surface admittance with Reynolds number because of the non-dimensionalization. If this variation of properties is not maintained, the surface must be regarded as specially tailored or designed for the task at hand. Examples will be shown illustrating the effect on the stability of the boundary layer of "normal" surfaces and those that have been specially "tailored."

The normal admittance Y_{11} is nearly purely imaginary for real values of c , having a real part proportional to damping and c_i which are small. The imaginary part changes sign as the effective wave speed $c_0^2 + \omega_0^2/\alpha^2$ is passed. A physical explanation for the effect this admittance has on the stability of the laminar boundary layer will be presented later.

The tangential admittance for this case vanishes because no tangential motion is considered in this particular model of a compliant boundary.

3.3 Admittances of a Rubber Surface

The following model is an illustration of a possible rubber surface. It yields a better physical representation of the dynamics of some practical boundary structure than that of the previous section. The general equations of motion for an elastic solid are

$$\begin{aligned} \rho_s \frac{\partial^2 \xi}{\partial t^2} &= \frac{\partial \sigma_{xx}}{\partial x} + \frac{\partial \sigma_{xy}}{\partial y} \\ \rho_s \frac{\partial^2 \eta}{\partial t^2} &= \frac{\partial \sigma_{xy}}{\partial x} + \frac{\partial \sigma_{yy}}{\partial y} \end{aligned} \quad (3.8)$$

Following the suggestion of Nonweiler (1961), the following form of stress tensor is assumed to exist in the boundary

$$\begin{aligned} \sigma_{mn} &= \left[E + (d_1 - 2d_2) \frac{\partial}{\partial t} \right] \frac{\partial \xi_k}{\partial x_k} \delta_{mn} \\ &+ \left[G + d_2 \frac{\partial}{\partial t} \right] \left(\frac{\partial \xi_m}{\partial x_n} + \frac{\partial \xi_n}{\partial x_m} \right) \end{aligned} \quad (3.9)$$

where standard tensor notation is used. ρ_s is the density of the material in the boundary, E and G represent the tensile and shear moduli, respectively, and d_1 , d_2 represent structural damping coefficients giving rise to stresses proportional to strain rates. This model as described is a Voigt solid. The constants used are assumed to be known constants of the material used in the boundary.

General solutions for the complex displacement amplitudes $\hat{\xi}$, $\hat{\eta}$ are

$$\begin{aligned} \hat{\xi}(y) = \frac{1}{\alpha} \left\{ \frac{A_1}{r_1} \sinh r_1 \alpha y + A_2 \cosh r_2 \alpha y \right. \\ \left. + A_3 \cosh r_1 \alpha y + r_2 A_4 \sinh r_2 \alpha y \right\} \\ \hat{\eta}(y) = \frac{1}{i\alpha} \left\{ A_1 \cosh r_1 \alpha y + \frac{A_2}{r_2} \sinh r_2 \alpha y \right. \\ \left. + r_1 A_3 \sinh r_1 \alpha y + A_4 \cosh r_2 \alpha y \right\} \end{aligned} \quad (3.10)$$

where the following abbreviations have been adopted

$$\begin{aligned} r_1^2 = 1 - (\epsilon/c_1)^2 & \quad r_2^2 = 1 - (\epsilon/c_2)^2 \\ c_1^2 = (E + 2G - i\alpha\epsilon d_1)/\rho_s & \quad c_2^2 = (G - i\alpha\epsilon d_2)/\rho_s \end{aligned} \quad (3.11)$$

in dimensionless form.

The perturbation velocities at the surface ($y = 0$) are found by inspection of (3.10)

$$\begin{aligned} \hat{u}_s = -i\epsilon (A_2 + A_3) \\ \hat{v}_s = -\epsilon (A_1 + A_4) \end{aligned} \quad (3.12)$$

Manipulation of (3.9) shows that the surface pressure \hat{p}_s can be expressed as

$$\begin{aligned} \hat{p}_s = -\sigma_{22} = - \left\{ E - i\alpha\epsilon(d_1 - 2d_2) \right\} (i\alpha \hat{\xi} + \hat{\eta}') \\ + (G - i\alpha\epsilon d_2) 2\hat{\eta}' \end{aligned}$$

or

$$\hat{p}_s = -\rho_s c_1^2 \hat{\eta}'(0) - i \alpha \rho_s (c_1^2 - 2c_2^2) \hat{\xi}(0) \quad (3.13)$$

where c_1^2 , c_2^2 are defined in (3.11). Thus

$$\hat{p}_s = i c_1^2 (A_2 + r_1^2 A_3) - i (c_1^2 - 2c_2^2) (A_2 + A_3) \quad (3.14)$$

The admittances Y_{11} and Y_{12} are specified by the ratios of \hat{u}_s , \hat{v}_s to \hat{p}_s , and the four constants A_i determine these admittances when three boundary conditions are specified to determine the constants.

Two boundary conditions that provide reasonable approximations to those that are expected at the interface between a rubber surface and a water boundary layer are that the shear stress vanishes at this interface and that the normal displacement vanishes at the lower boundary. These conditions can be stated mathematically as

$$\begin{aligned} \text{(i)} \quad \sigma_{xy} &= \frac{\partial \xi}{\partial y} + \frac{\partial \eta}{\partial x} = 0 && \text{at } y = 0 \\ \text{(ii)} \quad \eta &= 0 && \text{at } y = -H \end{aligned} \quad (3.15)$$

An additional boundary condition must be stated at the lower boundary of the surface. A boundary condition that leads to a simple result for the admittances is that the shear stress also vanishes at this boundary; i.e., the

lower surface slides without friction on a rigid substructure.

$$(iii) \quad \tau_{xy} = \frac{\partial \bar{\zeta}}{\partial y} = 0 \quad \text{at } y = -H \quad (3.16)$$

In terms of the four constants A_i introduced above, these boundary conditions specify three ratios

$$\begin{aligned} \frac{A_4}{A_1} &= -2/(r_2^2 - 1) \\ \frac{A_2}{A_1} &= -2r_2 \coth r_2 \alpha H / (1 + r_2^2) \\ \frac{A_3}{A_1} &= \frac{1}{r_1} \coth r_1 \alpha H \end{aligned} \quad (3.17)$$

From (3.17), (3.12), and (3.14), one can deduce

$$\begin{aligned} Y_{11} &= -i\epsilon r_1 (r_2^2 - 1) / \gamma \\ Y_{12} &= -\epsilon \beta / \gamma \end{aligned} \quad (3.18)$$

where

$$\begin{aligned} \beta &= (1 + r_2^2) \coth r_1 \alpha H - 2r_1 r_2 \coth r_2 \alpha H \\ \gamma &= \rho_3 \epsilon_2^2 \left\{ (1 + r_2^2)^2 \coth r_1 \alpha H - 4r_1 r_2 \coth r_2 \alpha H \right\} \end{aligned} \quad (3.19)$$

It is sometimes convenient to regard the disturbances that contribute to the admittances in (3.18) as shear waves propagating in an incompressible medium. This can be effected simply by letting $c_1^2 \rightarrow \infty$ so that $r_1 = 1$. This simplification reduces the relevant parameters to four, namely \tilde{c}_2 , d , ρ_s , and H , where

$$c_2^2 = \tilde{c}_2^2 (1 - \alpha e d) \quad (3.20)$$

Note that these parameters are functions of the Reynolds number as discussed in Section 2.2.

One can consider alternative boundary conditions to replace the assumption of (3.16). By requiring that both the normal and tangential displacement vanish at the lower boundary, the ratios specified in (3.17) are changed to

$$\frac{A_4}{A_1} = -2/(r_2^2 - 1)$$

$$\frac{A_2}{A_1} = \frac{r_2}{\Delta} \left(1 + \frac{r_1 r_2 \sinh r_1 \alpha H \sinh r_2 \alpha H - \cosh r_1 \alpha H \cosh r_2 \alpha H}{1 + r_2^2} \right) \quad (3.21)$$

$$\frac{A_3}{A_1} = \frac{r_2}{\Delta} \left(\frac{2}{1 + r_2^2} + \frac{\sinh r_1 \alpha H \sinh r_2 \alpha H}{r_1 r_2} - \cosh r_1 \alpha H \cosh r_2 \alpha H \right)$$

$$\Delta = r_1 r_2 \sinh r_1 \alpha H \cosh r_2 \alpha H - \cosh r_1 \alpha H \sinh r_2 \alpha H$$

The corresponding expressions for admittance can be deduced from (3.12) and (3.14). The final expression is rather long, and since no computations were made for a sur-

face with these boundary conditions, will not be written here.

3.4 Matching of Surface Shear Stress

It is generally sufficient to assume that the response of a compliant boundary, such as the rubber surface model considered previously, to the oscillating component of shear stress acting on the surface is negligible. If it is felt that this shear stress should be matched at the interface between boundary layer and compliant boundary, a simple iterative scheme can be proposed that will accomplish the matching.

This scheme is based on the premise that the shear stress at the interface is small. The first estimate considers the shear to vanish, permitting the computation of the tangential admittance Y_{12} . With this admittance, the eigenfunction ϕ_w may be found satisfying (2.29). Using ϕ_w one can compute the dimensionless shear stress at the boundary

$$\tau = \frac{1}{R} (\phi_w'' + \alpha^2 \phi_w) = \rho_s c_s^2 (\hat{\xi}'(0) + i\alpha \hat{\eta}(0)) \quad (3.22)$$

This value for τ is then inserted as an inhomogeneous term in (3.15i). After suitable normalization, this new boundary condition will effect (3.17) and give rise to a better estimate for Y_{12} . This process is repeated until adequate convergence of either Y_{12} or τ is obtained for two successive trials. At this time, both Y_0 and Y_{11} may be computed and the eigenvalue criterion \mathcal{E} may be evaluated.

It is not felt that the inclusion of surface shear will reveal any new effects, so no results of this computation will be presented.

3.5 Inviscid Liquid with Zero Mean Motion

Another simple example of a compliant boundary is a bed of inviscid liquid, such as a body of water. Defining φ as the velocity potential of the disturbances in the water, and using a linearized Bernoulli equation

$$p = -\rho_w \left(\frac{\partial \varphi}{\partial t} + g\eta \right) \quad (3.23)$$

where

$$\frac{\partial \eta}{\partial t} = \frac{\partial \varphi}{\partial y} \quad \text{at } y=0 \quad (3.24)$$

one can easily verify that

$$\begin{aligned} Y_{12} &= \alpha c / \rho_w (\alpha c^2 - g) \\ Y_{11} &= i\alpha c / \rho_w (\alpha c^2 - g) \end{aligned} \quad (3.25)$$

for deep water, and

$$\begin{aligned} Y_{12} &= \alpha c / \rho_w (\alpha c^2 - g \tanh \alpha H) \\ Y_{11} &= i\alpha c / \rho_w (\alpha c^2 \coth \alpha H - g) \end{aligned} \quad (3.26)$$

for water of a finite depth.

The vanishing of the denominator of (3.26), which yields an infinite admittance, is the condition usually applied for water waves; namely, a zero pressure perturbation on the surface, for which the wave speed is

$$c^2 = \frac{g}{\alpha} \tanh \alpha H \quad (3.27)$$

One expects wave speeds of interest to be in this range. Note that g here is expressed in dimensionless terms, and is directly related to the Froude number F of the boundary layer over the body of water

$$F^2 = U_0^2 / g\delta \quad (3.28)$$

The effect of surface tension can be represented by a simple modification of the Froude number, by including the inverse of the Weber* number $W^{-1} = T_* / \rho U_0^2 \delta$ in the following fashion

$$\tilde{F}^{-2} = F^{-2} + \alpha^2 W^{-1} \quad (3.29)$$

A decision should be made as to the manner in which the Reynolds number of the boundary layer is to vary in this case. Contrary to the arguments given in Section 2.2, the concept of a semi-infinite plate may not be very important for this configuration. A more realistic model would be to let the boundary-layer thickness and viscosity be fixed, and let the Reynolds number (and the Weber and Froude numbers) vary with the velocity.

The inviscid example presented here provides a good model for the generation of water waves by a shear flow, particularly in deep water where viscous effects have little importance.

3.6 Admittance of Coupled Helmholtz Resonators

A final example of the calculation of the admittance of a compliant boundary is that of the coupled Helmholtz resonators. This configuration was used by Meyer-Piening

* Defined in Section 12-5 of Ipsen (1960)

(1963) in a series of experiments on this flow. One can consider a two-dimensional array of Helmholtz resonators (small resonating chambers of fluid) that are coupled to each other and the fluid in the boundary layer by small openings (see Figure 3).

Each resonant cavity of compressible fluid behaves like a spring while the fluid in the small apertures represent the masses on which the springs act. There are several possible approaches to derive approximate solutions for this system. The analysis done by Meyer-Piening will be followed.

The motion of the fluid in each cavity must obey the wave equation for small disturbances. Using the numbering system of Figure 3, the pressure in the i th resonator must satisfy

$$\frac{\partial^2 p_i}{\partial t^2} - a^2 \frac{\partial^2 p_i}{\partial y^2} = 0 \quad (3.30)$$

for these essentially vertical oscillations. The parameter a is the speed of sound in the cavity and is assumed to be constant for these small disturbances. The pressure is assumed to be uniform across the section of the resonator. A velocity potential exists and is related to the pressure by the linearized Bernoulli equation

$$p_j = -\bar{\rho} \frac{\partial \phi_j}{\partial t} \quad (3.31)$$

where $\bar{\rho}$ is the mean density in the cavity. Solutions to (3.30) exist in the form

$$\begin{aligned} \phi_j &= \hat{\phi}_j \cos \frac{\omega}{a} y e^{-i\omega t} \\ p_j &= -i\bar{\rho}\omega \hat{\phi}_j \cos \frac{\omega}{a} y e^{-i\omega t} \end{aligned} \quad (3.32)$$

where the vertical velocity vanishes at the base of the cavity ($y = 0$ in this coordinate system).

By averaging ϕ over the cross section of the cavity,

one can neglect the effects of the side walls. The only other consideration is the effect of the pressure perturbation set up in the cavity on the motion of the small masses of fluid in the apertures. Since these small slugs of fluid have a finite mass, their acceleration causes a pressure difference across the apertures.

For the sake of the analysis, it will be assumed that the acceleration of the masses of fluid in all the apertures is proportional to the time rate of change in vertical velocity at the top of the cavities. This assumption approximates reality for small geometries at the top of the cavity. Thus the following constraints must be satisfied at the top of the cavity, using the notation of Figure 3.

$$\text{upper hole} \quad \bar{\rho} \frac{\partial^2 \phi_i}{\partial y \partial t} = - \frac{p_s - p_i}{l_2} \quad (3.34)$$

$$\text{left hole} \quad \bar{\rho} \frac{\partial^2 \phi_i}{\partial y \partial t} = - \frac{p_{i-1} - p_i}{l_3}$$

$$\text{right hole} \quad \bar{\rho} \frac{\partial^2 \phi_i}{\partial y \partial t} = - \frac{p_{i+1} - p_i}{l_3}$$

$$\text{solid boundary} \quad \bar{\rho} \frac{\partial^2 \phi_i}{\partial y \partial t} = 0$$

Averaging the boundary conditions at $y = H$, to account for the amount of boundary that is a rigid wall and that part that can communicate with regions at a different pressure, one finds

$$\begin{aligned} \bar{\rho} \frac{\partial^2 \phi_i}{\partial y \partial t} &= \frac{Q_2}{l_2} (p_i - p_s) \\ &+ \frac{Q_3}{l_3} (2p_i - p_{i-1} - p_{i+1}) \end{aligned} \quad (3.34a)$$

where

$$Q_2 = \frac{S_2}{S_1 + S_2} \quad Q_3 = \frac{S_3}{S_1 + S_3}$$

Regarding the last term on the right-hand side of (3.34a) as written in finite difference form, one can go to the limit of a second x derivative by introducing the distance between cavities L, and letting L approach zero

$$\bar{p} \frac{\partial^2 \phi}{\partial t \partial y} = \frac{Q_2}{l_2} (p_i - p_s) - \frac{Q_3}{l_3} L^2 \frac{\partial^2 p_i}{\partial x^2} \quad (3.35)$$

At this point recall that a traveling wave disturbance is causing the perturbation \hat{p}_i so that the second x derivative can be replaced by its operational equivalent $-\alpha^2$ yielding

$$\hat{p}_s = - \frac{l_2}{Q_2} (i \bar{p} \omega \cos \frac{\omega}{a} H) (-\omega \tan \frac{\omega}{a} H + \frac{Q_2}{l_2} + \frac{Q_3}{l_3} L^2 \alpha^2) \quad (3.36)$$

Using (3.36) and the definition of the normal admittance (2.20), one finally arrives at the admittance of this configuration

$$Y_{11} = \frac{-i Q_2 \tan \frac{\omega}{a} H}{l_2 \bar{p} (-\omega \tan \frac{\omega}{a} H + \frac{Q_2}{l_2} + \frac{Q_3}{l_3} L^2 \alpha^2)} \quad (3.37)$$

This can be compared to (3.6) if one realizes that there is only small x coupling (that provided by the tension in the membrane) and ω is replaced by αc . There is no provision for dissipation in this model, but it could be taken into consideration in a qualitative manner. Expanding the tangent for small values of its argument completes the comparison of these resonators with the membrane, showing the

principal effect to be that of the supporting spring of Section 3.2.

So similar are these cases that no calculations will be made for this configuration. It must be recognized, though, that a geometry such as this is a fruitful model for future investigations of the influence of a compliant boundary, but a more thorough analysis would have to be performed.

Chapter 4

COMPUTATION OF THE BOUNDARY LAYER ADMITTANCE

4.1 Solution of the Orr-Sommerfeld Equation far from a Boundary

In Chapter 2 it was shown that the Orr-Sommerfeld equation (2.8) governs the behavior of linear disturbances in a viscous shear flow. A technique for the numerical solution of the Orr-Sommerfeld equation is to be developed in subsequent sections. This technique is based on the observation that the equation takes a very simple form far from a boundary where the velocity \bar{U} approaches a constant value.

For these regions where $\bar{U}(y) = \bar{U}_0$, Equation (2.8) has constant coefficients and may be written

$$\phi^{IV} - (\alpha^2 + \beta^2)\phi'' + \alpha^2\beta^2\phi = 0 \quad (4.1)$$

where

$$\beta^2 = \alpha^2 + i\alpha R(\bar{U}_0 - c) \quad (4.2)$$

This constant coefficient equation has four solutions expressible in terms of exponential functions

$$\begin{aligned} \phi_1 &= e^{-\alpha y} & \phi_2 &= e^{\alpha y} \\ \phi_3 &= e^{-\beta y} & \phi_4 &= e^{\beta y} \end{aligned} \quad (4.3)$$

where the real part of $\beta > 0$.

Referring to the boundary condition (2.18), which states that ϕ, ϕ' tend to zero as $y \rightarrow \infty$, one must reject ϕ_2 and ϕ_4 for large positive y , and for cases where the flow extends to $-\infty$, one must reject ϕ_1 and ϕ_3 for large

negative y . Between these two extremes, there exists either a boundary or an unbounded shear flow for which (4.3) are not valid solutions. In the work that follows, it shall be considered that a boundary is located at $y = 0$ and the problem of interest is that of perturbations in a boundary layer lying above this boundary.

Since ϕ_1, ϕ_3 are the most general pair of bounded solutions that satisfy (2.18) outside of the boundary layer, at the outer edge* of the boundary layer a general solution of the Orr-Sommerfeld equation can be expressed as a combination of these two solutions.

Anticipating a numerical integration of (2.8) from the outer edge of the boundary layer (defined as $y = 1$) to the wall ($y = 0$), one can use this form of the solutions ϕ_1 and ϕ_3 to specify initial values for two numerical integrations of (2.8) to find the most general solution. These initial values are

$$\begin{array}{cccc} \phi_1 = 1 & \phi_1' = -\alpha & \phi_1'' = \alpha^2 & \phi_1''' = -\alpha^3 \\ \phi_3 = 1 & \phi_3' = -\beta & \phi_3'' = \beta^2 & \phi_3''' = -\beta^3 \end{array} \quad (4.4)$$

The given initial values are then integrated from $y = 1$ to $y = 0$. The two solutions ϕ_1, ϕ_3 should be linearly independent for α different from β . The details of this integration are discussed in the next section.

* Since the outer edge of the boundary layer is not precisely determined, it was located empirically for these computations. The point in the velocity profile was selected as the outer edge of the boundary layer if the integrations of the Orr-Sommerfeld equation starting at points farther removed from the wall yielded the same results.

4.2 Numerical Integration of the Orr-Sommerfeld Equation

When the coefficients of (2.8) vary (in the range $1 \leq y \leq 0$) no exact closed form solutions exist. In this interval, a numerical integration is used to solve the two initial value problems posed by (4.4). The use of these initial values insures that the final solution has the correct asymptotic behavior far from the surface, and that these are the only solutions of the four solutions possible that need to be considered.

The integration schemes that were considered were all single-step integration techniques suitable for this fourth order equation. This technique regards (2.8) as an algebraic equation for the fourth derivative

$$\phi^{IV} = F(\phi, \phi'', y) \quad (4.5)$$

Since at a station y , ϕ and its derivatives are known, the integration scheme can proceed to determine the desired quantities at the next station, $y-h$. This process continues until the wall ($y = 0$) is reached, and is schematically illustrated in Figure 4.

Several integration schemes were tried before the final form was selected. A trapezoidal, iterative integration formula provided reasonable results when approximately 250 integration steps were used. A non-iterative scheme based on the Taylor series expansion of the function about the point y still needed about 200 integration steps to yield satisfactory results. An iterative, modified Milne-Obrechhoff integration scheme provided excellent results which varied by less than one per cent when the number of steps was varied from 500 steps to 12 steps. The scheme that was finally selected was a modified Runge-Kutta integration that used 64 integration steps to perform the desired calculation. A description of the latter two techniques appears in Appendix B.

The selection of the Runge-Kutta integration scheme as the final form used in the computation of results was based on two considerations. It provided calculations of the eigenfunction ϕ at the wall sufficiently accurate to determine four digits of the wave speed c , and exhibited the most rapid speed of computation for this accuracy. One integration of the Orr-Sommerfeld equation is performed in 31/60 seconds on the IBM 7094 computer with the present FORTRAN coded computer program. This computational time could definitely be improved by the reprogramming of the numerical integration in appropriate machine language. It was felt that the simplicity of the present program outweighed the saving in time to be achieved from rewriting the program.

The accuracy of the scheme was verified by direct comparisons of the results with those of the Milne-Obrechhoff scheme, which was determined to have an exceptionally high accuracy, and by variations of the integration step size over several octaves above and below the finally accepted 64 step integration. Both of these comparisons indicated that the integration scheme provided the necessary accuracy for this type of calculation.

To determine whether the method itself was accurate, a comparison was made of the eigenfunction $\phi(y)$ with that found by Kurtz (1962). This comparison was performed by Mr. S. Chan* who reported excellent agreement of the test cases. It is felt that this comparison is significant because the technique used by Kurtz to solve the Orr-Sommerfeld equation is radically different from that described herein. The results of these two independent checks show that both the technique and the numerical integration used give valid solutions of the Orr-Sommerfeld equation.

It was observed that the solution ϕ_3 behaves the

* M.I.T. Electronics Systems Laboratory, unpublished communication.

same as the viscous asymptotic solution of (2.8), and henceforth will be referred to as the viscous solution. By appropriate combinations of ϕ_3 , one can calculate the Tietjen's function $\mathcal{F}(z)$ (Appendix A) which is tabulated in Miles (1962). Agreement was found to the number of digits presented in the tables.

In the range of Reynolds numbers that is important for boundary-layer stability, it is estimated that four decimal digits of complex c can be maintained. In the final form of the integration scheme, the relevant Reynolds number and wave number are limited by the inequality $\alpha R < 10^4$. Above this limit, an overflow of the viscous solution may develop for some phase speeds c : i.e., $|\phi_3'''| > 10^{38}$. It is possible to program around this occurrence without too much difficulty, but it was felt that smaller steps should be used for integrations at these high values of α, R . Furthermore, it was felt that Reynolds numbers beyond 10^4 were not of interest* so this restriction caused few limitations in the present computations.

4.3 Parasitic Growth of Truncation Errors

There is one feature of this numerical integration that causes significant problems when performing the actual computations. This difficulty arises because the "viscous" solution ϕ_3 has a much more rapid growth than the "inviscid" solution ϕ_1 . By this statement, it is meant that

$$\phi_3' / \phi_3 \gg \phi_1' / \phi_1 \quad (4.6)$$

for all finite intervals Δy in the range (1,0).

* For $R > 10^4$, $R_x > 3 \times 10^6$, above which natural transition is observed to occur for the smoothest flow conditions of the external stream. (cf. Schubauer and Skramstad (1947)).

Initially, the two solutions are linearly independent as shown by (4.4), but as the numerical integration proceeds, this independence is observed to disappear rapidly. Since the differential equation is of such a simple type (linear and non-singular) in the range of interest, it is certain that this loss of linear independence, which is impossible for an exact solution, arises because of the approximate nature of the numerical integration.

There are two possible sources of error that must be investigated. The first is an actual integration error caused by a poorly implemented numerical integration formula. The other type arises because of the nature of a digital computer operating in a floating point mode. A computer carries only a specified number of significant digits plus an exponent when representing a real number. From time to time, truncation or round-off of a result occurs, and this error is characterized as a truncation error.

The effect of integration errors is greatest on ϕ_3 , since this function exhibits a very rapid growth as the integration advances. As stated in the preceding section, it has been determined that the integration of ϕ_3 is within satisfactory limits. Judging from the behavior exhibited for $y > 1$, ϕ_1 should exhibit a slower growth than ϕ_3 and consequently the same integration scheme should be more than adequate to describe the variation of ϕ_1 .

However, it is noted that as the integration proceeds, ϕ_1 starts growing more rapidly than anticipated. This type of behavior is illustrated for a real function in Figure 5. It is regretted that an actual example of this phenomenon cannot be presented graphically, but ϕ_3 is a complex function that typically exhibits a growth in excess of 10^{12} , while ϕ_1 is observed to grow by a factor of (approximately) 10^5 . Figure 5 is used only to suggest the behavior of these

two functions. The point is that at $y = 0$, ϕ_1 is proportional to ϕ_3 . Since ϕ_3 is a solution, then ϕ_1 is still proportional to a solution of (2.8). The difficulty is that ϕ_1 satisfied boundary conditions at $y = 1$ that should have yielded a solution that is independent of ϕ_3 . It is also observed that the factor of proportionality that relates the resultant ϕ_1 to ϕ_3 exhibits a rapid variation when the initial conditions are changed slightly.

The conclusion is that quite arbitrary initial conditions at $y = 1$, when used for a numerical integration of (2.8) yield a solution proportional to ϕ_3 , and that the factor of proportionality is very sensitive to small changes in the initial data. It must be stressed that this factor of proportionality is a complex number, so at first glance, this dependence is not obvious if a comparison of only the real parts (or imaginary parts) is made.

This is an unfortunate occurrence, because other techniques of solution of the Orr-Sommerfeld equation indicate that the final eigenfunction remains of the same order throughout, so that the combination of ϕ_1 and ϕ_3 will probably result in the small difference of two very large numbers. If this technique for solving the Orr-Sommerfeld equation is to be a useful tool, the cause of this behavior must be explained and understood.

The explanation for this unusual phenomenon is based on two observations. The first of these is that ϕ_3 is the most rapidly growing solution of this equation by several orders of magnitude. When this is coupled with the second feature, the rather irregular number system used by the digital computer, the answer becomes clear.

Computation retaining only a fixed number of digits requires that ϕ_1 can be specified initially only to this number of significant figures. At the initial step then, one can re-

gard ϕ_1 as having a small portion of its initial conditions that provide suitable initial conditions for ϕ_3 . If by some rare circumstance, this small portion is not present initially, after one integration (and its accompanying truncation error) this portion will definitely be present.

It is this small initial error portion that is a complex multiple of ϕ_3 and eventually dominates the solution that started off as ϕ_1 if the integration proceeds far enough. It must be stressed that this error is not the result of any instability of the equation or numerical integration scheme as discussed by numerical analysts such as Urabe (1961) or Dahlquist (1962), but is an actual solution of the differential equation. This portion of the solution ϕ_1 is called the parasitic error.

An analogy might be drawn between the Orr-Sommerfeld equation and a noisy electronic circuit, which provides the same undesired output for an arbitrary noisy input. The techniques that can be used to remove this difficulty for the Orr-Sommerfeld equation have analogous techniques in electronics, as will be discussed in the next section.

As a consequence of this noise sensitivity, one can envision an analog computer solution of the Orr-Sommerfeld equation which always saturates the output for any arbitrary input, even the case for a shorted input.* This seeming paradox is explained by the infinitesimal contact noise at the shorted input that provides sufficient initial conditions for the viscous solution to grow to saturation. It is exactly the same phenomenon that causes the numerical (as opposed to analytical or mathematical) linear independence to be lost.

* Cf. Bismut (1963)

4.4 Parasitic Error Purification Scheme

A technique for removing or controlling this source of error must be found if this method of solution for the Orr-Sommerfeld equation is to be successful. There are two possible techniques that can be used to resolve this difficulty.

The first of these corresponds to improving the quality of the analogous electrical signal by improving the quality of the electrical network. On the digital computer, this corresponds to carrying more significant figures in the computation of ϕ_1 . Double precision arithmetic can increase the number of significant decimal digits to 16 and requires a growth of ϕ_3 on the order of 10^{25} before this problem again becomes important. Furthermore, modern digital computers such as the IBM 7094 have provision for automatically performing these double precision operations by means of built-in hardware.

In Table 4.1 an estimate is given of the penalties in computation time imposed by double precision arithmetic. The operation time for sample single and double precision arithmetic operations is given for the IBM 7090 and 7094 digital computers.

Floating Point Operation	Machine Instruction	Machine Cycles	
		7094	7090
Addition (Subtraction)	FAD(FSB)	12	15
	DFAD(DFSB)	13**	61*
Multiplication	FMP	5	13
	DFMP	9**	69*
Division	FDP	9	13
	DFDP	19**	90*

Table 4.1. Execution time in Machine Cycles for Selected Floating Point Arithmetic Instructions on the IBM 7090-7094 Computers.

Note: Prefix D signifies double precision operation

*Double precision operations for the 7090 are available only as specially-coded subroutines. The times quoted are approximate times for the FORTRAN II double precision arithmetic package.

**Double precision operations are automatic on the 7094 only through an assembly language such as FAP.

Core storage cycle time: 7090 2.18 microseconds
7094 2.0 microseconds

It is obvious that even for a laborious, hand-coded numerical integration utilizing double precision arithmetic for every arithmetic operation appearing in the numerical integration, this alternative is costly in computation time, with execution times typically 40% slower. If it is desired to keep the programming in a simpler, compiler language, such as FORTRAN II, the time loss is prohibitive. However, it must be stressed that inefficiency and high investment in programmer time are the only disadvantages to this means of solving the problem, and this technique definitely will work.

To continue with the electronic analogy, the second technique that can be used to control the parasitic solution corresponds to the utilization of selective filters. By using

this technique, the parasitic solution can be filtered from the more slowly growing solution ϕ_1 . In other words, ϕ_1 is to be purified of its parasitic error.

The root of this technique is based on the introduction of controlled amount of the viscous solution ϕ_3 into the slowly growing solution. If sufficient care is taken about the amount of parasite that is permitted to grow, it can be insured that the part of the slowly growing solution that is linearly independent of ϕ_3 is never truncated from ϕ_1 . In this technique it is recognized that since both ϕ_1 and ϕ_3 are solutions* of (2.8), a combination of these two solutions is also a solution

$$\tilde{\phi}_1 = \phi_1 + A\phi_3$$

Assume that $\tilde{\phi}_1(y)$ is a solution of (2.8) at station y and that any parasite in $\tilde{\phi}_1$ does not dominate the solution; i.e., there is an arbitrary number of digits in $\tilde{\phi}_1$ independent of ϕ_3 . Then one can write $\tilde{\phi}_1$ as an independent part ϕ_1 and a parasite

$$\tilde{\phi}_1(y) = \phi_1(y) + \epsilon \phi_3(y) \quad (4.7)$$

After a numerical integration to $(y-h)$, the parasite is larger relative to ϕ_1 than at station y . Define a new function $\tilde{\tilde{\phi}}_1$ at $(y-h)$ in the following manner

$$\tilde{\tilde{\phi}}_1(y-h) = \tilde{\phi}_1(y-h) - A\phi_3(y-h) = \phi_1(y-h) + (\epsilon - A)\phi_3(y-h) \quad (4.8)$$

If ϵ were known, one could select the constant A so that the contribution $(\epsilon - A)\phi_3$ would exactly vanish (except for a small numerical truncation error). However, it is not necessary to totally discard the parasite, but merely to

* By "solution" it is meant that at station y , the four complex numbers $\phi, \phi', \phi'', \phi'''$ are values of a function that satisfies (2.8) and that approaches 0 as $y \rightarrow \infty$.

insure that it does not dominate $\phi_1(y-h)$. This can be done with the aid of an operator F that expresses some relationship between $\tilde{\phi}_1$ and its derivatives

$$F(\tilde{\phi}_1, y-h) = 0 \quad (4.9)$$

For the moment, regard F as an arbitrary operator involving ϕ and one derivative with the restriction that

$$F(\phi_3, y-h) \neq 0 \quad (4.10)$$

The only restriction on F other than that presented by (4.10) is that the solution of the differential equation

$$F(\chi) = 0$$

has a solution that always behaves much differently than the rapidly growing solution ϕ_3 , in that it does not have such rapid growth.

For example, a possible choice for the auxiliary constraint F is the inviscid equation (the Orr-Sommerfeld equation for infinite Reynolds number)

$$F(\phi, y) = (\bar{U}(y) - c)(\phi'' - \alpha^2 \phi) - \bar{U}''(y) \phi \quad (4.11)$$

It must be stressed that $\tilde{\phi}_1$ is not a "solution" of (4.11), but is a solution of (2.8) that merely satisfies the relationship between its derivatives as shown by (4.11). Any auxiliary differential constraint provides this kind of relationship between the derivatives of $\tilde{\phi}_1$, but the fact that ϕ and three derivatives are given at station $(y-h)$ means that any initial value problem for a relationship like (4.11) is over-specified.

With the aid of this auxiliary relationship, one can continuously filter out part of the parasitic solution at every stage of the numerical integration, since the constant A can now be determined to be

$$A(Y-h) = F(\tilde{\phi}_1, Y-h) / F(\phi_3, Y-h) \quad (4.12)$$

The "solution" that had part of the parasitic solution filtered out at every integration step is called the "purified solution." It is not a true solution of Equation (2.8) in the sense that no analytic solution would take on the values of the "purified solution" at the points of integration. It is rather the value of a different combination of the two independent solutions (ϕ_1 and ϕ_3) at every integration station. If the purification constants A have been saved after their evaluation, a single solution can be constructed at every integration station ($Y=nh$) by use of the following formula

$$\phi_1(nh) = \tilde{\phi}_1(nh) + \left\{ \sum_{m=0}^{n-1} A(mh) \right\} \phi_3(nh) \quad (4.13)$$

It must be stressed that this recombination must take place in a reverse order than that for which the A's were computed. If a direct combination were attempted, small errors in the values of the initial A at ($Y=1$) would cause large errors in the value of A at ($Y=0$), because the magnitudes of the purification constants descend very rapidly. It is exactly this difficulty that the purification scheme tends to correct in the integration of the more slowly growing solution.

4.5 Numerical Determination of the Eigenvalue Criterion

To solve the eigenvalue problem numerically, one does not need to know the functions $\phi_1(y)$, $\phi_3(y)$ but only their values at the wall. Thus the results of the numerical integration are eight complex numbers defined at ($y = 0$).

$$\phi_1, \phi_1', \phi_1'', \phi_1''', \phi_3, \phi_3', \phi_3'', \phi_3'''$$

Because of the purification scheme, these two pairs of four numbers are numerically linearly independent. The value of the eigenfunction Φ is found by letting

$$\Phi = \phi_1 + B \phi_3 \quad (4.14)$$

where B is selected from consideration of the requirement that Φ satisfy (2.29), which is rewritten below

$$G(\Phi) = (1 - c Y_{12}) \left(\Phi_w' + \frac{\bar{U}_w'}{c} \Phi_w \right) + \quad (4.15)$$

$$\frac{i Y_{12}}{\alpha R} \left(\Phi_w''' - \alpha^2 \Phi_w' \right)$$

The previous two equations determine B to be

$$B = - \frac{G(\phi_1)}{G(\phi_3)} \quad (4.16)$$

It is this final eigenfunction $\bar{\Phi}$ that is used to determine the boundary-layer admittance Y_0 from its defining equation (2.31).

4.6 Construction of the Eigenfunction

Although it is not necessary for the computation of the boundary-layer admittance, it still may be of interest to investigate the actual behavior of the eigenfunction $\bar{\Phi}(y)$. The use of the purification scheme requires that some thought be given to the method of combination. It can be easily shown that the correct combination of the two solutions of (2.8) is

$$\bar{\Phi}(nh) = \hat{\bar{\Phi}}_1(nh) + \left(B + \sum_{m=0}^{n-1} A(mh) \right) \phi_3(nh) \quad (4.17)$$

This should be compared with (4.13) in which only the "inviscid" part of the solution was required. The notation is that used in the previous sections.

With the use of this eigenfunction, one may compute the distribution of amplitude of the velocity components

$$\begin{aligned} \hat{u}(y) &= \bar{\Phi}'(y) \\ \hat{v}(y) &= -i\alpha \bar{\Phi}(y) \end{aligned} \quad (4.18)$$

and also the vorticity and Reynolds stress distributions

$$\hat{\zeta}(\gamma) = -\Phi''(\gamma) + \alpha^2 \bar{\Phi}(\gamma)$$

(4.19)

$$\hat{\tau}(\gamma) = -\text{Real Part} \{ i\alpha \Phi' \bar{\Phi}^* \}$$

where * indicates the complex conjugate.

These are useful in the study of the physical phenomena represented by the mathematical solutions. The distribution of the disturbance amplitudes can also be compared to the available measurements of disturbances in the boundary layer. This will be discussed in Section 10.2.

Chapter 5

DETERMINATION OF THE EIGENVALUES

5.1 Selection of the Eigenvalue Criterion

The techniques described in Chapters 3 and 4 exist in the form of subroutines written for a digital computer. Examples of these routines are shown in Appendix C. Given a value of α , R , and c , these routines numerically determine Y_{11} , Y_{12} , and Y_0 so that the eigenvalue criterion \mathcal{E} can be evaluated. In this section, both R and α will be regarded as fixed and the details of the computation of the eigenvalue c will be considered.

With this limitation in mind, it is sufficient to take \mathcal{E} as a function of c alone, so that the eigenvalue c_e is a solution of the following equation

$$\mathcal{E}(c_e) = 0 \quad (5.1)$$

This function is known numerically in the sense that, given a value for c , $\mathcal{E}(c)$ can then be determined. Furthermore, it is anticipated that the functional relationship is analytic even though no closed form solution is known.

The selection of the exact form of the various possible relations for $\mathcal{E}(c)$ is important, for numerically the only test that is made is that

$$|\mathcal{E}| < \epsilon \quad (5.2)$$

for some arbitrarily small tolerance ϵ . It is generally sufficient to use the simple form

$$\mathcal{E} = \Delta Y = Y_0 - Y_{11} \quad (5.3)$$

when investigating the Class A disturbances, since both Y_0 and Y_{11} are of order unity. However, the Class B disturbances are generally located in the neighborhood of the poles of Y_{11} so that in this case, it is more useful to consider

$$\mathcal{E} = \mathcal{E} = Y_0 / Y_{11} - 1 \quad (5.4)$$

or alternatively, the difference in impedances

$$\mathcal{E} = \Delta Z = Y_0^{-1} - Y_{11}^{-1} \quad (5.5)$$

In general, (5.4) is preferable to (5.5) since it may also be used for computations of the Class A waves. It goes without mentioning that these functions all have the same desired roots, so that the manipulations can be regarded as a readjustment of the topology near these roots.

Furthermore, it is desirable to consider only analytic functions of the admittances, since they are in general analytic functions of c . Thus, it is wise to reject such non-analytic relations as

$$\mathcal{E} = (Y_0 - Y_{11}) / |Y_{11}| \quad (5.6)$$

although it might work in some cases.

If both \mathcal{E} and c were real, the eigenvalue problem would degenerate into a trivial exercise of finding the roots of a real function, as illustrated in Figure 6. There are several well-known techniques for determining the roots of functions using numerical methods. Only the simplest of these methods can be generalized for complex variables.

Landahl (1964) discusses in detail the effect of

the location of the zeros of a complex function $\mathcal{E}(c)$ on the form of the curve $c_i = 0$ in an Argand diagram of \mathcal{E}_i vs \mathcal{E}_r . (As before, subscripts r and i refer to the real and imaginary parts, respectively, of a complex variable.) By correct interpretation of these curves, Landahl is able to evaluate the marginal stability of dynamic systems. The basic idea of this technique can be used to great advantage in this problem.

In Figure 7, an example of this Argand diagram is shown for a case of a boundary layer over a compliant boundary. The loci plotted are for constant real and imaginary parts of c on an $\mathcal{E}_r, \mathcal{E}_i$ plot for Figure 7(a), and the real and imaginary parts of \mathcal{E} on a c_r, c_i plot in 7(b). The zeros of this function are well separated, and the diagram is detailed only for the sheet on which the zero at $c = 0.87 - 0.06i$ lies. A branch point is observed near $c = 0.72 - 0.01i$. The important feature is that in the neighborhood of the zero, $\mathcal{E}(c)$ is single-valued, and the branch points indicated on the sketch correspond to saddle points in the c plane. The existence of these saddle points can cause some numerical difficulties, as is discussed in the next section.

5.2 The Inverse of the Eigenvalue Criterion

While the method mentioned in the preceding section is useful for locating one or two eigenvalues, it does not provide the most efficient procedure for use in an automatic, numerical computation, because of the human judgment that must be provided to make it successful. It does provide a useful technique for making estimates of the initial locations of eigenvalues, and also suggests a basis for a more refined technique to perform the actual computations.

In the neighborhood of an isolated zero, the simplest form of the eigenvalue criterion is

$$\mathcal{E}(c) = g(c)(c - c_e) \quad (5.6)$$

where $g(c)$ is a slowly varying function of c in the neighborhood of the zero, c_e . One can approximate $g(c)$ by $g(c_e)$ so that

$$\mathcal{E}(c) \approx A + Bc \quad (5.7)$$

Two estimates of the eigenvalue, c_1 and c_2 are sufficient to determine the constants A and B so that the next estimate c_3 can be made.

$$c_3 = -\frac{A}{B} = \frac{c_1 \mathcal{E}(c_1) - c_2 \mathcal{E}(c_1)}{\mathcal{E}(c_1) - \mathcal{E}(c_2)} \quad (5.8)$$

The value of the criterion at c_3 is then calculated. If it is within tolerance, then $c_3 = c_e$. If not, then one must determine whether it is a better estimate than c_1 or c_2 . If it is not, further computation is useless with this method. The third estimate generally is better than one of the first two.

One can proceed by using c_3 and the better of c_1 and c_2 to calculate a fourth estimate, and so on until the evaluated $\mathcal{E}(c)$ is within tolerance.

It should be recognized that this method discards the results of previous calculations and thus does not proceed in the most efficient manner. It would be better if all preceding estimates could be used in making the next estimate. The use of three points requires the assumption that

$$\mathcal{E}(c) = A + Bc + Dc^2 \quad (5.9)$$

which corresponds to the following form for $\mathcal{E}(c)$

$$\mathcal{E}(c) = g_1(c)(c - c_{e1})(c - c_{e2}) \quad (5.10)$$

However, there are two solutions to (5.9), and these solutions are not complex conjugates since in general (5.9) has complex coefficients. Thus there is no criterion to determine which of these solutions is the desired eigenvalue.

It is at this point that a simple observation can be made; namely, that the inverse function $c(\mathcal{E})$ is simpler to solve than any general function $\mathcal{E}(c)$, and is as easy to evaluate. By inspection of Figure 7, it is seen that the possibility exists that $c(\mathcal{E})$ may be double-valued, but for the bulk of calculations of interest, it behaves locally as a single-valued function. Then it is of interest to consider the inverse of the eigenvalue criterion

$$c = c(\mathcal{E}) \quad (5.11)$$

and the associated eigenvalue

$$c_e = c(0) \quad (5.12)$$

If there are k estimates for the eigenvalue, then the next estimate may be found by the use of the Lagrangian interpolation formula

$$c_{k+1} = \sum_{e=1}^k c_e \prod_{\substack{j=1 \\ j \neq e}}^k \left(\frac{-\mathcal{E}_j}{\mathcal{E}_e - \mathcal{E}_j} \right) \quad (5.13)$$

There is no ambiguity about branch points with this form of higher order curve fitting, but it must be stressed that this technique will work only when the eigenvalues are well separated and the actual branch point is removed from both eigenvalues. If the eigenvalues are located close together, one can still use (5.9) as the basis for an estimate, and it should work quite well, except for the possibility of jumping from one eigenvalue to the next on successive estimates.

It should be noted that (5.9) would be of little use for the configuration shown in Figure 7, for which the branch point is remote from a zero of $\mathcal{E}(c)$. It should also be stressed that if an estimate from (5.13) is in the neighborhood of the branch point, then this procedure also will fail. In general, however, when two roots are located close together, the physical situation is very unstable, and the entire configuration would probably be rejected if the desired goal is to find boundaries with improved stability characteristics. If a thorough investigation of the instability is needed, it can be found manually, by the techniques outlined in Landahl's paper and in Section 5.1.

It is generally found that proper convergence can be obtained with three to four estimates using this method, whereas it takes nearly a hundred calculations to map out Figure 7 and on the average, five to six using formula (5.8).

5.3 Calculation of the Group Velocity

The computation of the spatial amplification rates by Gaster's transformation (2.41) requires the knowledge of the group velocity defined in (2.42). This necessitates a numerical differentiation, one of the most inaccurate numerical operations.

However, in this problem, $c_r(\alpha)$ is a very well behaved function, so that generally the differentiation proceeds without too much difficulty. The technique used first replaces the values of c_r with those found by a least squares fit of a quadratic through seven neighboring points. The original eigenvalues are retained in performing the fit and the new values substituted only after those points are no longer needed to calculate the other smoothed points. The values of these new points are given in Table 5.1 for the case of equally-spaced abscissas.

After the function is smoothed in this manner, a standard difference formula is used to compute the derivatives, using central differences where possible. In these formulas, x_i represents the abscissa, y_i the ordinate, and the points are numbered consecutively from 1 to N. In practice, these formulas are modified to handle unequally-spaced abscissas, but the calculations were generally performed for equal intervals of α . The spacing is indicated here by h.)

The differentiation formulas are

$$y'_i = \frac{1}{2h} (-y_i + y_{i+1}) \quad (\text{interior point})$$

$$y'_1 = \frac{1}{2h} (-3y_1 + 4y_2 - y_3) \quad (\text{first point})$$

$$y'_n = \frac{1}{2h} (y_{n-2} - 4y_{n-1} + 3y_n) \quad (\text{last point})$$

$$y_{1_{LS}} = \frac{1}{42}(32y_1 + 15y_2 + 3y_3 - 4y_4 - 6y_5 - 3y_6 + 5y_7)$$

$$y_{2_{LS}} = \frac{1}{42}(15y_1 + 12y_2 + 9y_3 + 6y_4 + 3y_5 + 0y_6 - 3y_7)$$

$$y_{3_{LS}} = \frac{1}{42}(3y_1 + 9y_2 + 12y_3 + 12y_4 + 9y_5 + 3y_6 - 6y_7)$$

$$y_{i_{LS}} = \frac{1}{42}(-4y_{i-3} + 6y_{i-2} + 12y_{i-1} + 14y_i + 12y_{i+1} + 6y_{i+2} - 4y_{i+3})$$

$$y_{N-2_{LS}} = \frac{1}{42}(-6y_{N-6} + 3y_{N-5} + 9y_{N-4} + 12y_{N-3} + 12y_{N-2} + 9y_{N-1} + 3y_N)$$

$$y_{N-1_{LS}} = \frac{1}{42}(-3y_{N-6} + 0y_{N-5} + 3y_{N-4} + 6y_{N-3} + 9y_{N-2} + 12y_{N-1} + 15y_N)$$

$$y_{N_{LS}} = \frac{1}{42}(5y_{N-6} - 3y_{N-5} - 6y_{N-4} - 4y_{N-3} + 3y_{N-2} + 15y_{N-1} + 32y_N)$$

Table 5.1. Least-Square Curve Fitting

5.4 Prediction of the Eigenvalues

The root-seeking techniques discussed in Sections 5.1 and 5.2 will work only when provided with at least two initial estimates as to the location of the eigenvalues. It is clear from that discussion that these estimates need to be reasonably near the actual root so that the possibility of finding an estimate on another sheet is reduced.

Usually, an educated guess is sufficient for the location of the first eigenvalue sought. The computer is programmed to go on to the next desired value of α at a fixed R . The eigenvalue last calculated is used as a first estimate of the location of the next eigenvalue, while a small constant is added to provide the second estimate. After two roots have been found, they are extrapolated to give an estimate for the next value of α and at this first value of R , this small constant is added to give a second estimate. This prediction process proceeds using as many previous estimates as are available for that value of R .

As the computation moves to a new value of R , prediction becomes available now from extrapolation on R and α . One new estimate for the second Reynolds number considered is the root at the same α with a small constant added to bring it closer to the values expected at the new R . The prediction then proceeds as in the preceding paragraph. At the third and subsequent value of R , the extrapolation can be attempted for both α and R .

Although the results of an extrapolation can often be inaccurate, it is sometimes found in this problem that one of the two initial estimates is within tolerance. If not, the third estimate generally is within tolerance, except in certain exceptional cases where the topology of the inverse eigenvalue criterion becomes more complicated as the calculation proceeds. Generally though, this process of using all

of the previously determined information about the stability loci helps to shorten considerably the time needed to locate a total stability diagram, and is an important feature of the efficiency of the root-seeking technique.

Chapter 6

STABILITY OF A LAMINAR BOUNDARY LAYER OVER A RIGID SURFACE

6.1 Eigenvalues for the Blasius Boundary Layer

The numerical techniques described in the preceding sections were first used to calculate the eigenvalues for the Blasius boundary layer over a rigid surface. This selection was the obvious one because of the abundance of both theoretical and experimental studies of this configuration. Using the general formulation of the boundary conditions for flow over a general flexible surface by means of the traveling wave admittances, it is seen that this case is a simple specialization, and can be used to verify the numerical techniques and results.

The boundary conditions at a rigid surface are that both tangential and normal velocities vanish at the boundary. Since Y_{12} then vanishes, Equation (2.29) can be simplified to

$$\Phi'_w + \frac{\bar{U}_w'}{c} \Phi_w = 0 \quad (6.1)$$

The boundary-layer admittance Y_0 is then simply

$$Y_0(\alpha, c, R) = \frac{-\alpha^2 R \Phi_w}{\Phi_w'''' - \alpha^2 \Phi_w} \quad (6.2)$$

The eigenvalue criterion is then that Y_0 vanishes. This occurs for

$$\Phi_w = \Phi'_w = 0 \quad (6.3)$$

Equation (6.3) is exactly the condition that the velocity perturbations vanish, so the boundary conditions are exactly the same as those normally considered. It is felt that this formulation has distinct advantages over the approach taken by Kurtz (1962) wherein pressure infinities are sought. There is no difference in results, but the restoration of the usual boundary conditions is comforting.

The values of the velocity profile $\bar{U}(y)$ and $\bar{U}'(y)$ were made available for the numerical integration in the form of a table containing the computed values at every integration station. This table was prepared from a direct numerical integration of the Blasius differential equation.

The eigenvalues were located using the techniques described in Chapter 5. It generally took less than five tries to locate an eigenvalue, and three were usually sufficient when enough previous points were located to attempt an intelligent prediction of the eigenvalue at the point under consideration.

In Figure 8, the loci of constant c_r and c_i are presented on a conventional α, R plot. In this presentation, the abscissa is the Reynolds number based on boundary-layer thickness δ , as defined by (2.10), and the ordinate is the dimensionless wave number α . In all of these computations, α is regarded as a real parameter.

Figure 8 is limited to the following range of α , R .

$$1000 < R < 5000 \quad (28000 < R_x < 695,000)$$

$$0 < \alpha < 1.4$$

It is felt that in this range, the significant amplification occurs, and it is this range that is influenced significantly by compliant boundaries. Although it is not evident from

Figure 8, both the loci of c_i and c_r are double-valued in α . The c_i curves form open loops at high R (as is seen from the drawing) and the c_r curves form loops open at low R . All computations that yielded Class A waves (Tollmien-Schlichting waves) for the Blasius boundary layer never showed a value for c_r that exceeded 0.51. It is observed that this is slightly beneath the point in the velocity profile for which \bar{U}'''' is a minimum, which corresponds to the point of maximum production of vorticity by the mean flow. (For a parallel flow, \bar{U}' corresponds to the vorticity and \bar{U}'''' is the Laplacian of the vorticity, analogous to a vorticity source term.) This is merely an observation and no reason has been determined as to why the Class A wave speed should be bounded by this value.

Using the results of Section 2.6, one can compute the spatial amplification rates $\alpha_i \omega / U_0$, which are presented in Figure 9. The ordinate of this figure is now the dimensionless frequency of the disturbance $\omega_r (\omega_* \omega / U_0^2)$. The justification that this is the most significant form of the results is implied in Section 2.2, for it is this form alone which has no reference to the growth of the boundary layer for the semi-infinite flat-plate problem. The spatial amplification rates were computed using the group velocity as described in Section 5.3.

It is noted that the curves of constant α_i are closed, and reach a maximum value on the figure.

$$\frac{\alpha_i \omega}{U_0} = -7.5 \times 10^{-6} \quad \text{at} \quad \begin{cases} R = 3500 \\ \omega_r = 95 \times 10^{-6} \end{cases}$$

This maximum considered together with the critical Reynolds number

$$R_c = 1804. \quad \alpha_c = 1.1.$$

might be regarded as providing a simple measure of the stability of the boundary layer.

However, when considering the effect of the compliant boundary on the stability of the laminar boundary layer, it is found that there is no simple measure of the stabilizing (or destabilizing) influence of the boundary. For this reason, it is felt that Figure 9 in its entirety provides the best means of comparison of the effectiveness of compliant boundaries in altering the stability of the system, and that any other presentation contains less significant information about the stability. Since the conventional α, R plot is so well known and understood, this will always be shown for comparison purposes.

6.2 Comparison of the Stability of the Blasius Boundary Layer with Experiments and with other Theories

It is traditional to compare the results of new calculations with previous work done in the same area, and this paper is no exception. In Figure 10, a summary of this comparison is given. Selected points from the neutral curves of other authors are plotted on the α, R plane. The results of Lin (1945) and Schlichting (1935) are analytical results based on the asymptotic solutions of (2.8). (By analytical it is meant that they are based on analytical, not numerical solutions of the Orr-Sommerfeld equation.) The other authors all used solely numerical techniques and were selected because they represent recent significant contributions to the knowledge of these eigenvalues.

A detailed comparison of the results shows general agreement on the location of the lower branch of the neutral curve but a wide discrepancy in the neighborhood of the critical Reynolds number. In this region there is satisfactory agreement between the present results and those found by Kurtz and Crandall (1962) and Brown (1959). Since the other

authors generally used the displacement thickness as their length scale, alternative scales based on displacement thickness are provided along the edges of the figure. The numerical factor relating the Reynolds number and wave number is given by

$$\delta = 3.5 \delta^*$$

to the accuracy of the sketches.

It should be noted that there is general disagreement as to the location of the upper branch of the neutral curve at the low Reynolds presented in this figure. In Brown's report where a comparison is made of several solutions of an earlier vintage, the same feature is obvious. At the present time, there are several solutions that yield distinct upper branches at these Reynolds numbers. The present calculations yield an upper branch that lies slightly below the other calculations and slightly above the experimental points.

Part of this comparison is detailed in Figure 11, which presents the neutral curve in the ω_r , R plane. Neutral curve measurements by Schubauer and Skramstad (1947) are presented on the same figure. It is seen that there is excellent agreement on the location of both the upper and lower branches for Reynolds numbers in excess of 2500. At lower values of R, there is considerable scatter in the experimental results, and several points were observed at frequencies higher than those predicted by the present calculations. It must also be mentioned that the data was taken from a small figure in their report, and some inaccuracies might have resulted in the transfer, perhaps requiring a fourfold increase in the diameter of the experimental "points."

It is not felt that the low Reynolds number discrepancies cast doubt on the numerical results in this area. The experimental error can be very high for measurements of this kind at such low values of the Reynolds number. In the region of the minimum critical Reynolds number, the slope of

the streamlines is of order 0.01. From the other information available in their report, one can deduce that the product of velocity and boundary layer thickness at the critical Reynolds number is

$$U_0 = 0.328 \text{ ft}^2/\text{sec}$$

For the low air speed of 32.8 ft/sec, a boundary-layer thickness of 0.12 in. would be observed. A hot wire of 0.001 in. would occupy about one per cent of the velocity profile, which is roughly the same ratio as the streamline slope. Thus the relative position of the hot wire would have to be determined to within a wire diameter as the wire is traversed downstream. If the wire is located in the region of the fluctuation profile where u' is decreasing with distance from the wall (past the maximum of the fluctuation) and the wire is not properly positioned to account for boundary-layer growth, an apparent amplification might be measured, while on the other side of the maximum, an apparent damping might appear. These effects are suggested in (2.43) as an apparent error term in the determination of spatial amplification from parallel flow theory. Both calculated and measured disturbance distributions show that there is a very rapid variation in the neighborhood of the maximum. (See Figure 14).

While it cannot be determined from the description given in their report, at which location in the profile the experimental measurements were made, to locate a neutral disturbance Schubauer and Skramstad would have to traverse the wire several inches downstream to get a measurable change in amplitude. During this traversal, the wire would have to be accurately positioned upward a distance of the order of the wire diameter to achieve the same similar distance from the surface. It is not clear that any amplification or decay

measured under these difficult experimental conditions can be solely attributed to parallel flow amplification or boundary-layer thickening. Later measurements at Reynolds numbers for which the boundary-layer growth is not as rapid do not exhibit this discrepancy, as shown in the next section.

6.3 Calculation of Spatial Amplification

In their report, Schubauer and Skramstad performed some calculations to deduce the conventional amplification rates c_i (see their Fig. 28). These, and the corresponding theoretical predictions are presented in Figure 12 plotted versus α for two values of the Reynolds number. It is seen here that the agreement between theory and experiment improves as the Reynolds number is increased, with almost perfect agreement for a Reynolds number of 7702.

From the description given in their report, there seem to be two sources of inaccuracies in the reduction of the experimental data. The first source of difficulty is performing the measurements at low Reynolds numbers, as discussed in the last section. The second is more basic as regards their use of the measured phase speeds to transform the measured spatial amplification to c_i .

As explained in Section 2.6, the group velocity should be used for this transformation. However, the group velocity cannot be measured directly and although it is possible to measure the phase speed c_r as a function of α , the wave length of a constant frequency disturbance changes so rapidly with Reynolds number, that a derivative of experimentally determined values measured under these conditions would be very inaccurate. The difference between the phase and group velocities at the higher of these two Reynolds numbers is less than 15%. However, the agreement between these two curves is exact for all practical purposes,

and the reason for this exact agreement must be regarded as unknown.

An added check on the validity of these results was made from an earlier figure in their report (Fig. 23). In this figure, Schubauer and Skramstad presented actual measured spatial amplification, in other words their raw data. An attempt was made to duplicate the experiment on the computer by using (2.41) and (2.43) to calculate amplification rates and amplification from the computed eigenvalues.

The results of this calculation are presented in Figure 13 and are compared to selected experimental points. The experiment consisted of vibrating a ribbon at a fixed frequency $\omega_* \nu / U_0^2$ (listed on the right of the figure) and measuring the amplitude of the disturbance at several downstream locations. The theoretical points were determined from the area under a curve of $\alpha_i \nu / U_0$ versus R^2 for constant frequency. There was excellent agreement for all values checked, even those that do not appear on the figure.

The agreement between these results leaves no doubts that the observed phenomena were those described by the theory of stability of parallel shear flows, and that the accuracy of these calculations is high when compared to these experimental results. Furthermore, since of all available theories, these computations yield the lowest value for the location of the upper branch of the neutral curve, and since the experimentally determined upper branch is at most only slightly lower than that predicted by these calculations, it is felt that they are inherently more accurate than preceding work.

6.4 Stability of the Boundary Layer under an Adverse Pressure Gradient

As a further example of the stability of the boundary layer over a rigid surface, a similarity profile representing a boundary layer in an adverse pressure gradient was selected. The velocity profile used was one of the Falkner-Skan family of similarity solutions for an external velocity proportional to $x^{-0.05}$. A sketch of this profile and its second derivative appears in Figure 15. An inflection point appears in the profile for $y = 0.255$ at a mean velocity of 0.41.

It is felt that a similarity solution represented a more meaningful example than a profile from the Karman-Pohlhausen family (for instance) since the similarity solution satisfies the boundary-layer equations and thus has a more accurate representation for its second derivative, whereas an approximate solution usually satisfies only some integral of the boundary-layer equations and thus can present inaccurate second derivatives. Of course, a calculation on any desired profile could be performed with an expenditure on the order of three to five minutes on the computer to completely map out the eigenvalues.

The two stability loci appear as Figures 16 and 17. Figure 16 presents the loci of constant phase speed on the α , R diagram, while Figure 17 presents the more meaningful ω_r , R plot.

Comparisons with the zero pressure gradient case show that amplification rates, phase speeds and frequencies are higher for the adverse pressure gradient, and that the critical Reynolds number is decreased. Thus by any criterion, an adverse pressure gradient is clearly destabilizing. Furthermore, it must be recognized that the frequencies, spatial amplification rates and phase speeds are independent of the choice of length scale used, although it is felt that this length scale

corresponds to the same boundary-layer thickness used before.

It should be stressed that the decrease in critical Reynolds number tells only a small part of the destabilizing influence of the adverse pressure gradient, and the magnitude of the total destabilization can only be determined by a complete comparison of Figure 17 with Figure 9. Although conclusions as to relative stability are easy to draw in this example, the same conclusions are seldom as clear cut for the examples of compliant boundaries.

Chapter 7

STABILITY OF THE LAMINAR BOUNDARY LAYER OVER SELECTED COMPLIANT BOUNDARIES

7.1 The Three Classes of Disturbances

As mentioned in the Introduction, one expects three possible types of disturbances to arise when investigating the stability of the laminar boundary layer over compliant boundaries. The first of these disturbances is named Class A, and is essentially a Tollmien-Schlichting wave modified by the presence of the compliant boundary. It is observed that the amplification of this class of disturbances is moderately influenced by variations of the type of boundary considered and the parameters of the boundary. Since a rigid surface is the limiting case of an arbitrarily stiff compliant boundary, the Class A eigenvalues approach those of the rigid surface as the stiffness is increased. Thus the results of this chapter should always be compared to the corresponding situation for a rigid surface; namely, the discussion of the Blasius boundary layer presented in the last chapter.

When it is said that the Class A eigenvalues are only moderately sensitive to variations of the surface parameters, it is only by comparison with the behavior of the other two types of possible eigenvalues. The Class B disturbances are waves that exist principally in the boundary, influenced (and excited) by the presence of the boundary layer. They generally occur for higher values of both α and c than do the Class A waves. The investigations to date generally reveal pairs of Class B disturbances, one that has always been observed to be damped in time traveling upstream, and a downstream moving wave that may be either amplified or damped, depending upon the parameters of the problem. Hains (1963) calculated unstable upstream traveling Class B dis-

turbances for the Poiseuille flow over membrane boundaries, but these always seemed to occur for unrealistic choices of physical parameters.

In these investigations, the parameters were selected with the aim that they represent a realistic range of values that might be anticipated for a boundary layer of water traveling over a boundary with properties similar to those of a rubber mat. While no attempt was made to perform an exact physical modeling, it is expected that the range of parameters investigated will not produce misleading results. In particular, when a four parameter surface is studied, all four parameters are selected to have realistic, non-zero values as might be found in the laboratory. The price that is paid is the neglect of interesting but unrealistic results that some investigators have observed.

It is for this reason that no Class C disturbances are presented as numerical results. Class C disturbances were found for very compliant surfaces when the restoring forces in the boundary were insufficient to maintain an undamped oscillation. The amplification rates for these disturbances were observed to be quite high and appeared to arise from a merger of the Class A and Class B disturbances.

This conclusion was reached from the circumstances under which these Class C disturbances appeared. All of the calculated Class C waves were found in the search for Class A disturbances. It was noted that the wave speeds were high compared to the other Class A waves found, and at first they were thought to be Class B disturbances. However, the amplification rates were much higher than either Class A or Class B amplification rates. All of the disturbances found in this family were unstable and there was no apparent dependence of the amplification rates on the wave number. Furthermore, the flexibility of the membranes for which these disturbances appeared was very high which, together with the other observa-

tions, tends to support their classification as Class C disturbances. No stability boundaries could be presented for these disturbances since no neutral disturbances were located. It was also observed that small changes in the damping had negligible influence on the stability of these eigenvalues, as predicted by Landahl (1962).

In the following sections, the results of some sample calculations of eigenvalues of Classes A and B are presented for two types of compliant boundaries. The important features of these disturbances are discussed, including the spatial amplification rates, oblique disturbances, and the effect of the compliant boundaries on the group velocity of the waves.

7.2 Effect of a Membrane on Boundary-Layer Stability - Class A Waves

A desired goal is to design boundaries that will delay the transition of the laminar boundary layer. Thus interest focuses on the influence of the compliant boundary on the Class A disturbances which appear to lead to the transition of the boundary layer over a rigid surface. In this section, the effect of the type of membrane discussed in Section 3.2 is considered. The parameters describing the physical properties of the surface were varied with Reynolds number in the manner specified in Section 2.2, and were selected as representative of the range of values expected to be physically significant.

In Figure 18, the influence of disturbance propagation speed c_0 (in vacuum, as is sometimes described) of the membrane is presented. The true extent of the effect of the boundary, and the variation of its parameters is best illustrated on an ω_r, R plot. As the wave speed c_0 is decreased, the neutral curve gradually shifts to lower frequencies. The slight increase in critical Reynolds numbers is not due to the

wave speed c_0 , for it is noted that when c_0 is decreased from 0.90 to 0.80, the critical Reynolds number decreases slightly. Thus the chief effect of this wave propagation speed is to reduce the frequency of the band for which instabilities occur.

As additional calculations were made at values of c_0 lower than those shown on Figure 18 (with the other parameters held fixed), it was observed that other types of disturbances appeared. Thus, for this example of a relatively compliant boundary, the range of c_0 over which an improvement in stability characteristics was noted was from infinity down to about 0.75. Below this value (for this surface) other types of disturbances became unstable, so the question of the Class A waves becomes moot. In general, wave speeds on the order of unity had the most significant effect on reducing the frequency of the unstable disturbances.

The influence of the cutoff frequency ω_0 can be discussed in the light of the results presented in Figure 18. The inclusion of ω_0 reduces the compliance of the membrane at low wave numbers, for which a simple, infinite membrane is obviously unstable (i.e., $\alpha = 0$ is the only member of the discrete eigenvalue spectrum for an infinite membrane). It further causes a decrease in compliance at lower Reynolds numbers by (2.16). Its only dynamic effect is to add dispersion to the membrane by increasing the effective wave speed to $\sqrt{c_0^2 + \omega_0^2/\alpha^2}$. Thus it is desirable to keep the cutoff as low as possible (but a zero value is unrealistic) so that the frequency band of instability can be brought to lower values. A constant value of $\omega_0 = 0.10$ at $R_0 = 5000$ was used throughout the calculations, corresponding to a dimensionless frequency $\omega_0 \nu / U_0^2 = 20 \times 10^{-6}$. This might seem a low frequency but for a 30 ft/sec boundary layer in water, corresponds to a cutoff frequency of about 300 c/sec, which is easily obtainable with known materials. Reductions below

this value have little effect on the stability of the Class A disturbances in these examples.

The most significant effect of the membrane on the critical Reynolds number is the relative value of the damping coefficient d , as shown in Figure 19. The value of the damping coefficient d varies with Reynolds number as shown in (2.15). Damping has an adverse effect on the stability of Class A waves in the sense that an increase in the value of the damping causes an increase in the extent of the unstable region, either in the width of the unstable frequency band or the unstable Reynolds numbers.

The example shown in Figure 19 is for a relatively stiff membrane, yet the effect is readily apparent, and becomes more pronounced as the compliance of the boundary is increased. The three neutral curves presented in Figure 19 illustrate the expansion of the unstable region very clearly for a variation in damping coefficient over three octaves. The case of zero damping is purposely not shown since it is felt that lack of dissipation would provide misleading results for a true physical situation; i.e., it is impossible to construct a boundary of this type free from dissipation.

It is difficult to describe with any measure of certainty what is meant by a value for d of 0.05, except some intuitive notion that it represents a small quantity, and one expects that the decay of disturbances in the boundary under vacuum conditions should be correspondingly small. For the membrane, it is unclear exactly what mechanism provides this damping or how to proceed to measure it. All that is certain is that it is present, and that it must be kept as small as possible.

The best description of the influence of compliant boundaries on the stability of the Class A waves is given in Figure 20. This figure presents the local spatial amplifica-

tion rate $\alpha_i \nu / U_0$ as a function of R^2 (which is proportional to x for the Blasius boundary layer, as discussed in Section 2.2). This curve is shown for constant frequency ($\omega_* \nu / U_0^2$) disturbances for a rigid surface and two membranes. It is derived by cutting a relief map of Figure 9 or 21(b) at constant frequency. The membranes cause not only a reduction of the distance over which the disturbance is amplified, but also a decrease at the magnitudes of the spatial amplification rates. The natural logarithm of the total amplification of this frequency is proportional to the area under one of these curves, as shown by (2.43).

It is also significant to note that the critical Reynolds number for these surfaces is actually lower at this frequency than for the rigid boundary, but that the total amplification is far less. This same type of phenomenon was noted by Karplus (1963) in his studies of transition of channel flow with membrane walls. In his report it is stated that for some cases, transition occurred earlier in the channel for the compliant boundaries than for the rigid boundaries, but that the level of the turbulence appeared to be lower. This indicates the same general trend, but should not be taken as a parallelism in view of the different physical circumstances investigated and the tentative nature of his results.

This phenomenon is a perfect example of misleading conclusions that might be drawn if the critical Reynolds number is the sole criterion of relative stability.

Figure 21 presents the details of the eigenvalues for one of the membranes shown. Only the Class A waves are shown in this figure, and the two presentations should be compared with Figures 8 and 9 to detail the differences caused by the compliant boundary.

7.3 Modifying the Membrane to Improve its Performance

Up to this point the effect of the mass per unit length parameter m has not been discussed for the membrane. This is because the mass is a "passive" parameter; i.e., its influence does not depend on the value of α or c . However, m itself must vary with R according to (3.7), which indicates a decrease in compliance at low values of the Reynolds number where the boundary layer is thinner. In view of the non-dimensionalization used, the choice of $m = 1$ at $R_0 = 5000$ should be justified. For a boundary layer moving at 30 ft/sec in water, if the membrane is composed of a material of twice the specific gravity of water, then it needs to be 0.01-inch thick to have this value for the mass parameter m . This is clearly possible to consider, but a final judgment of this model will be reserved until a realistic look at the dynamics of a better rubber surface model is taken (Section 7.6).

A simple technique for improving the performance of this membrane model for Class A waves involves the variation of the mass of membrane. One can make the parameter m in (3.7) independent of Reynolds number by "tailoring" the surface so that its moving thickness* (and thus its physical mass per unit length) varies in the same manner as the boundary-layer thickness. This technique makes the surface as compliant at low Reynolds numbers as at high values. The surfaces that were considered by Landahl (1962) should be considered as these "tailored" membranes.

In Figure 22 the effect of this "tailoring" is presented for a sample membrane. The advantage of maintaining the same low level of compliance at low Reynolds numbers is evident for R below the normalizing value R_0 , and of course the effect is reversed above R_0 . The tailoring has a favorable effect on the stability of the Class A waves, if

*This corresponds to an interpretation of the membrane as a thin coating on a spongy substructure (the spring) free to perform only vertical oscillations.

other parameters are held constant.

However, it might be difficult to maintain the other parameters constant while tailoring the mass of the membrane. Figure 23 shows the effect of a variation in the damping of the membrane. The stability boundaries are now radically altered by changes in the damping. Needless to say, the maintenance of low damping is more critical for the case of the tailored membrane, and since the damping is probably the most difficult property to specify, this method of improving the performance of the boundary for the Class A waves is not recommended. Furthermore, this type of tailoring can be expected to have an adverse effect on Class B waves. The very critical nature of the damping noted by Landahl (1962) was due to the fact that he used just this kind of surface model.

The locus of eigenvalues are shown only for c_r , c_i and should be compared to Figures 21(a) and 8. The loci in the ω_r , R plane can be deduced from Figures 22 and 23.

7.4 Class B Waves in a Membrane

The existence of other types of disturbances was predicted by Benjamin (1960) and some examples of these disturbances were found by Landahl (1962). These Class B disturbances are fundamentally different from the Class A disturbances. Undamped Class B waves appear only for very compliant boundaries, and the damping in the boundary tends to stabilize Class B disturbances.

Examples of Class B eigenvalues are shown in Figure 25 and can be compared directly to the corresponding Class A Waves. It is immediately apparent that Class B waves occur

at much higher values of both wave number and frequency than Class A waves, that the phase speeds are higher than the Class A phase speeds and decrease with wave number so that the group velocity is less than the phase velocity. The contour lines of constant c_i or α_i are more widely spaced for the Class B disturbances, but in this example, the critical Reynolds number of the Class B waves is greater, so that the amplification begins farther downstream than for the Class A waves. A small increase in the damping can be expected to move all unstable Class B waves off Figure 25, but this, of course, would have an adverse effect on the Class A waves. The biggest difficulty encountered in finding Class B disturbances is the determination of stability boundaries; either no unstable waves existed or the violently unstable Class C disturbances were found.

The results shown in Figure 25 differ markedly from those of Landahl (1962). The main reason for this difference is the interpretation of the Reynolds number in Section 2.2. As mentioned before, Landahl's dimensionless parameters are consistent with an interpretation of the variation in Reynolds number arising from varying ν , so that his surfaces were more compliant at lower values of R than are these membranes. The result is that at low values of R , both dimensionless m and d appear larger, which tends to delay the onset of unstable Class B waves.

As shown from the examples in Figure 19, it is possible to specify surfaces for which no unstable Class B waves could be found (they were sought for values of α up to 3, and no trend of instability was noted at even that large value of α).

The differences in the perturbation distribution for the two types of disturbances is indicated in Figure 26, while the difference in variation of phase and group

velocities is indicated in Figure 27. Comment on these two figures is reserved until a later section (Chapter 10).

7.5 Oblique Disturbances

In Section 2.5, the justification for consideration of two-dimensional disturbances was given by a detailed inspection of Squire's transformation (2.37). In view of the improved stability characteristics that have been found for the membranes under consideration, it is necessary to investigate the oblique disturbances to insure that they are not more unstable than the two-dimensional disturbances; thus partially negating these improvements.

If it is assumed that the tension in the membrane is uniform in all directions, the transformations given by (2.40) are valid and govern the variation of the two-dimensional parameters. In Figure 28 are shown the results of this calculation as a series of neutral curves for disturbances traveling at some angle Θ to the direction of flow. These should be compared to Figures 8 and 21(a). For this particular case, the two-dimensional disturbances happen to be most critical, but it is felt that this is fortuitous.

In Figure 29, the critical Reynolds number is plotted as a function of the angle of the disturbance. This is compared to the manner in which rigid surface critical Reynolds numbers vary with the direction of the disturbances, and with the variation of flexible surface critical Reynolds numbers if Squire's theorem were valid.

Thus, Figure 29 demonstrates that Squire's theorem is definitely invalid and that three-dimensional disturbances are unquestionably more important than they are in the rigid surface case. While this example does not indicate any oblique disturbance more unstable than the two-dimensional dis-

turbance, the possibility clearly exists.

Furthermore, this consideration need only apply to the Class A waves, for the oblique Class B waves are definitely more stable than the two-dimensional disturbances. This is because the membrane is less compliant for three-dimensional disturbances, as demonstrated in Section 2.5. In addition, the "tailored" membrane surface is probably more sensitive to oblique disturbances because of its extremely low compliance and because of its strong dependence on the damping.

It is clear that these three-dimensional effects are an important consideration to be studied before deciding whether any given model of compliant boundary will yield improved stability characteristics.

If a detailed analysis of the three-dimensional growth of an initial disturbance is considered in detail, as was done by Criminale and Kovaszny (1962), one would find that disturbances over a compliant boundary spread more rapidly in the third dimension than do those over a rigid surface. Furthermore, since the second order spanwise terms found by Benney (1961) have only small pressure perturbations associated with them, the present approach should provide a sufficient start for the more complete analysis of three-dimensional effects.

7.6 Effect of a Rubber Surface on Boundary-Layer Stability

Investigation of the rubber surface model discussed in Section 3.3 introduces a new degree of freedom into the motion of the compliant boundary; namely, the boundary is free to move in the tangential direction. It can easily be shown that tangential motion at the boundary does not alter the stability problem for the Class A waves to any significant degree. The analysis in Appendix A derives the asymptotic

solutions of the Orr-Sommerfeld equation given both tangential and normal admittances.

Since the spring-supported membrane was taken as a model for just this type of surface, it is not surprising that there are few differences in the effect of these models on the stability problem. Since the speed of compression waves is generally much higher than the shear wave propagation speed, the effect of the latter only is investigated in this section by regarding the compressive wave speed c_1 as infinite. The same reactions to variations of shear wave speed c_2 and damping d_2 are as evident for this model as for the membrane; namely, a decrease of c_2 reduces the frequency of the unstable region, and an increase in damping tends to cause the neutral curve to expand to lower R and higher ω (and α).

A significant difference noted in the rubber model is the absence of an explicit cutoff frequency and the presence of a length H . The effect of the thickness of the surface H on the neutral curve is shown in Figure 30. It is clear that surfaces thicker than the boundary layer have more favorable stability characteristics.

This result appears to contradict the interpretation of the "tailored" membrane given in Section 7.3, where it was assumed that the mass per unit length of the membrane was proportional to the thickness. However, the total moving mass of the membrane was assumed to be known, and the spring support had to be regarded as massless. In this case, since the bottom of the surface is constrained to have no vertical motion, the moving mass of rubber is in a thin layer near the top.

One can easily see that in the limit as the product αH approaches zero (i.e., zero thickness), the expressions for the admittances simplify to

$$\begin{aligned}
 Y_{11} &\rightarrow \frac{i c \alpha H}{\rho_s (c^2 - 2c_2^2)} \rightarrow 0 \\
 Y_{12} &\rightarrow \frac{c}{\rho_s (c^2 - 2c_2^2)}
 \end{aligned}
 \tag{7.1}$$

Since at $y = -H$ no vertical motion of the boundary was permitted, the normal admittance of the surface approaches that of a rigid surface, while the tangential admittance remains finite. The latter occurs because the lower surface could slide freely on the substructure (3.16).

Also note that wave propagation speed becomes non-dispersive as the "shallow" surface wave speed approaches twice the "deep" surface wave speed c_2 , in a manner analogous to water wave theory. It is readily seen that (7.1) are exactly the same as (3.26), the equations for the admittances of water of finite depth in the limit as $\alpha H \rightarrow 0$. It should be recalled that shallow water theory predicts a non-dispersive propagation of disturbances compared to dispersive deep water waves.

There is no simple analogy between deep water waves and the case of large thickness except the observation that for $H > 3$ thickness effects cease to be important. Furthermore, some numerical difficulty is experienced when (3.18) is used to calculate the admittances in the Class A wave regime when $r_2 \rightarrow 1$ ($c \ll c_2$). In this case, both numerator and denominator involve the difference of numbers close to unity, causing a bad numerical scatter in these admittances. In the absence of a simple limiting form that does not suffer from this numerical defect, double precision techniques should be used to numerically calculate the admittances for these limiting cases.

The behavior of the Class A disturbances for this surface model is different only in detail from those investigated in pre-

ceding sections. In Figures 31 to 34 examples of Class A response are shown. It should be noted that this behavior is reminiscent of the behavior of the "tailored" membrane surface of Section 7.3, rather than the dimensionally correct membrane model. However, damping is not as critical for these examples as it is for the "tailored" membrane. It should also be noted that the parameters are lower to achieve a comparable stabilizing effect on the boundary layer, which implies that the membrane model is inherently more compliant than the present model, and that the appearance of transverse admittance seems to cause a slightly destabilizing effect. This point will be discussed further in Chapter 10.

In Figure 34, the u velocity perturbations and Reynolds stresses are again plotted for the rubber surface model. Note that now the Reynolds stress does not fall to zero at the boundary since the boundary is free to move tangentially.

It should be stressed that the results presented are only as good as the model used to calculate them, and this model was selected mainly for convenience. These calculations should be repeated to determine the nature of the eigenvalues for more realistic models of actual design configurations, if that is the desired goal.

Chapter 8

JETS, WAKES, AND SHEAR FLOWS

8.1 Compliant Boundary Model for the Stability of Jets, Wakes, and Shear Flows

Apart from the use of the Orr-Sommerfeld equation there appears to be little similarity between the compliant boundaries investigated in the preceding sections and unbounded jets, wakes, and shear flows. Actually, the same techniques, including the same computer programs, can be used to analyze these seemingly different situations.

The point of similarity is quite simple. The unbounded flow is divided into two sections, one extending to $+\infty$ the other to $-\infty$. Either section can be regarded as a boundary layer (in the same sense that it has solutions that die off at ∞ , and must satisfy additional conditions at some finite point) and the other as a compliant boundary. If the mean flow is neither purely symmetric nor anti-symmetric, then the Orr-Sommerfeld equation must be satisfied in both sections, but there are important simplifications that can result when symmetry (or antisymmetry) exists.

One can regard the two sections of the shear flow as being separated by an imaginary membrane which is massless, infinitely flexible, and infinitely extensible. Across this imaginary boundary, there can exist no discontinuities in ϕ or its derivatives. Since there are three disposable constants in the system, the matching of ϕ , ϕ' , ϕ'' can easily be performed. However, ϕ''' will in general still be discontinuous, which gives a criterion analogous to \mathcal{E} in (2.33). The values of α , c , R for which the discontinuity in ϕ''' vanishes are eigenvalues of the problem.

8.2 Stability of Symmetric and Antisymmetric Profiles

There are significant simplifications that result in the analysis of stability of a symmetric or antisymmetric unbounded shear flow. In these cases, it is necessary to integrate only over one half of the profile and use symmetry to formulate the eigenvalue criterion.

In cases of this kind, one can investigate either symmetrical (varicose) or antisymmetrical (sinuous) perturbations. The sinuous disturbances are the most critical and are observed experimentally. For these disturbances, the following boundary conditions are satisfied at the plane of symmetry.

$$\begin{aligned}\phi_w' &= 0 \\ \phi_w''' &= 0 \quad Y=0\end{aligned}\tag{8.1}$$

For symmetric profiles, for which \bar{U}_w' vanishes, one can easily recognize the type of compliant surface that models these boundary conditions. Inspection of (2.29) reveals that setting $Y_{12} = 0$ will cause the first equation of (8.1) to be satisfied. With this simplification, (2.31) becomes

$$Y_0(\alpha, c, R) = -\alpha^2 R \phi_w / \phi_w'''\tag{8.2}$$

To satisfy the second equation in (8.1), one has a boundary model of zero normal impedance (i.e., an infinitely compliant surface or a free streamline) and yet of zero tangential admittance.

A suitable eigenvalue criterion for the symmetric case is then

$$E(\alpha, c, R) = Y_0^{-1} = -\phi_w''' / \alpha^2 R \phi_w = 0 \quad (8.3)$$

For antisymmetric profiles, the interpretation is not as simple, since $\bar{U}_w' \neq 0$. For this case one expects both Y_{11}^{-1} and Y_{11}^{-1} to vanish, corresponding to a free boundary, but both of these conditions are equivalent. Thus (8.1) itself is the only consistent technique to achieve this end, and one must recognize that this will also satisfy the requirements for a surface with no impedance.

8.3 Asymmetric, Unbounded Shear Flows

When there is no plane of symmetry, one needs to solve the Orr-Sommerfeld equation for the entire shear flow. This can be done by dividing it into two distinct sections, and performing the integration of the Orr-Sommerfeld equation separately for both sections. The results of these two integrations are four sets of complex numbers, two from the "upper" portion of the profile, and two from the "lower" portion, that are solutions of the Orr-Sommerfeld equation at $y = 0$ (with the correct asymptotic behavior as $y \rightarrow \pm \infty$).

Recognizing that the division of the profile into two sections was an artificial process which could have been done at any location in the profile, one cannot permit a discontinuity in the final eigenfunction ϕ or in any of its derivatives at the junction point.

This condition requires that for a continuous solution, the four sets of complex numbers cannot be independent. Labeling the upper portion a and the lower portion b, the eigenvalue criterion can be simply stated as

$$E(\alpha, C, R) = \begin{vmatrix} \phi_{1a} & \phi'_{1a} & \phi''_{1a} & \phi'''_{1a} \\ \phi_{3a} & \phi'_{3a} & \phi''_{3a} & \phi'''_{3a} \\ \phi_{1b} & \phi'_{1b} & \phi''_{1b} & \phi'''_{1b} \\ \phi_{3b} & \phi'_{3b} & \phi''_{3b} & \phi'''_{3b} \end{vmatrix} = 0 \quad (8.4)$$

It is obvious that when (8.4) is satisfied, if the upper portion is regarded as a boundary layer and the lower portion as a compliant boundary, both normal and tangential admittances will be matched.

This process is much less straightforward than the requirements of Section 2.3 and equation (2.31), for the admittance of the "compliant boundary" is dependent upon the actual solution in the boundary layer. In some respects, this problem is similar to that considered in Section 3.4, but the iterative analysis is made unnecessary by the existence of (8.4).

It should also be noted that both (8.4) and (8.3) may not be sufficiently normalized to permit a simple judgment of when the eigenvalue criterion is zero numerically. For use in an automatic root-seeking scheme, one needs to specify some size that is acceptable as zero. For the compliant boundary, this tolerance was small compared to unity. This is not always the case in these computations, as is discussed in the next section.

8.4 Stability of the Two-Dimensional Jet

Numerical results were obtained for the two-dimensional similar jet

$$\bar{U}(y) = \text{sech}^2(y) \quad (8.6)$$

which has also been investigated by Tatsumi and Kakutani (1958). This profile arose from a similarity solution of the boundary-layer equations, and is discussed in detail in the above reference.

The results of these calculations are presented in Figure 35. Since the computer programs were not originally written to perform this type of calculation, it is satisfying to note that the results appear consistent with those of previous investigators along the upper branch of the curve, even for low values of R .

There is some doubt as to the accuracy of the results for the lower branch because small errors in the initial conditions at $y = 1$ can cause large errors in the solutions for small values of α . It should be noted that \bar{U}_0 in (4.2) is now zero, so the initial integration step takes the solution from the asymptotic form of zero velocity and second derivative to finite values of both quantities. It is felt that this is a possible source of error for small values of α .

Initially, calculations were made for $\text{sech}^2(3y)$, and as $\alpha \rightarrow 0$, it was noted that αc approached a finite, negative limit. For high values of R , c_r is in the range of $\bar{U}(y)$, and this limit appears in error. More refined calculations of $\text{sech}^2(6y)$ and $\text{sech}^2(9y)$ show that the position of the zero crossing of c_r can be postponed to lower and lower values of α , but it was always observed to occur.

This error has three possible causes. The first, initial errors (which imply that the initial values do not represent solutions that decay as $y \rightarrow \infty$) are alleviated by moving the start of integration further out in the profile,

as discussed in the preceding section.

The second source of error might be the purification scheme, which is superfluous for small αR . To remove this doubt, cases were run with the purification scheme disabled, and no changes in eigenvalues were noted.

An additional source of error, and one that is very difficult to remove in the limited time available, was that mentioned at the end of the preceding section: namely, a satisfactory normalization of the eigenvalue criterion was lacking. Attempts were made to check this by tightening the tolerance as $\alpha \rightarrow 0$, but since it is essential to compute for as many values of R and α as possible to insure efficient use of the available computer time, both R and α usually were varied over several orders of magnitude. Thus the present location of the lower branch on Figure 35 must be regarded as tentative.

It is felt that these computations are in substantial agreement with those of Tatsumi and Kakutani (1958), within the limits imposed by their expansion technique, for points near the critical Reynolds number and, furthermore, give a more complete picture of the unstable region, including those frequencies that might be expected to appear in the natural transition of a two-dimensional jet.

Chapter 9

BOUNDARIES EXHIBITING A SPATIAL VARIATION OF PROPERTIES

9.1 Occurrence of Spatial Variation of Boundary Parameters

The simple models for compliant boundaries considered in Chapter 3 had one feature in common. This feature was that the parameters characterizing the dynamics of the boundary were not functions of position. The "tailored" membrane surfaces of Section 7.3 exhibited a variation in thickness of the same nature as the growth of the boundary layer, which is within the limits of this theory.

The reasons for this restriction are clear. The separation of variables used for the perturbation stream function (2.7) is valid only if the coefficients and boundary conditions of the Orr-Sommerfeld equation are independent of x . Equivalently, these sinusoidal traveling waves are solutions for the motion of a compliant boundary only if the coefficients in the equation for the boundary are independent of x .

However, the experimental configurations investigated by Kramer (1957) (1960) exhibited a periodic variation of the structure of the boundary with space. Other phenomena, such as panel flutter, are based on the ordinary construction practice of providing some extra support for the structure at regular intervals.

One must determine whether this spatial variation of the properties of the boundary have an important influence on the resultant stability problem. The possibility also exists of some kind of resonance phenomena between traveling waves in the boundary layer and the period structure of the boundary. This periodic structure will cause a coupling between wave numbers, thereby providing a linear mechanism for the transfer of

disturbance energy to adjacent wave numbers, and must therefore be carefully investigated.

The type of variation to be investigated in the following sections is a small sinusoidal perturbation in the stiffness and damping of the membrane model for the compliant boundary. This model should provide all the essential features of the influence of the periodic variation of properties, and still not introduce undue complications into the analysis.

The analysis used will take a slightly different approach to the stability problem than that of the previous sections. Since a pure sinusoidal wave is not in itself a solution of the equation of motion of the boundary, an expansion in terms of sinusoidal traveling waves will be sought. Because the problem remains linearized, one can still use every Fourier component of this expansion to provide a relationship between the pressure perturbation of the boundary layer and the motion of the boundary.

Thus the problem to be solved is the equation of motion of the membrane with periodic coefficients and a driving term caused by the pressure perturbations in the boundary layer. This should be compared to the approach taken in Section 2.3 in which the only reference to the dynamics of the boundary appeared in the boundary conditions of the Orr-Sommerfeld equation.

9.2 Membrane Supported by a Spring of Varying Stiffness

As an example of the analysis of a structure exhibiting a small sinusoidal spatial variation of properties, consider the membrane of Section 3.2 with the following changes

$$\omega_0^2 = \omega_1^2 + 2\epsilon \omega_2^2 \cos 2\alpha_0 x$$

$$d = d_1 + 2\epsilon d_2 \cos(2\alpha_0 x + \mathcal{K})$$
(9.1)

The first equation in (9.1) represents a small ($\epsilon \ll 1$) periodic variation in the stiffness of the supporting spring with a wavelength π/α_0 . It will be seen that the damping can be regarded as having a similar periodic variation, and allowance is made for an arbitrary phase lag \mathcal{K} between the damping and spring variations.

Since the solution of (3.4) for $\epsilon = 0$ are known to be sinusoidal traveling waves, the solution for $\epsilon \neq 0$ can be expanded about this known result. The factor of two in the argument of the cosine in (9.1) appears as a result of Floquet's theorem, quoted in Stoker (1950) and Morse and Feshbach (1953), which states that equations with coefficients periodic in 2π can have solutions periodic in either 2π or 4π . With this fact in mind, one seeks to expand the solution of (3.4) in the following form

$$\eta(x,t) = e^{i(\alpha x - \omega t)} \sum_{n=-\infty}^{\infty} \hat{w}_n e^{in\alpha_0 x}$$

$$p(x,t) = e^{i(\alpha x - \omega t)} \sum_{n=-\infty}^{\infty} \hat{p}_n e^{in\alpha_0 x}$$
(9.2)

where it is anticipated that the \hat{w}_n and \hat{p}_n are of higher order in ϵ than \hat{w}_0 , \hat{p}_0 , the solutions of the zeroth order problem.

It is also known from the discussion of Chapter 2 and the linearity of the problem, that each component \hat{p}_n is

related to each \hat{w}_n by the normal admittance of the boundary layer.

$$\hat{p}_n = i\omega \hat{w}_n Y_0^{-1}(\alpha + n\alpha_0, \omega) = i\omega Z_n \hat{w}_n \quad (9.3)$$

The interpretation of (9.3) is that Z_n is the Fourier transform of a Green's function relating the velocity of the wall ($-i\omega \hat{w}_n$) to the pressure (\hat{p}_n). The function Z_n can be regarded as a known function of (α, ω) for a given boundary-layer profile at a given Reynolds number. It is found in the manner described in Chapter 4.

Inserting (9.2) into (3.4), and using the new definitions given in (9.1), one arrives at the equation

$$\begin{aligned} & \sum_{n=-\infty}^{\infty} \left\{ [C_0^2 (\alpha + n\alpha_0)^2 - \omega^2 - i\omega d_1 + \omega_1^2 + \frac{i\omega}{m} Z_n] \hat{w}_n \right. \\ & + \epsilon \hat{w}_{n-2} [\omega_2^2 + d_2 e^{iKx}] \\ & \left. + \epsilon \hat{w}_{n+2} [\omega_2^2 + d_2 e^{-iKx}] \right\} e^{i(\alpha + n\alpha_0)x} = 0 \end{aligned} \quad (9.4)$$

Equation (9.4) is satisfied only if the coefficient of every component of the Fourier series is set equal to zero. This yields a three term recursion formula for \hat{w}_{n-2} , \hat{w}_n , and \hat{w}_{n+2} . It should be noted that the added terms are periodic in 2π (or rather π/α_0), since no reference to odd powers of ϵ appear for an expansion around $\epsilon = 0$.

The three term recursion formula of (9.4) can be solved by the following infinite determinant, analogous to Hill's determinant.

$$\begin{vmatrix}
 \vdots & \vdots & \vdots & \vdots & \vdots & \vdots & \vdots \\
 \vdots & \vdots & \vdots & \vdots & \vdots & \vdots & \vdots \\
 \dots & F_{-4} & -\epsilon H & 0 & 0 & 0 & \dots \\
 \dots & -\epsilon G & F_{-2} & -\epsilon H & 0 & 0 & \dots \\
 \dots & 0 & -\epsilon G & F_0 & -\epsilon H & 0 & \dots \\
 \dots & 0 & 0 & -\epsilon H & F_2 & -\epsilon H & \dots \\
 \dots & 0 & 0 & 0 & -\epsilon G & F_4 & \dots \\
 \vdots & \vdots & \vdots & \vdots & \vdots & \vdots & \vdots \\
 \vdots & \vdots & \vdots & \vdots & \vdots & \vdots & \vdots
 \end{vmatrix} = 0 \quad (9.5)$$

where

$$\begin{aligned}
 F_n &= C_0^2 (\alpha + n\alpha_0)^2 - \omega^2 - i\omega d_1 + \omega_1^2 + \frac{i\omega}{m} Z_n \\
 G &= \omega_2^2 + i\omega d_2 e^{i\chi} \\
 H &= \omega_2^2 + i\omega d_2 e^{-i\chi}
 \end{aligned} \quad (9.6)$$

One can approximate the solution of this determinant by the following sequence of equations

$$\begin{aligned}
 F_0 &= 0 \quad (\text{to order } \epsilon^2) \\
 F_0 - \epsilon^2 GH (F_{-2}^{-1} + F_2^{-1}) &= 0 \quad (\text{to order } \epsilon^4) \\
 F_0 - \epsilon^2 GH (F_{-2}^{-1} + F_2^{-1}) - \epsilon^2 GH \{ F_0 (F_{-2}^{-1} F_{-4}^{-1} + F_2^{-1} F_4^{-1}) \\
 + \epsilon^2 GH F_4^{-1} F_{-4}^{-1} (F_0 + F_2^{-1} + F_{-2}^{-1}) \} &= 0 \quad (\text{to order } \epsilon^6)
 \end{aligned} \quad (9.7)$$

The first equation in this sequence poses the same eigenvalue problem as (3.6), while the second equation provides the lowest order correction term that takes the periodic variation of the coefficients into account. Since the solution is aperiodic, the correction terms effect only those components with wave numbers differing by $2\alpha_0$.

Consider for the moment the same approach to the eigenvalue problem taken previously; namely, α is regarded as a real, fixed parameter and one attempts to find the complex frequency ω corresponding to this α . Solutions for ω can be found from the series

$$\omega = \omega^{(0)} + \epsilon^2 \omega^{(2)} + \dots \quad (9.8)$$

This expansion shows that the lowest order estimate $\omega^{(0)}$ can be found from

$$F(\alpha, \omega^{(0)}) = 0 \quad (9.9)$$

and the next estimate for the eigenvalue is found to be

$$\omega^{(2)} = \frac{GH(\bar{F}_2^{-1}(\alpha, \omega^{(0)}) + \bar{F}_2^{-1}(\alpha, \omega^{(0)}))}{\left(\frac{\partial F}{\partial \omega}\right)_{\omega = \omega^{(0)}}} \quad (9.10)$$

Succeeding estimates require the solution of a quadratic, but for small ϵ , (9.10) provides a sufficient trend. Thus, (9.10) demonstrates that the correction in the amplification rate $\hat{\omega}_1$ will be of order ϵ^2 for aperiodic solutions and can be found in a straightforward manner.

9.3 Parametric Resonant Conditions

When $\alpha = n\alpha_0$, a condition of resonance exists, and the assumptions made in the derivation must be carefully investigated. The reason for the caution is as follows. Because of the substitution of (9.1) into (3.4), and the insertion of a sinusoidal time dependence, one expects that the resultant equation can be transformed into Mathieu's equation (9.11), and that results analogous to those found from the stability of Mathieu's equation are valid.

$$f'' + (\gamma + \epsilon \cos 2\alpha_0 x) f = 0 \quad (9.11)$$

All of the critically stable solutions of (9.11) have an eigenvalue relationship similar to (9.10), except for the subharmonic resonant solution, which yields a correction proportional to $|\epsilon|$. The possible existence of such subharmonic solutions must be investigated for this case in which only periodic solutions are considered.

One seeks periodic solutions of (9.11) in the form

$$\begin{aligned} f &= f_0 + \epsilon f_1 + \dots \\ \gamma &= \gamma_0 + \epsilon \gamma_1 + \dots \end{aligned} \quad (9.12)$$

where

$$\begin{aligned} \gamma_0 &= n^2 \alpha_0^2 \\ f_0 &= \frac{\sin(n\alpha_0 x)}{\cos} \end{aligned} \quad (9.13)$$

One expects the correction in f to be expressible in a Fourier series, and to be found (along with the correction terms in γ) from a consistent expansion of (9.11) in powers

of ϵ . This is the approach described by Stoker (1950).

Starting from the basic solutions in (9.13), one requires that the corrections also be periodic in π/α_0 or $2\pi/\alpha_0$, which will determine the lowest order correction to γ . The criterion for all of the corrections is that a solution that grows in a manner proportional to x is excluded. For instance, the expansion of the cross terms for $n = 1$ are

$$\begin{aligned} \cos \alpha_0 x \cos 2\alpha_0 x &= \frac{1}{2} (\cos \alpha_0 x + \cos 3\alpha_0 x) \\ \sin \alpha_0 x \cos 2\alpha_0 x &= \frac{1}{2} (-\sin \alpha_0 x + \sin 3\alpha_0 x) \end{aligned} \quad (9.14)$$

Writing the expansion of (9.11) to order ϵ , to get the basic equation for f_1 , one finds

$$\begin{aligned} f_1'' + \alpha_0^2 f_1 &= -\frac{1}{2} (\cos \alpha_0 x + \cos 3\alpha_0 x) - \gamma_1 \cos \alpha_0 x \\ \text{or} \\ f_1'' + \alpha_0^2 f_1 &= -\frac{1}{2} (-\sin \alpha_0 x + \sin 3\alpha_0 x) - \gamma_1 \sin \alpha_0 x \end{aligned} \quad (9.15)$$

from which the first-order correction for γ can be found by excluding secular growth of f_1

$$\gamma_1 = \pm 1/2 \quad (9.16)$$

For all other basic solutions ($n \neq 1$), γ_1 vanishes. Thus, it is only for the subharmonic response of Mathieu's equation that the perturbation in the eigenvalue is of order ϵ .

By appropriate manipulation, equation (3.4) can be written in the following form

$$f'' + [\gamma + \epsilon(k_1 e^{2i\alpha_0 x} + k_2 e^{-2i\alpha_0 x})]f = -g(x) \quad (9.17)$$

where

$$k_1 = (\omega_2^2 + i\omega d_2 e^{i\omega t}) / c_0^2$$

$$k_2 = (\omega_2^2 + i\omega d_2 e^{-i\omega t}) / c_0^2$$
(9.18)

$$\gamma = (\omega_1^2 - i\omega d_1 - \omega^2) / c_0^2$$

and $g(x)$ represents the pressure excitation from the boundary layer

$$g(x) = p(x) / m c_0^2 \quad (9.19)$$

The pressure term is completely determined by the motion of the boundary in the following form

$$g(x) = \int_{-\infty}^x f(x-\xi) G(\xi) d\xi \quad (9.20)$$

where $G(x)$ has as its Fourier transform, the impedance of the boundary layer. Thus (9.17) and (9.20) are in the form of a modified Mathieu equation with an integral of the Volterra type over a known kernel; i.e., an integro-differential equation.

The solutions derived in the last section are found

directly from the Fourier transform of (9.17), and will yield the same eigenvalue problem for $n > 1$.

Applying Stoker's technique to (9.17), one defines

$$f = f_0 + \epsilon f_1 + \epsilon^2 f_2 + \dots \quad (9.21)$$

$$\gamma = \gamma_0 + \epsilon \gamma_1 + \epsilon^2 \gamma_2 + \dots$$

The differential equations that must be satisfied are then

$$\epsilon^0: f_0'' + \gamma_0 f_0 + \int_{-\infty}^x f_0(x-\xi) G(\xi) d\xi = 0 \quad (9.22a)$$

$$\begin{aligned} \epsilon^1: f_1'' + \gamma_0 f_1 + \int_{-\infty}^x f_1(x-\xi) G(\xi) d\xi = \\ -\gamma_1 f_0 - k_1 f_0 e^{2i\alpha_0 x} - k_2 f_0 e^{-2i\alpha_0 x} \end{aligned} \quad (9.22b)$$

$$\begin{aligned} \epsilon^2: f_2'' + \gamma_0 f_2 + \int_{-\infty}^x f_2(x-\xi) G(\xi) d\xi = \\ -\gamma_2 f_0 - \gamma_1 f_1 - k_1 f_1 e^{2i\alpha_0 x} - k_2 f_1 e^{-2i\alpha_0 x} \end{aligned} \quad (9.22c)$$

To evaluate the perturbation in the eigenvalue at the subharmonic, set the basic solution

$$f_0 = e^{i\alpha_0 x} \pm e^{-i\alpha_0 x} \quad (9.23)$$

This form satisfies (9.22a) since the pressure is simply related to the displacement for sinusoidal motion (9.3). It is for this subharmonic that an inhomogeneous term arising from

the product of f_0 with the sinusoidal coefficients is also a solution of the homogeneous equation. This will yield solutions similar to those of (9.15) unless the coefficient of that term vanishes. Thus for this case the perturbation in the eigenvalue is

$$\gamma_1 = \begin{cases} \pm k_1 \\ \pm k_2 \end{cases} \quad (9.24)$$

Introducing an expansion for ω

$$\omega = \omega^{(0)} + \epsilon \omega^{(1)} + \dots \quad (9.25)$$

gives a new condition for the perturbations in amplification rates valid at the subharmonic

$$\omega^{(1)} = \pm (\omega_2^2 + i\omega d_2 e^{\pm i\chi_1}) / (2\omega^{(0)} - id_1) \quad (9.26)$$

where $\omega^{(0)}$ satisfies (9.9). Note that there is no reference to the fluid dynamics in (9.26) except implicitly through the value of $\omega^{(0)}$. This is because the subharmonic resonance, and the suppression of secular instability, is essentially governed by the inhomogeneous equation and the lowest order mode.

9.4 The Altered Stability Problem

The preceding two sections have demonstrated the manner in which the eigenvalue ω is affected by a small periodic variation in the properties of a membrane both for aperiodic solutions and for the subharmonic case. The occurrence of "normal" harmonics can easily be handled by

(9.10), if one recognizes that for $\alpha = n\alpha_0$, the term F_{-n} is singular, but enters into the eigenvalue problem only as F_{-n}^{-1} , thereby causing no substantial difficulties.

Furthermore it must be stressed that the change in amplification rate ω_i can be substantial, since the change in ω is a complex number and is small compared only to the actual magnitude of the complex number. Thus $\epsilon^2 \omega_i^{(2)}$ may actually be large compared to $\omega_i^{(0)}$ and still represent a valid expansion.

Sample calculations were made to determine the first correction to the frequency $\omega^{(2)}$. These calculations were performed for two eigenvalues; the first an amplified Class A wave and the other, a neutral Class B wave for a given compliant boundary.

In these calculations the wave number α_0 was varied from 0.03125 to 5.0. The ratio of the sinusoidal variation in damping to the sinusoidal variation in cutoff frequency was varied from 0 to 1000 and the phase angle \mathcal{K} was varied from 0 to 180 degrees.

For the Class A disturbance, two cases were noted. Below the subharmonic resonant value of α_0 , the phase angle \mathcal{K} that demonstrated the largest stabilizing effect was zero degree, while above the resonance, it was 180 degrees. The ratio of damping variation to frequency variation for greatest stabilization was small in the neighborhood of resonance (most variation in the spring) and large away from resonance (all damper).

For the Class B wave, the computations showed that the perturbation in damping should be very small, while the phase angle \mathcal{K} was around zero degree for greatest stabilization below subharmonic resonance, with the opposite being true above resonance.

However, these results must be regarded as very tentative, for the choice of sinusoidal variation in properties that is stabilizing at one wave number can be very destabilizing at different wave numbers. Much more extensive parametric studies of this situation are needed. The studies can easily be based on the present techniques.

Chapter 10

CONCLUSIONS

10.1 Boundary-Layer Stabilization with Compliant Boundaries

The results presented in the preceding chapters indicate that the stability of the laminar boundary layer can be altered by the use of compliant boundaries. In general, the more compliant the boundary, the more pronounced is its stabilizing (or destabilizing) influence on the boundary layer when compared to a similar situation in the presence of a rigid surface.

The general effect of the variations of the parameters of the boundary has been discussed in Chapter 7. The most interesting feature is the adverse effect of damping, or dissipation terms in the boundary, on the stability of the Class A waves. Both Landahl (1962) and Benjamin (1963) discuss the reasons for this behavior at some length on the basis of the models for the dynamic systems that they have selected. This fact will be demonstrated additionally here for a boundary with both normal and tangential admittances.

To show this, it is necessary to refer to a result from the asymptotic theory as outlined in Appendix A. Using the notation defined in the appendix, the eigenvalue criterion for neutral disturbances can be written from (A.31) as

$$(u+iv - \frac{i\bar{U}'_w}{\alpha} Y_{11} - c Y_{12}) = (1 - c Y_{12}) \mathcal{F}(z) \quad (10.1)$$

The result quoted is the simplified form suitable for large αR , but small α and c , and will suffice for the following discussion.

One can approximately separate the normal and tangential admittances into two portions

$$\begin{aligned} Y_{11} &= dY_r - iY_i \\ Y_{12} &= -X_r - idX_i \end{aligned} \tag{10.2}$$

where the factor d is retained to demonstrate how the (small) damping coefficient enters into this relationship (for neutral disturbances). The coefficients X_r , X_i , Y_r , Y_i are all positive for Class A disturbances, and may be either positive or negative, depending on whether c is less than or greater than the propagation speed in the boundary. The following discussion is accurate only for Class A waves, for the asymptotic theory itself can be expected to fail for the Class B waves.

Upon insertion of (10.2) into (10.1), the left-hand side becomes

$$\left(u - \frac{\bar{U}'_w}{\alpha} Y_i + cX_r \right) + i \left\{ v - d \left(\frac{\bar{U}'_w}{\alpha} Y_r + cX_i \right) \right\} \tag{10.3}$$

The imaginary part v is determined by the curvature of the velocity profile at the critical point. In the graphical solution of (10.1) described by Landahl (1962), one can see that an increase in v for fixed α and c will cause the low Reynolds number intersection to move to a higher value of αR . This is the principal stabilizing effect of a favorable pressure gradient. The small imaginary corrections to v are negative, thus demonstrating that an increase in damping acts to decrease v and thus αR at fixed α and c , therefore decreasing the critical Reynolds number.

Arguments of this kind can be made on the basis of v alone, since u is generally large compared to v . Further-

more, (10.3) shows that a partial cancellation of the effective real part of the admittance results since the effects of normal and of tangential admittance have opposite sign. Since it is normal admittance that causes the motion of the unstable region to lower values of α or of ω , tangential admittance tends to reduce this phenomenon. In this sense, the tangential admittance can be regarded as having a slightly destabilizing influence, but since it is physically impossible to construct a boundary that only moves vertically, this characterization is meaningless. It is more accurate to say that the results derived for a membrane show a greater influence on the boundary-layer stability than could be achieved with an actual boundary of the same compliance.

However, the repeated emphasis throughout this paper has been that critical Reynolds number alone is an insufficient criterion for comparisons of relative stability, and it has been suggested that spatial amplification rates presented in a frequency Reynolds number diagram give a greater depth of understanding to the results.

Inspection of Figure 27 reveals that a primary result of the presence of the compliant boundary is an increase in the group velocity of the disturbances. Since the energy is convected with the group velocity in a dispersive system, this is interpreted to mean that the disturbance energy passes through the unstable region in space (a finite Reynolds number band) more rapidly in the presence of a compliant boundary. Thus for a given temporal amplification rate (which was not altered greatly by the presence of the boundary) there is less time for the wave to be amplified before passing to higher stable Reynolds numbers.

Furthermore, the wavelengths of the unstable disturbances are greater and the frequencies lower for a boundary layer in the presence of a compliant boundary. It must be

stressed that for a given mass and damping, this downward shift of the unstable region is a function of the propagation speed only. It must be concluded that the dispersion in the system is increased by a low value (within limits) of the propagation speed.

By means of the numerical solutions and analytical arguments, the effect of the compliant boundary may be qualitatively and quantitatively described. One can specify optimum ranges of parameters for configurations under specific constraints only after extended parametric studies of the desired configurations. The general notions discussed in this paper can be used to evaluate these studies intelligently, but the actual specification of an optimum configuration will still require much judgment.

10.2 The Mechanisms Causing Instability

In a system as complicated as that under consideration, it is dangerous to state unequivocally that any specific factor is the cause of the instability. It is generally agreed that a basic contributor to the unstable behavior is the small but finite viscosity of the boundary layer. Lin (1955) discusses the effect of the Reynolds stresses (shown in Figures 26 and 34 for both Class A and B disturbances) acting "on the wall in the direction of propagation of the disturbance wave" as revealing a mechanism for the conversion of energy in the mean flow into the disturbance. Landahl (1962) further remarks that the Class A waves are energy deficient in the sense that an increase in dissipation in a compliant boundary causes an increase in the disturbance amplitude to recover the dissipated energy from the mean flow, and the mechanism for this recovery can only be the Reynolds stresses. Benjamin (1963) amplifies on this argument for his descriptions of a more general class of coupled systems.

Figures 26 and 34 indicate that the Reynolds stresses

appearing for Class A waves are relatively unchanged from the picture that can be obtained from the boundary layer traveling over a rigid surface. One can then conclude that the essential mechanism for the instability of the Class A disturbances is essentially as summed up in Lin's monograph.

However, the story is entirely different for the Class B disturbances. Consider first the two plots for Class B waves in a membrane, shown in Figure 26. Note that the Reynolds stress at the surface of the membrane must vanish by (2.29)

$$\tau_w = -\alpha \text{RealPart} \{ i \phi_w' \phi_w^* \} = \frac{\alpha \bar{U}_w'}{c} \text{RealPart} \{ i \phi_w \phi_w^* \} = 0$$

However, these approximately neutral disturbances show a peak in amplitude for the Reynolds stress in the region immediately adjacent to the wall. There is unquestionably a conversion of these stresses into pressure work (pressure in phase with the vertical velocity) at the wall.

The Class B example in Figure 34 is for the rubber surface model, in which the Reynolds stresses at the wall do not vanish. In the example of the highly damped disturbance, the sign of these stresses changes at the wall, supporting Lin's contention of the effect of their action. The chief feature that one notes in the calculations is that the Class B waves do not have a small real part of the Reynolds stresses as do the Class A. The phase shifts that are the factor that determines the relative size of the real and imaginary parts of the Reynolds stresses (the imaginary part has no physical significance but is generally large compared to the real part) are very large for Class B waves, indicating that their behavior is radically different from that of the Class A waves. It must be concluded that the action of compliant surface in a Class B wave is a more effective mechanism for generating

Reynolds stresses than the phase differences across the critical layer.

Thus it is demonstrated that the mechanism of the instability of the Class A disturbances is the same as that for the boundary layer over a rigid surface, thus justifying their consideration as Tollmien-Schlichting waves. The mechanism for the generation of Class B waves is the phase shifts that generate large Reynolds stresses, originating from large surface admittance. Finally, the Kelvin-Helmholtz (or Class C) instability is caused by too compliant a boundary and is essentially an inviscid phenomenon.

10.3 Suggestions for Future Investigation

It is felt that future study is needed to determine optimum parametric relationships for realistic models of compliant boundaries. The chief expenditure for these studies would be computer time and careful judgment in evaluating the results, but it is hoped that the techniques presented in this report will make these costs slight. It would also be desirable to have experiments in this area of the same high caliber as those performed by the National Bureau of Standards group, but the difficulty in performing such experiments is recognized. It might be more efficient to attempt to correlate the spatial amplification criteria of these stability calculations with actual measurements of transition points for a variety of pressure gradients and surface models. It is expected that the spatial amplification calculations will aid in the formulation of such transition criteria.

Along this line, further investigation is needed into the justification of these spatial amplification techniques and a direct calculation of the imaginary parts of wave number would be desirable. This study in depth is needed because of the utility of these results in providing relative stability

criteria, and the reasons mentioned in the preceding paragraph.

The techniques used to solve the Orr-Sommerfeld equation can be adapted to handle a variety of other fluid dynamic stability problems, such as the compressible flow boundary layer, or the addition of nonNewtonian fluids. The inherent speed of these calculations would provide a distinct advantage in computations of boundary-layer stability at supersonic Mach numbers, if the techniques can be successfully adapted.

It is also felt that the remarks on the observed boundedness of c_r for Class A waves (Section 6.1) should be carefully investigated. At the present, this is only set forth as an observation, but it may have more general validity.

Finally, the calculations of the stability of jets, wakes and shear flows should be extended, perhaps to include compressibility effects. One can consider the formation of a wake (or a high-speed jet) as a laminar core surrounded by a rapidly expanding asymmetric shear flow. Thus studies of two-dimensional calculations might be used to shed some light on the large-scale breakup of these configurations. Further extensions to axisymmetric geometries are probably possible using the present techniques, and definitely warrant more complete study. The problem of wave generation by wind can also be investigated in a straightforward manner as the problem of an asymmetric shear flow with a density discontinuity at the interface, or in the manner suggested in Section 3.5.

REFERENCES

- Benjamin, T.B. 1959 "Shearing Flow Over a Wavy Boundary."
J. Fluid Mech. 6, p. 161.
- Benjamin, T.B. 1960 "Effects of a Flexible Boundary on Hydrodynamic Stability." J. Fluid Mech. 9, p. 513.
- Benjamin, T.B. 1963 "The Threefold Classification of Unstable Disturbances in Flows Over Flexible Surfaces."
J. Fluid Mech. 16, p. 436.
- Benney, D.J. 1961 "A Nonlinear Theory for Oscillations in Parallel Flow." J. Fluid Mech. 10, p. 209.
- Bismut, M. 1963 "Ecoulement Perturbe Entre Plaques Paralleles Recherche Par Calcul Analogique Des Valeurs Propres Des Coeficients De L'Equation D'Orr-Sommerfeld." Communication Presented at the International Colloquium on Analog and Numerical Calculation in Aeronautics, Liege, Sept. 1963.
- Brown, F.M.N. 1963 "Boundary Layer Transition." Dept. of Aero. Eng., U. of Notre Dame, Indiana.
- Brown, W.B. 1955 "Extension of Exact Solution of the Orr-Sommerfeld Equation to Reynolds Numbers of 4000." Rept NAI 55-548, Northrop Aircraft Inc.
- Brown, W.B. 1959 "Numerical Calculation of the Stability of Cross Flow Profiles in Laminar Boundary Layers on a Rotating Disc and on a Swept Back Wing and an Exact Calculation of the Stability of the Blasius Velocity Profile." Report NAI 59-5, Northrop Aircraft Inc.
- Brown, W.B. 1961 "A Stability Criterion for Three-Dimensional Boundary Layers and Flow Control." G.V. Lachman (Ed) Vol. 2, Pt III, pp. 913-923, Pergamon Press.
- Collatz, L. 1951 Numerische Behandlung Von Differentialgleichungen. Springer Verlag Ohg

- Criminale, W.O. Jr. and Kovaszny, L.S.G. 1962 "The Growth of Localized Disturbances in a Laminar Boundary Layer." J. Fluid Mech. 14, p. 59.
- Dahlquist, G.G. 1962 "Stability Questions for Some Numerical Methods for Ordinary Differential Equations." Technical Report sponsored jointly by U.S. Navy Office of Naval Research and U.S. Army Research Office, Contracts Nonr 233(24) and DA-04-495-ORD-1630.
- Drazin, P.G. and Howard, L.N. 1962 "The Instability of Long Waves of Unbounded Parallel Inviscid Flow." J. Fluid Mech. 14, p. 257.
- Dunn, D.W. 1953 "On the Stability of the Laminar Boundary Layer in a Compressible Fluid for the Case of Three Dimensional Disturbances." Doctoral Dissertation, Dept. of Math. Massachusetts Institute of Technology.
- Gaster, M. 1962 "A Note on the Relation Between Temporally-Increasing and Spatially-Increasing Disturbances in Hydrodynamic Stability." J. Fluid Mech. 14, p. 222.
- Hains, F.D. 1963 "Comparison of the Stability of Poiseuille Flow and the Blasius Profile for Flexible Walls." Boeing Scientific Research Laboratories, Flight Sciences Laboratory Report No. 75.
- Hildebrand, F.B. 1956 Introduction to Numerical Analysis. McGraw Hill Book Co. Inc. Chapter 6.
- Ipsen, D.C. 1960 Units, Dimensions, and Dimensionless Numbers. McGraw Hill Book Co. Inc.
- Karplus, H.B. 1963 "Turbulent Flow Transition Near Solid and Flexible Boundaries." IIT RES. INST. REPT. NO. IITRI 1205-1.

- Klebanoff, P.S., Tidstrom, K.D., and Sargent, L.M. 1962
 "The Three Dimensional Nature of Boundary Layer
 Instability." J. Fluid Mech. 12, p. 1.
- Kramer, M.O. 1957 "Boundary Layer Stabilization by Distributed
 Damping." J. Aero. Sci. 24, p. 459.
- Kramer, M.O. 1960 "Readers Forum." J. Aero/Space Sci. 27, p.68.
- Kramer, M.O. 1960 "Boundary Layer Stabilization by Distributed
 Damping." J. Amer. Soc. Nav. Engrs. 72, p. 25.
- Kurtz, E.F. Jr. and Crandall, S.H. 1962 "Computer-Aided
 Analysis of Hydrodynamic Stability." J. of Math
 and Physics, XLI, p. 264.
- Landahl, M.T. 1962 "On the Stability of a Laminar, Incompres-
 sible Boundary Layer Over a Flexible Surface."
J. Fluid Mech. 13, p. 609.
- Landahl, M.T. 1964 "Graphical Techniques for Analyzing
 Marginally Stable Dynamic Systems." AIAA Preprint
 LJ-80.
- Lees, L. 1947 "The Stability of the Laminar Boundary Layer
 for a Compressible Fluid." NACA Rept No. 876.
- Lin, C.C. 1945 "On the Stability of Two-Dimensional Parallel
 Flows." Pt I, II, III, Quart. Appl. Math. 3, pp. 117,
 218, 277.
- Lin, C.C. 1955 The Theory of Hydrodynamic Stability.
 Cambridge Univ. Press.
- Linebarger, J.H. 1961 "On the Stability of a Laminar Boundary
 Layer Over a Flexible Surface in a Compressible Fluid."
 S.M. Thesis, Dept. of Aero. and Astro. Massachusetts
 Institute of Technology.
- Meyer-Piening, H.R. 1963 "Viscous Flow Over a Compliant Surface."
 Massachusetts Institute of Technology, Aeroelastic and
 Structures Research Lab. Rept ASRL 1015.

- Miles, J.W. 1960 "The Hydrodynamic Stability of a Thin Film in Uniform Shearing Motion." J. Fluid Mech. 8, p.593.
- McLachlan, N.W. 1947 Theory and Applications of Mathieu Functions. Oxford Univ. Press.
- Morse, P.M. and Feshbach, H. 1953 Methods of Theoretical Physics. Vols. I, II. McGraw Hill Book Co. Inc., New York.
- Nonweiler, T. 1961 "Qualitative Solutions of the Stability Equation for a Boundary Layer in Contact with Various Forms of Flexible Surfaces." A.R.C. Rept. No. 22,670.
- Powers, J.O., Heichs, G., and Shen, S.F. 1963 "The Stability of Selected Boundary Layer Profiles." U.S. Naval Ordnance Laboratory, Aerodynamics Research Report No. 186.
- Schlichting, H. 1933 "Zur Entstehung der Turbulenz Bei der Plattenstromung." Nachr. Ges. Wiss. Gottingen. Math.-Phys. Klasse, pp. 181-208.
- Schlichting, H. 1935 "Amplitudenverteilung und Energiebilanz der Kleiner Storungen Bei der Plattenstromung." Nachr. Ges. Wiss. Gottingen, Math.-Phys. Klass Bd I, p. 47.
- Schlichting, H. 1955 Boundary Layer Theory. Pergammon Press, New York
- Schubauer, G.B. and Skramstad, H.K. 1948 "Laminar Boundary Layer Oscillations and Transition on Flat Plate." NACA Rept. No. 909.
- Squire, H.B. 1933 "On the Stability of the Three Dimensional Disturbances of Viscous Flow Between Parallel Walls." Proc. Roy. Soc. A, 142, p. 621.

- Stoker, J.J. 1950 Nonlinear Vibrations. Interscience,
New York
- Tatsumi, T. and Kakutani, T. 1958 "The Stability of a
Two-Dimensional Laminar Jet." J. Fluid Mech. 4, p. 261.
- Tokita, N. and Boggs, F.W. 1962 "Final Report of Theoretical
Study of Compliant Coatings to Achieve Drag Reduction
on Underwater Vehicles." U.S. Rubber Company report.
- Urabe, M. 1961 "Theory of Errors in Numerical Integration of
Ordinary Differential Equations." J. Sci. Hiroshima
Univ. (Ser. A 1) 25, pp. 3-62.

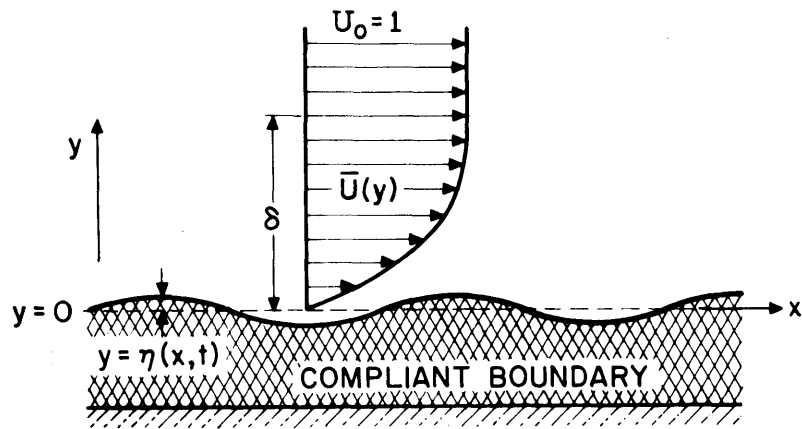


Figure 1. Boundary Layer Over a Compliant Boundary

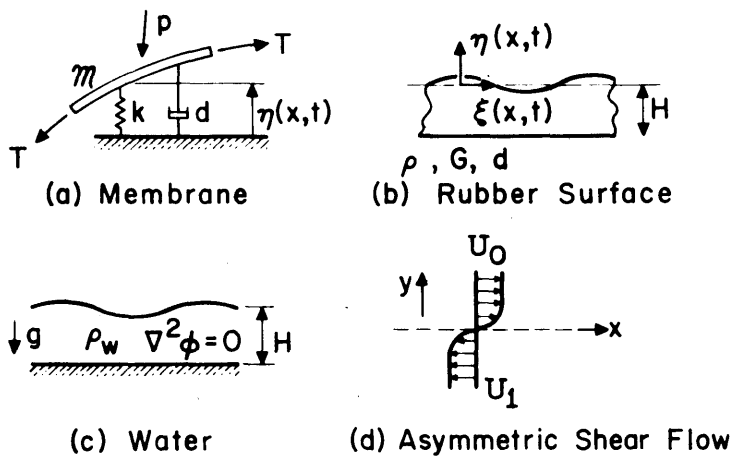


Figure 2. Examples of Flexible Surfaces

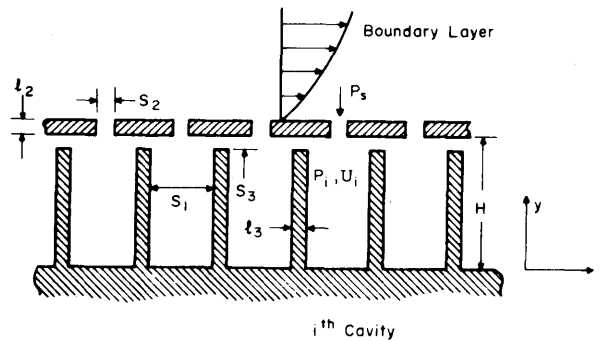


FIGURE 3 Two-Dimensional Array of loosely coupled Helmholtz Resonators

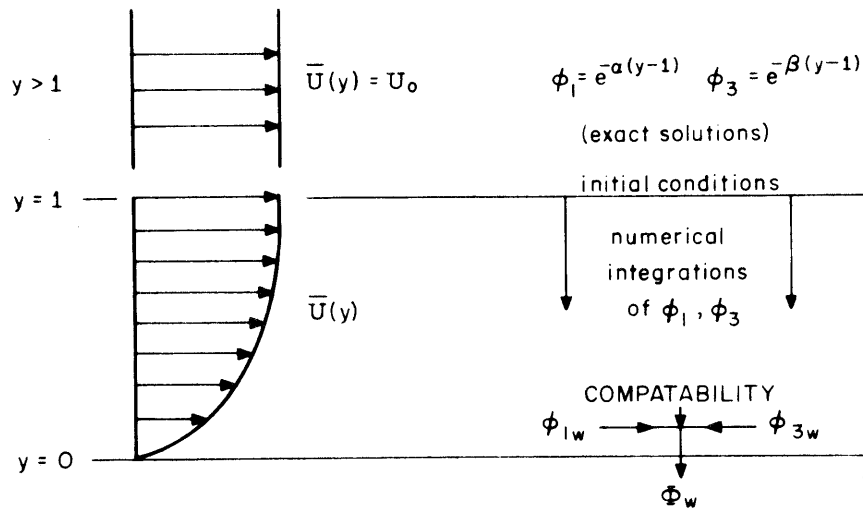


FIGURE 4 Integration of the Orr - Sommerfeld Equation

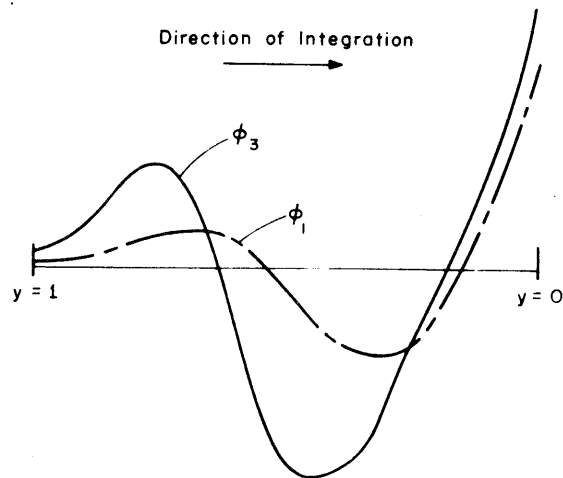
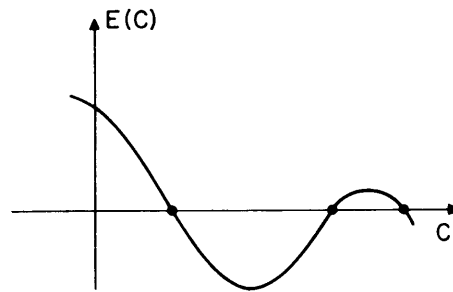
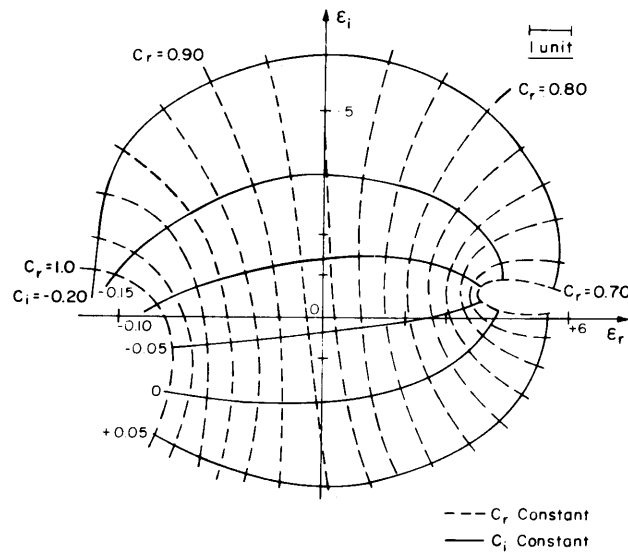


FIGURE 5 Growth of Parasitic Solutions (Schematic)

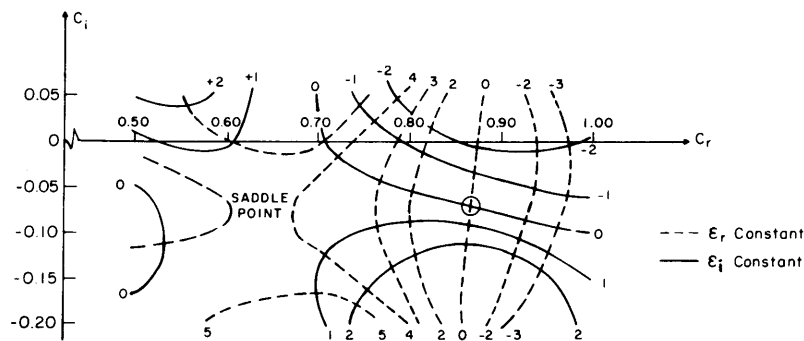


• Eigenvalues C_e for which $E(C_e) = 0$

Figure 6. Illustration of Eigenvalue Problem



7(a) Argand Diagram - C Plane Mapped on E Plane



7(b) Argand Diagram - E Plane Mapped on C Plane

Figure 7. Topology of Eigenvalue Criterion - Membrane Surface
 $c_0 = 0.90$ $d_0 = 0.05$ $\omega_0 = 0.10$ $m_0 = 1.0$ $R_0 = 5000$
 $R = 2000$ $\alpha = 1$

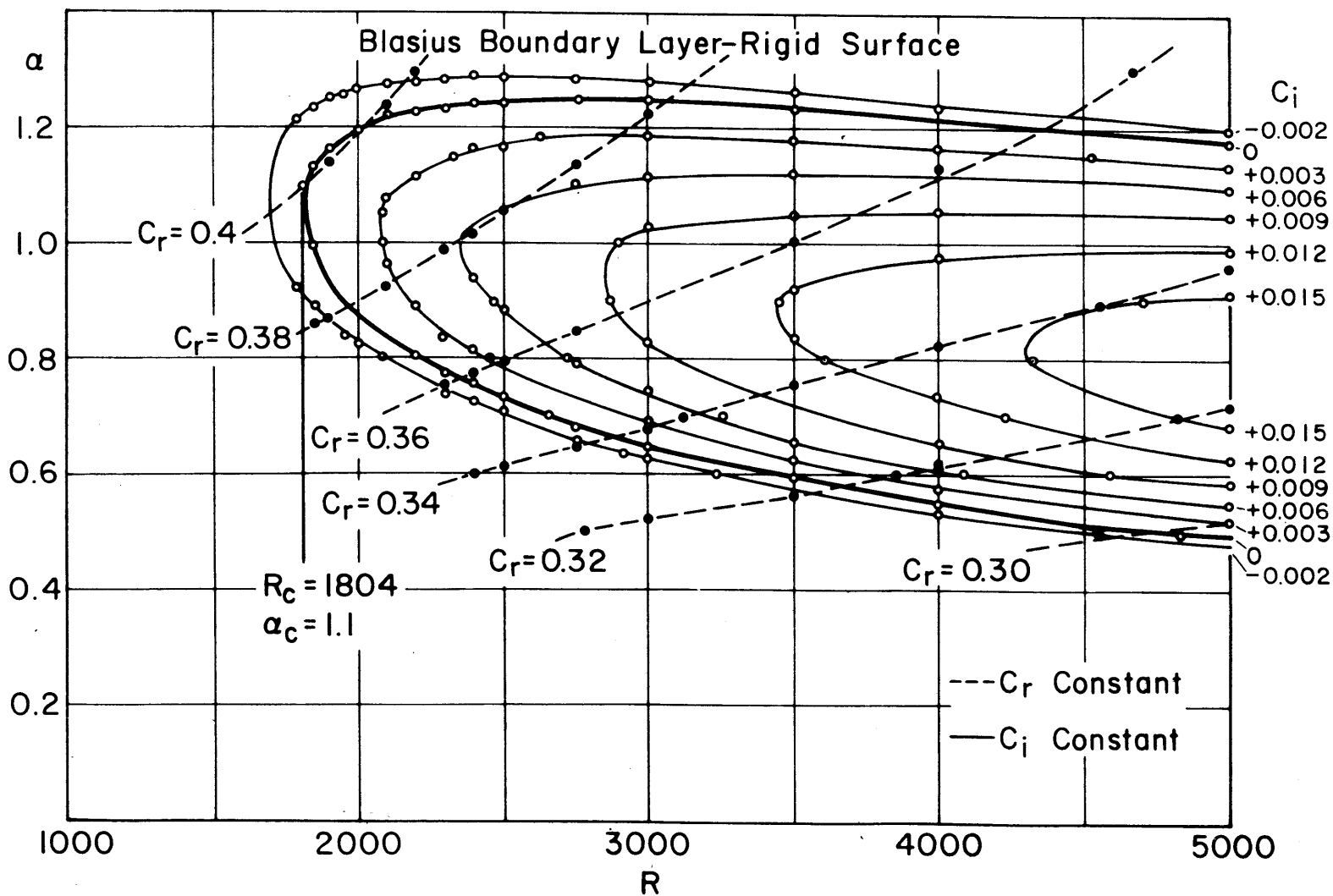


Figure 8. Eigenvalues c_r , c_i for the Blasius Boundary Layer over a Rigid Surface

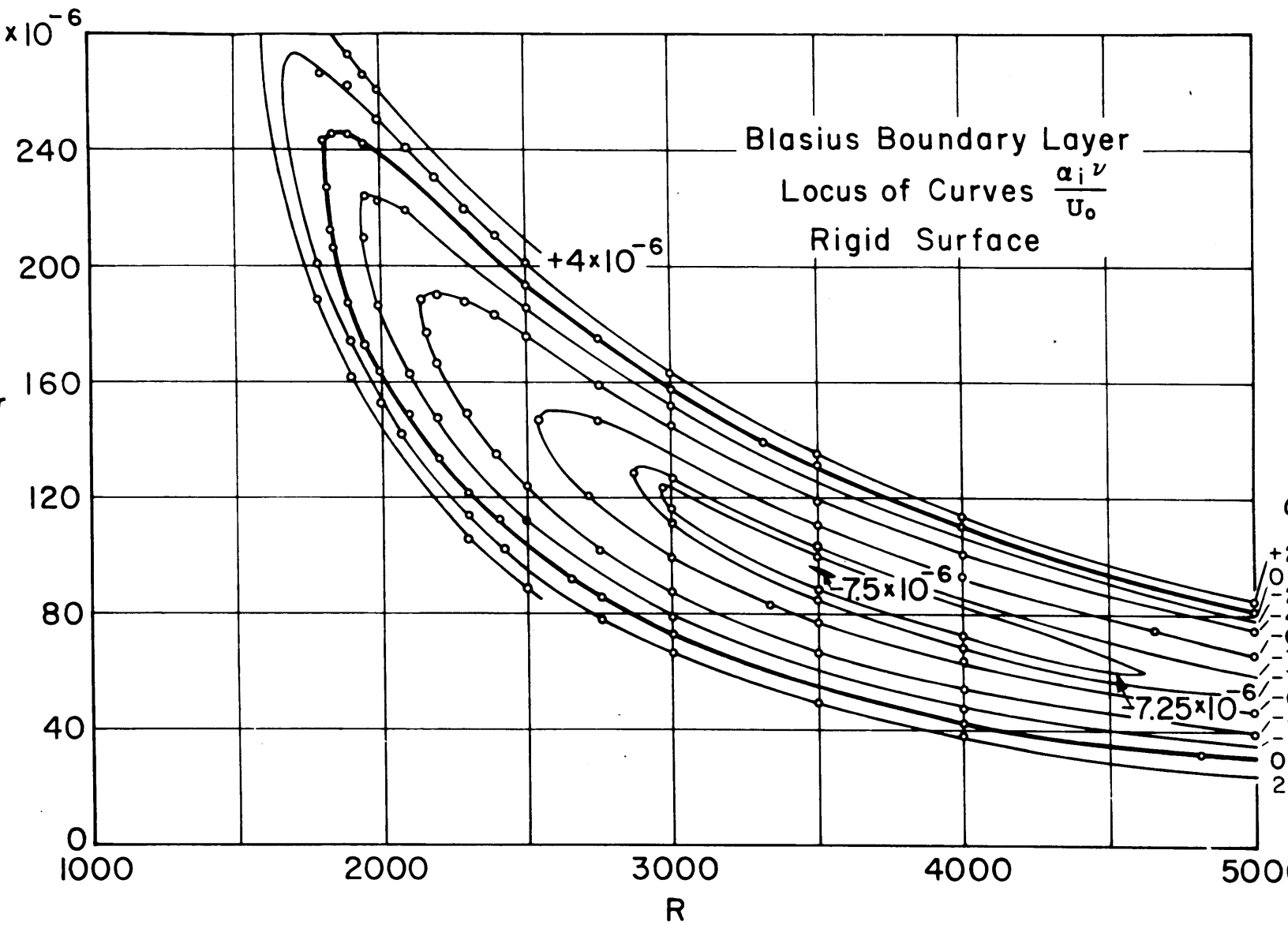


Figure 9. Spatial Amplification Rates for the Blasius Boundary Layer over a Rigid Surface

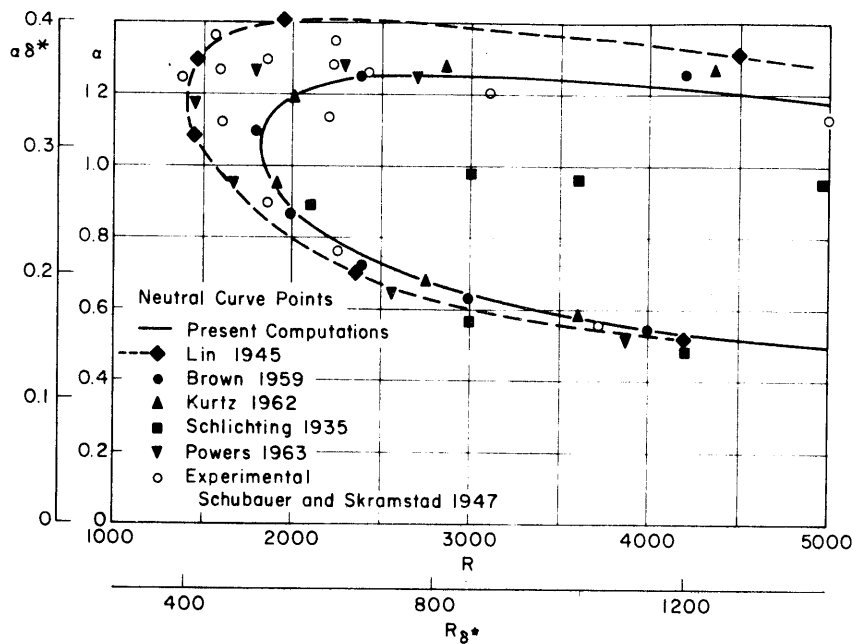


Figure 10. Comparisons of the Neutral Curves for the Blasius Boundary Layer over a Rigid Surface

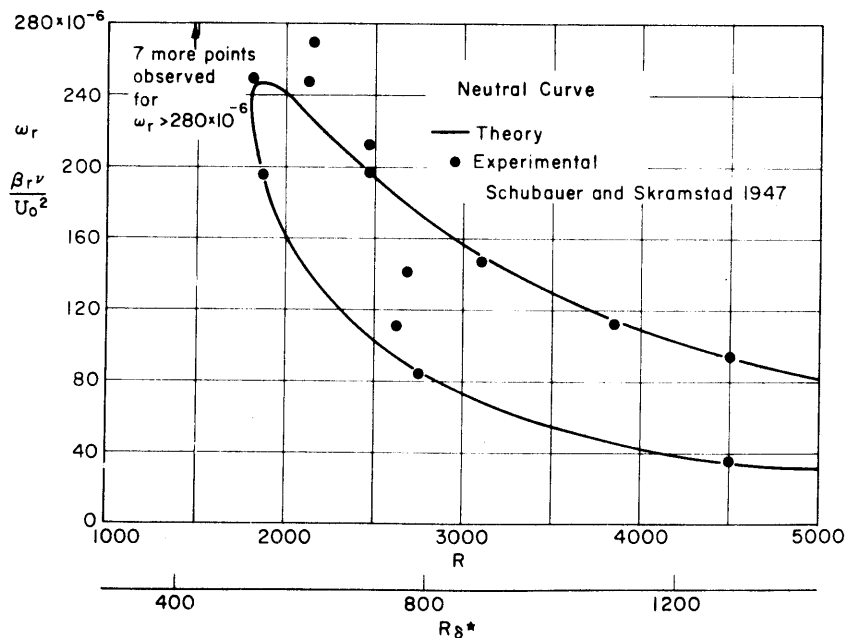


Figure 11. Comparisons with Experimental Results for the Blasius Boundary Layer over a Rigid Surface

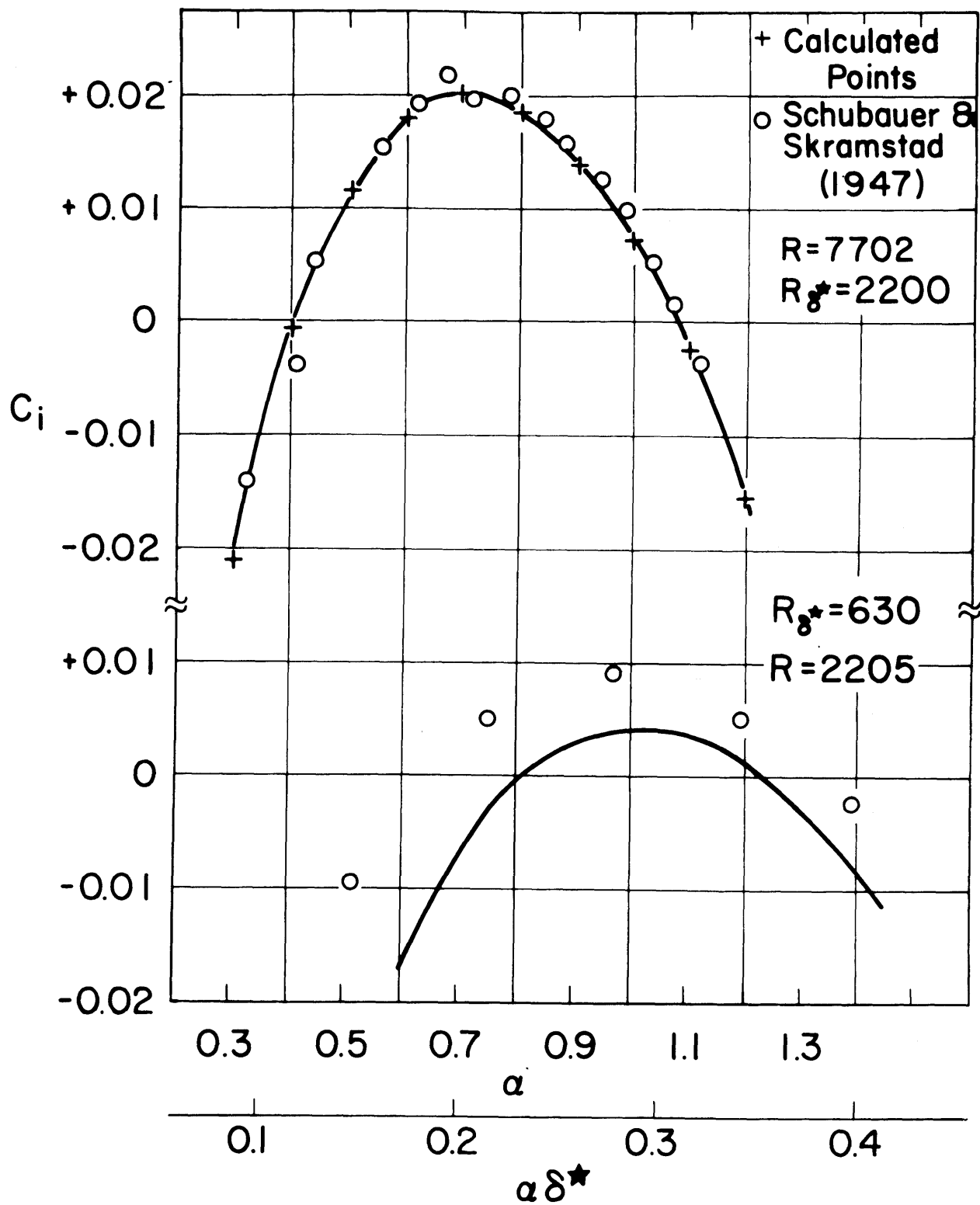
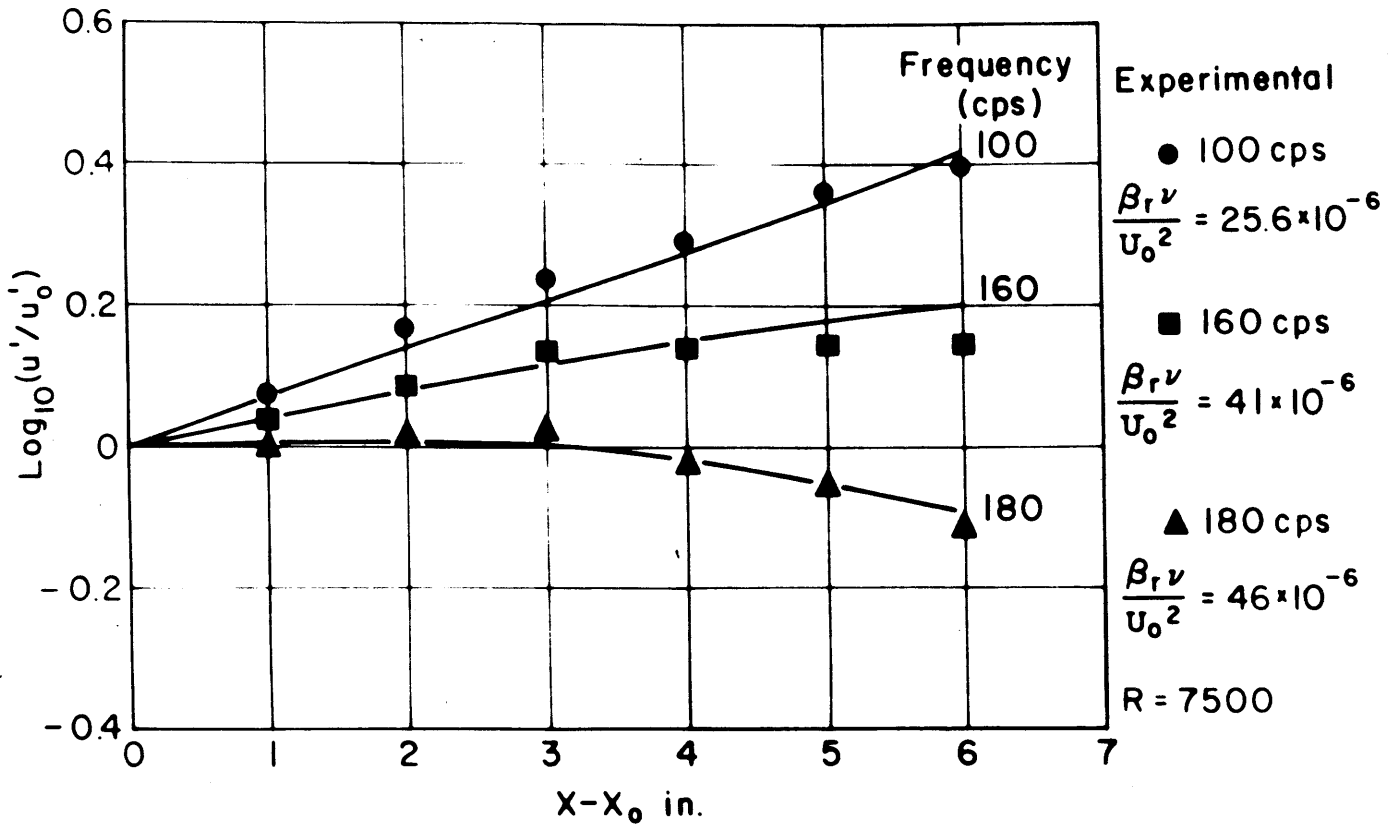


Figure 12. Comparison with Experiment - Temporal Amplification Rates



$U_0 = 64 \text{ ft/sec}$

Ribbon 4 ft from leading edge of plate

$X_0 = 2 \text{ in. behind ribbon}$

Ref: Schubauer and Skramstad [1947]

Figure 13. Comparison with Experiment - Spatial Amplification

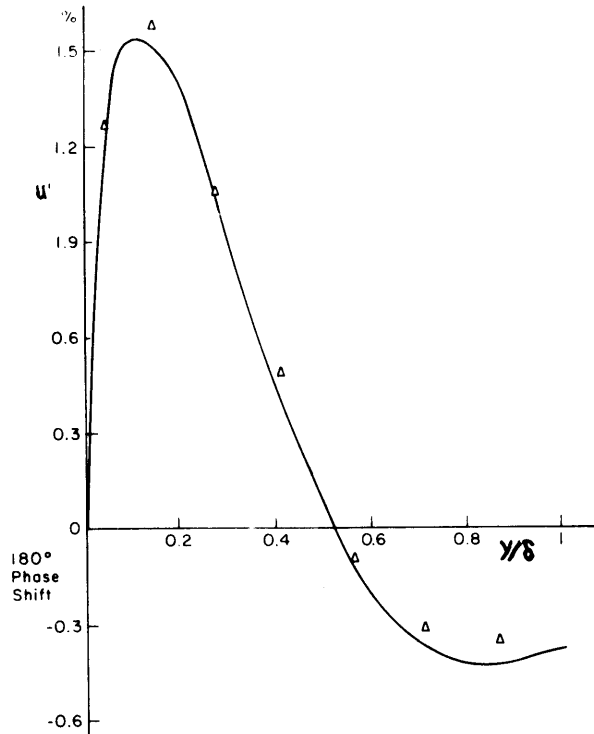


Figure 14. u Perturbation Amplitude Distribution
 ▲ Experimental Points - Schubauer and Skramstad (1947)
 $R = 3000 \quad \alpha = 1.24$

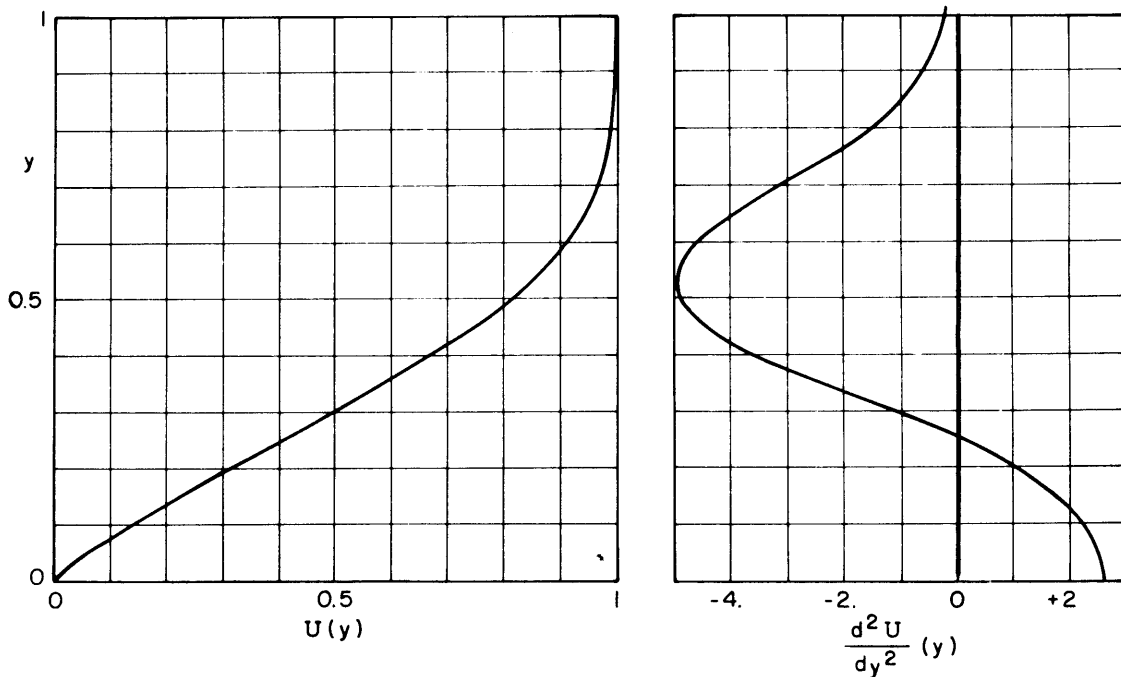


Figure 15. Falkner-Skan Profile $\bar{U} = cx^m$ -- $m = -0.05$

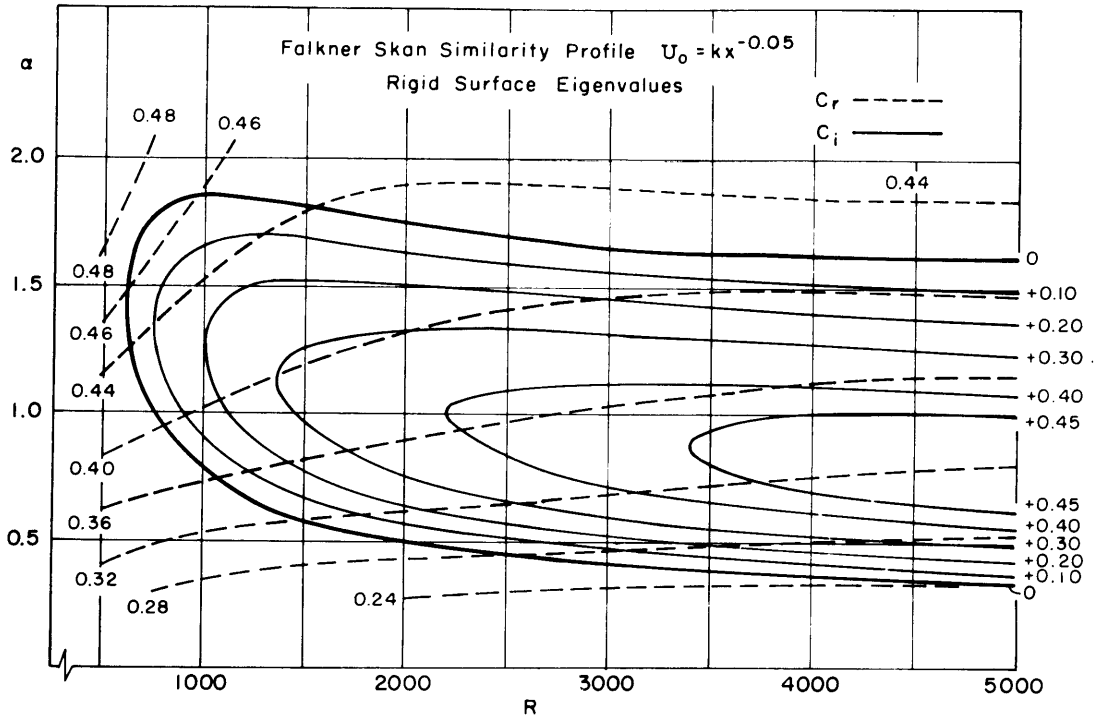


Figure 16. Eigenvalues $c_r - c_i$ for the Falkner-Skan Flow over a Rigid Surface

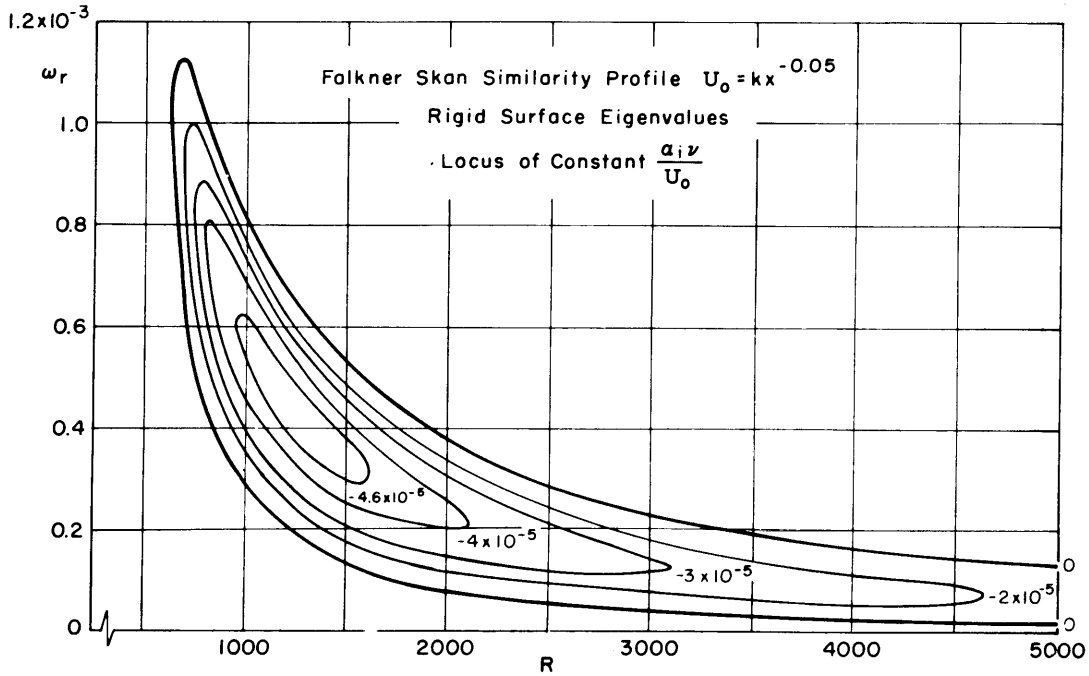


Figure 17. Spatial Amplification Rates for the Falkner-Skan Boundary Layer over a Rigid Surface

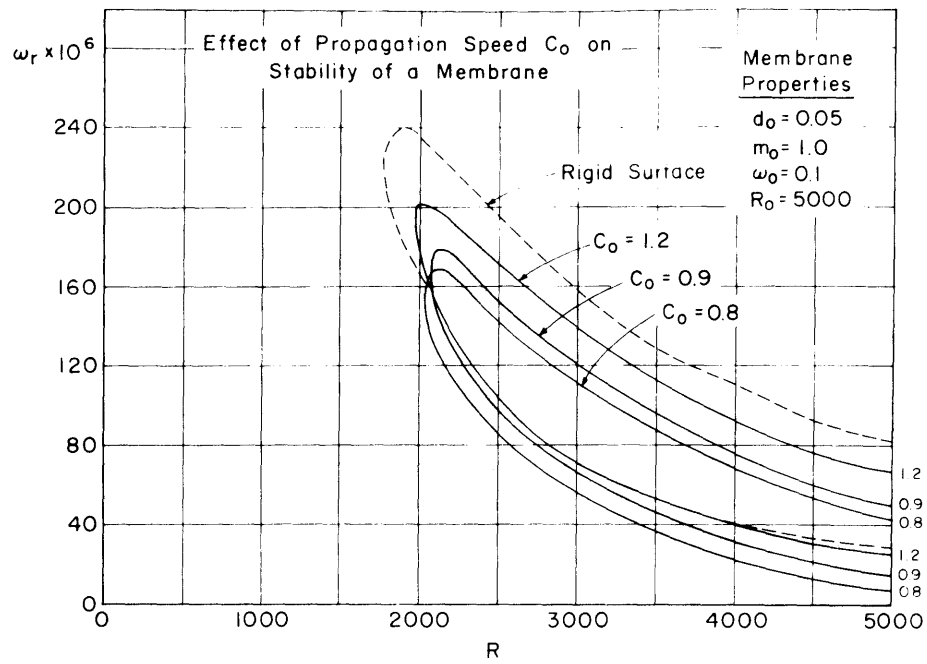


Figure 18

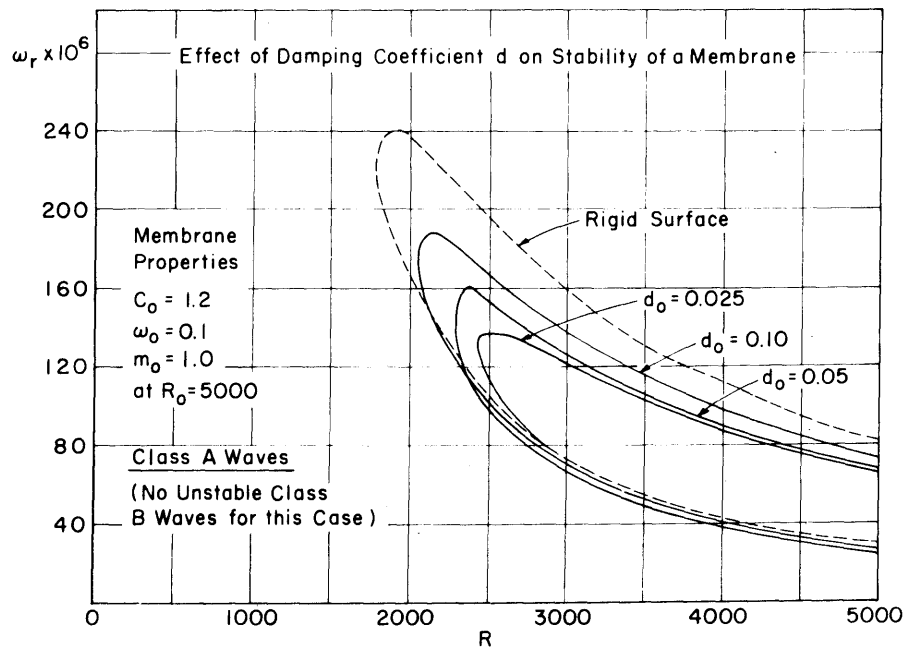


Figure 19

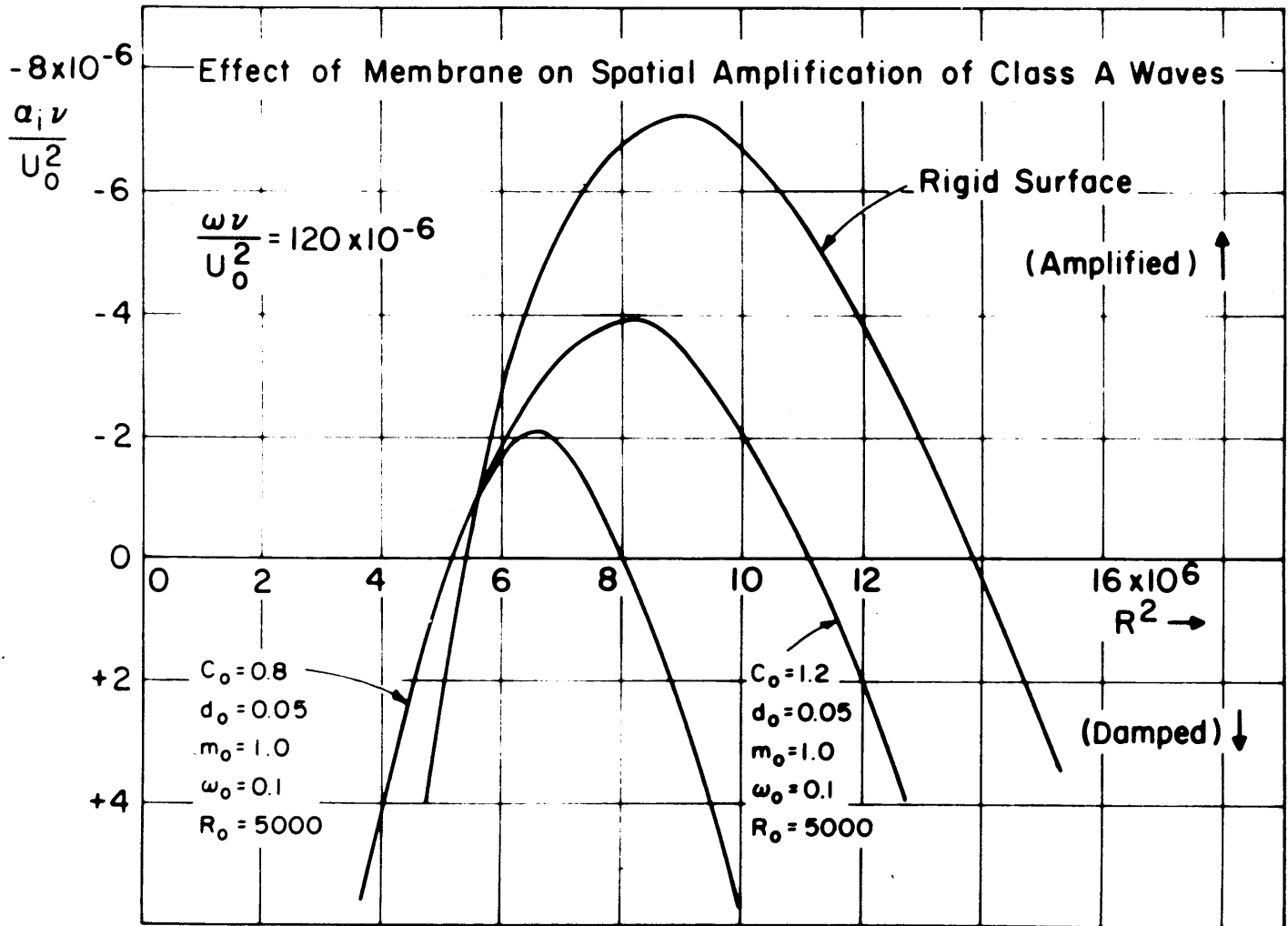


Figure 20

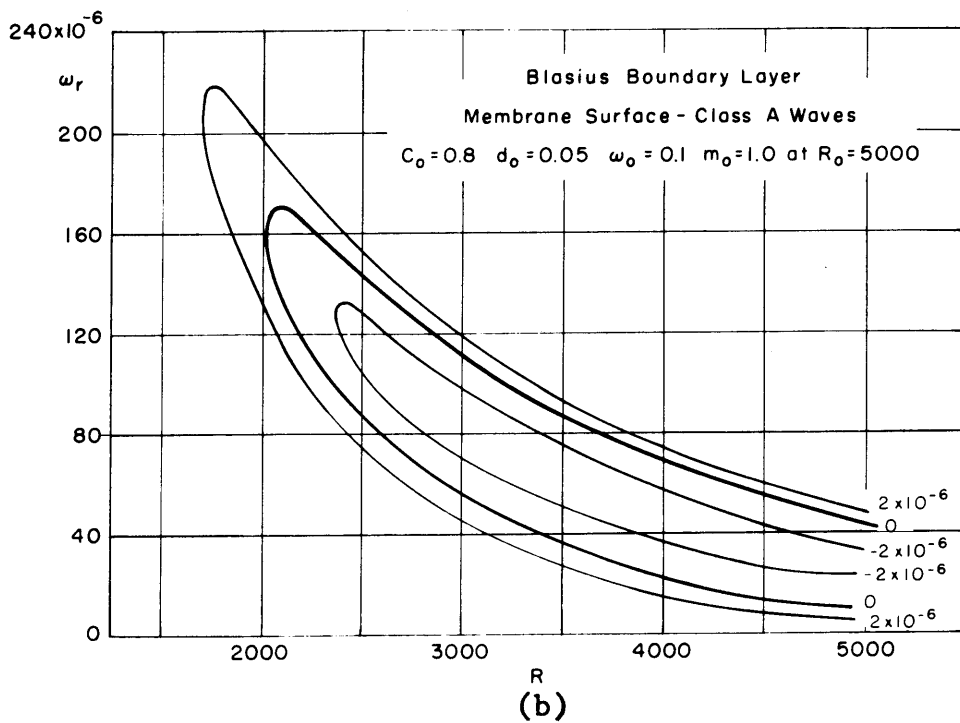
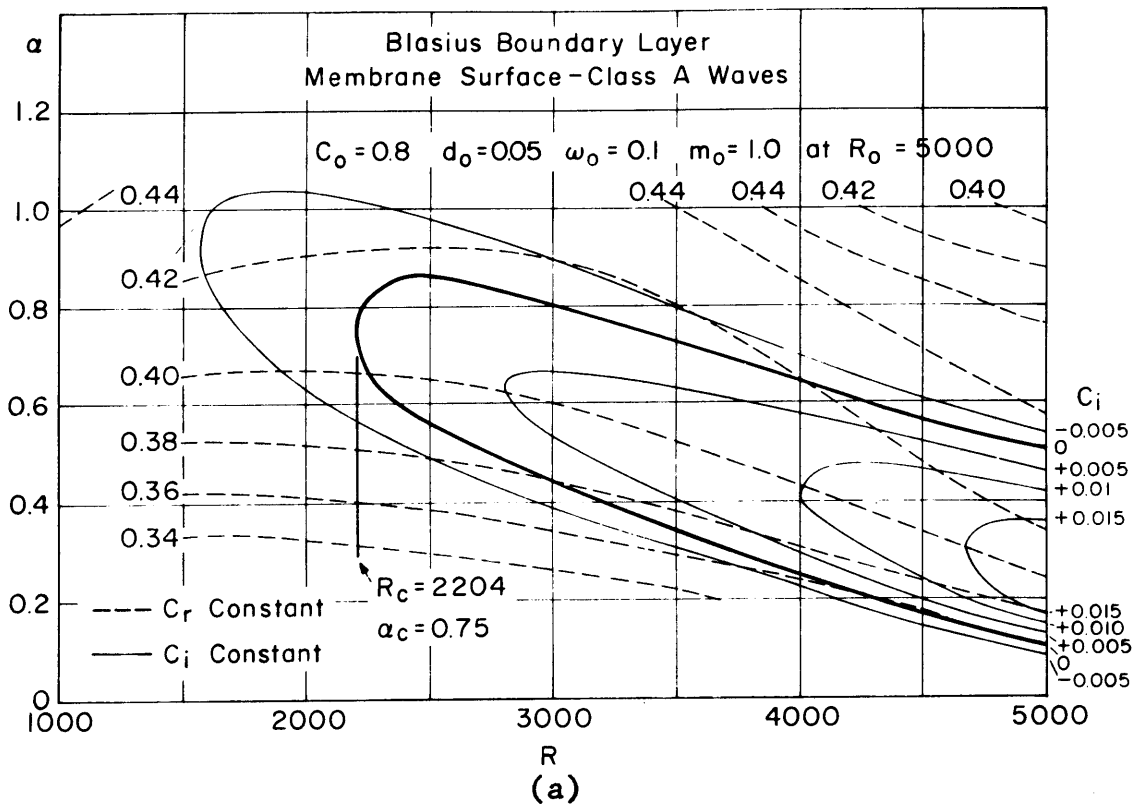


Figure 21. Eigenvalues for a Membrane Surface - Class A Waves

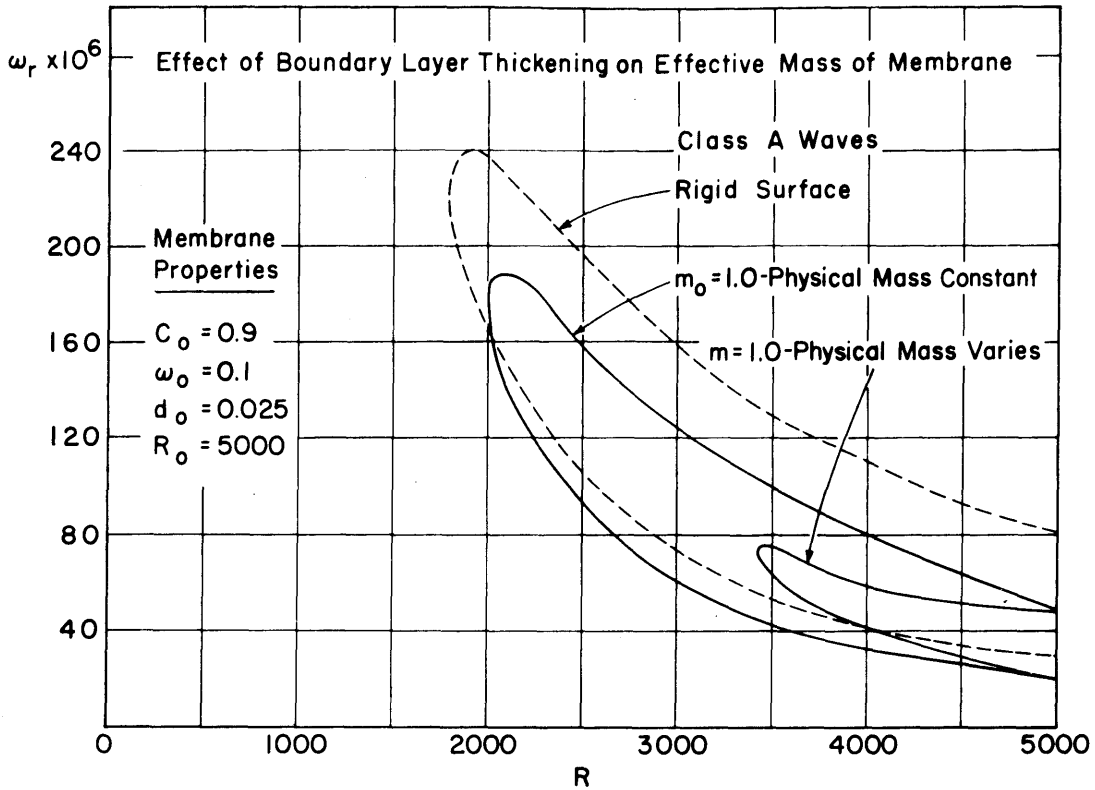


Figure 22

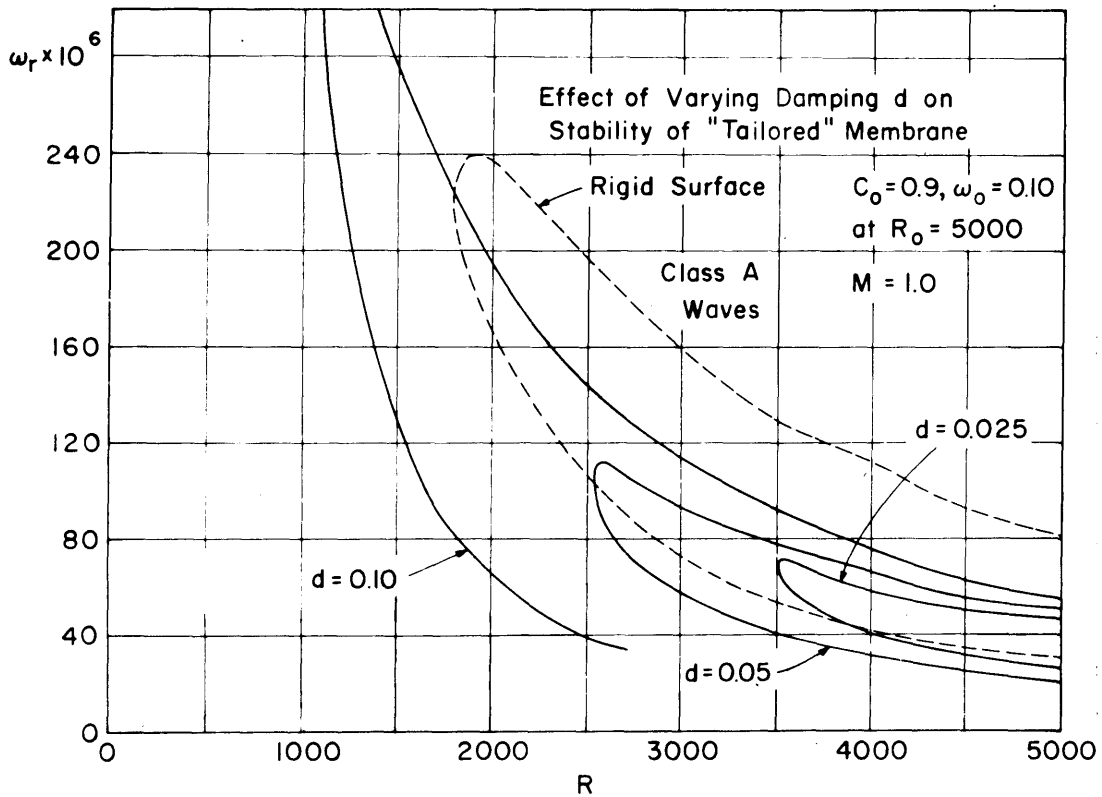


Figure 23

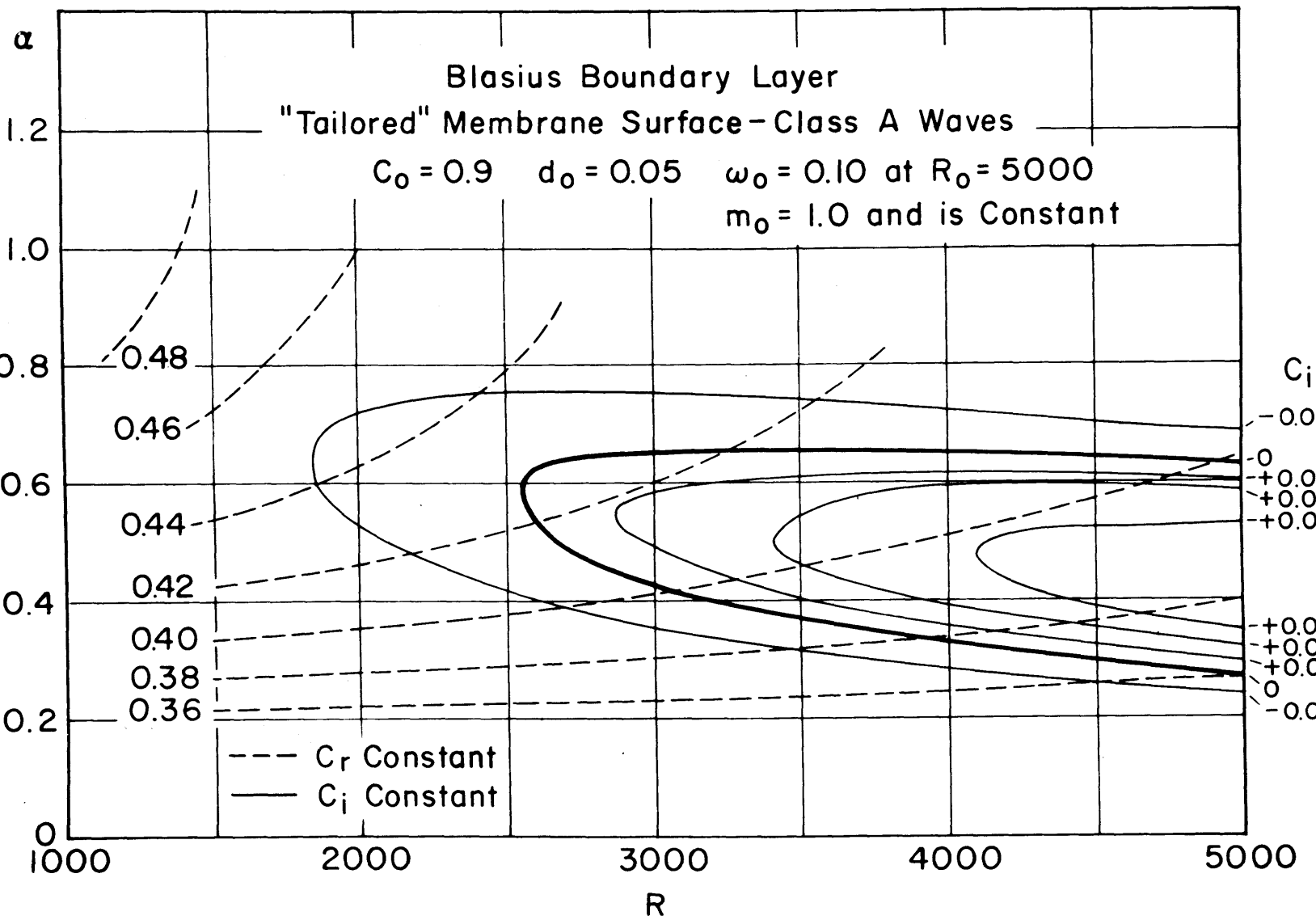


Figure 24. Eigenvalues for a "Tailored" Membrane Surface - Class A Waves

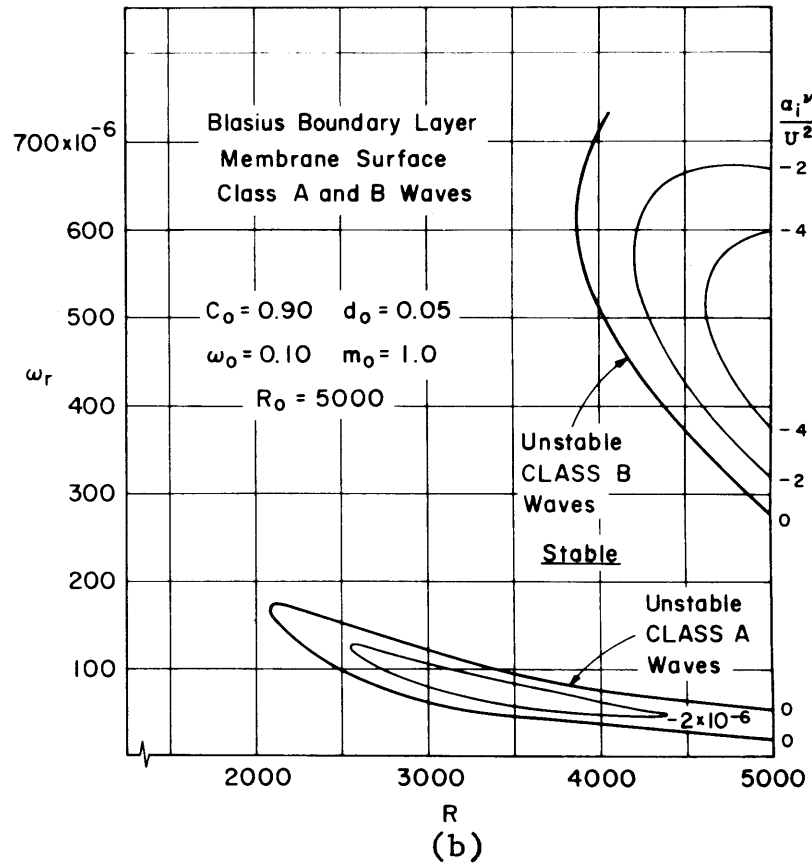
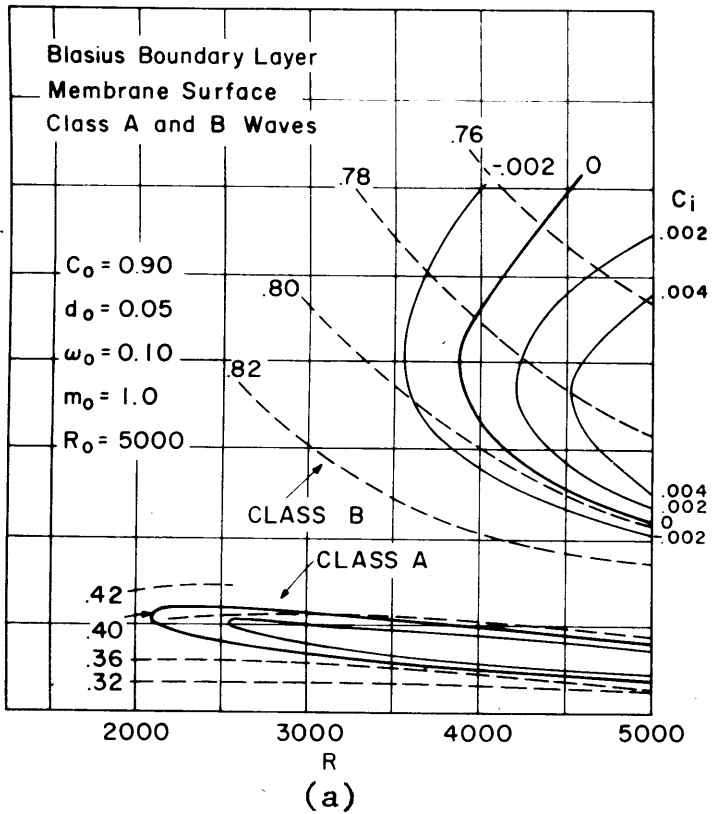


Figure 25. Eigenvalues for a Membrane Surface - Class A and B Waves

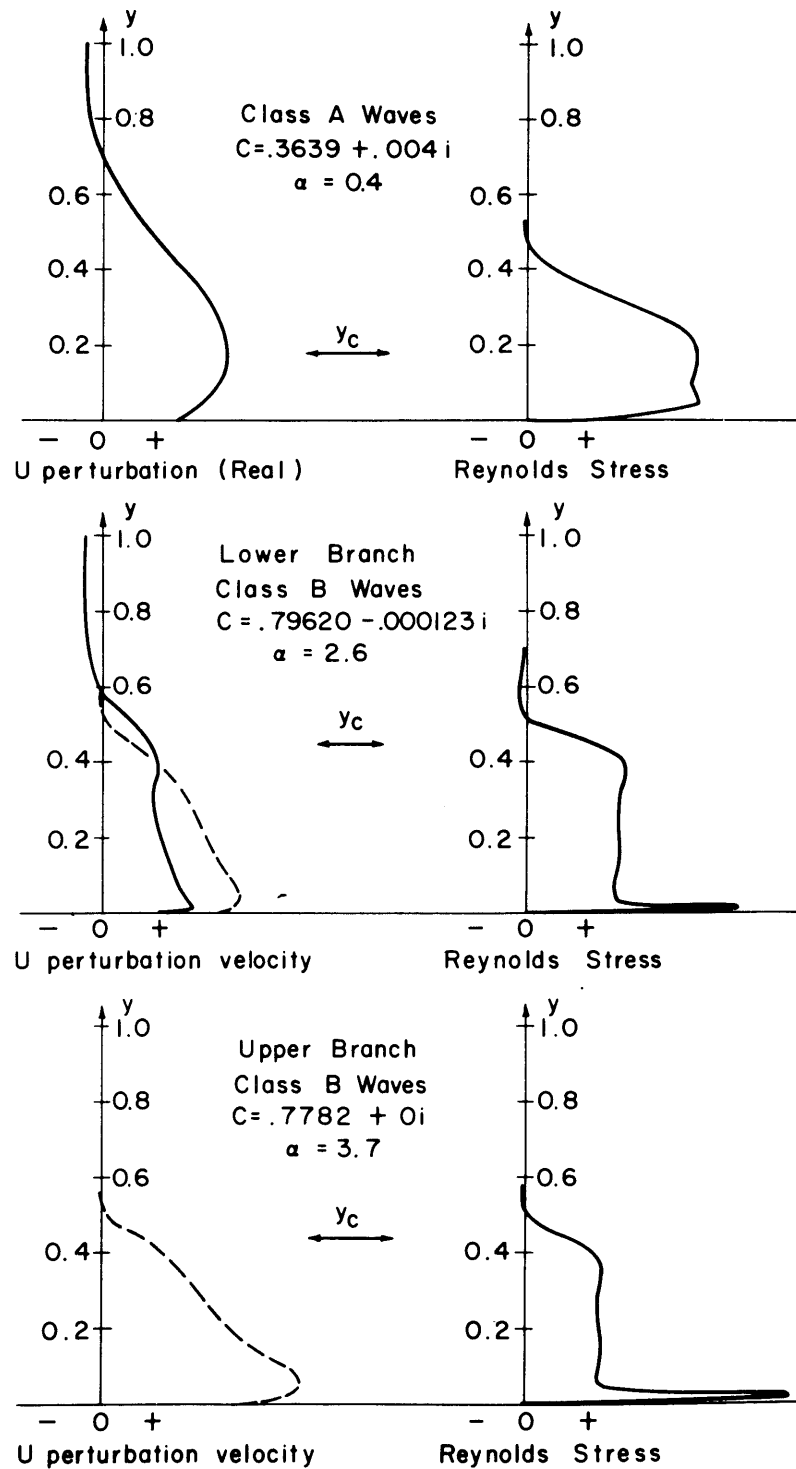


Figure 26. Disturbance Amplitude Distribution - Membrane Surface
 $c_o = 0.90$ $d_o = 0.05$ $\omega_o = 0.10$ $m_o = 1.0$ $R_o = 5000$
 ---- 90° out of phase

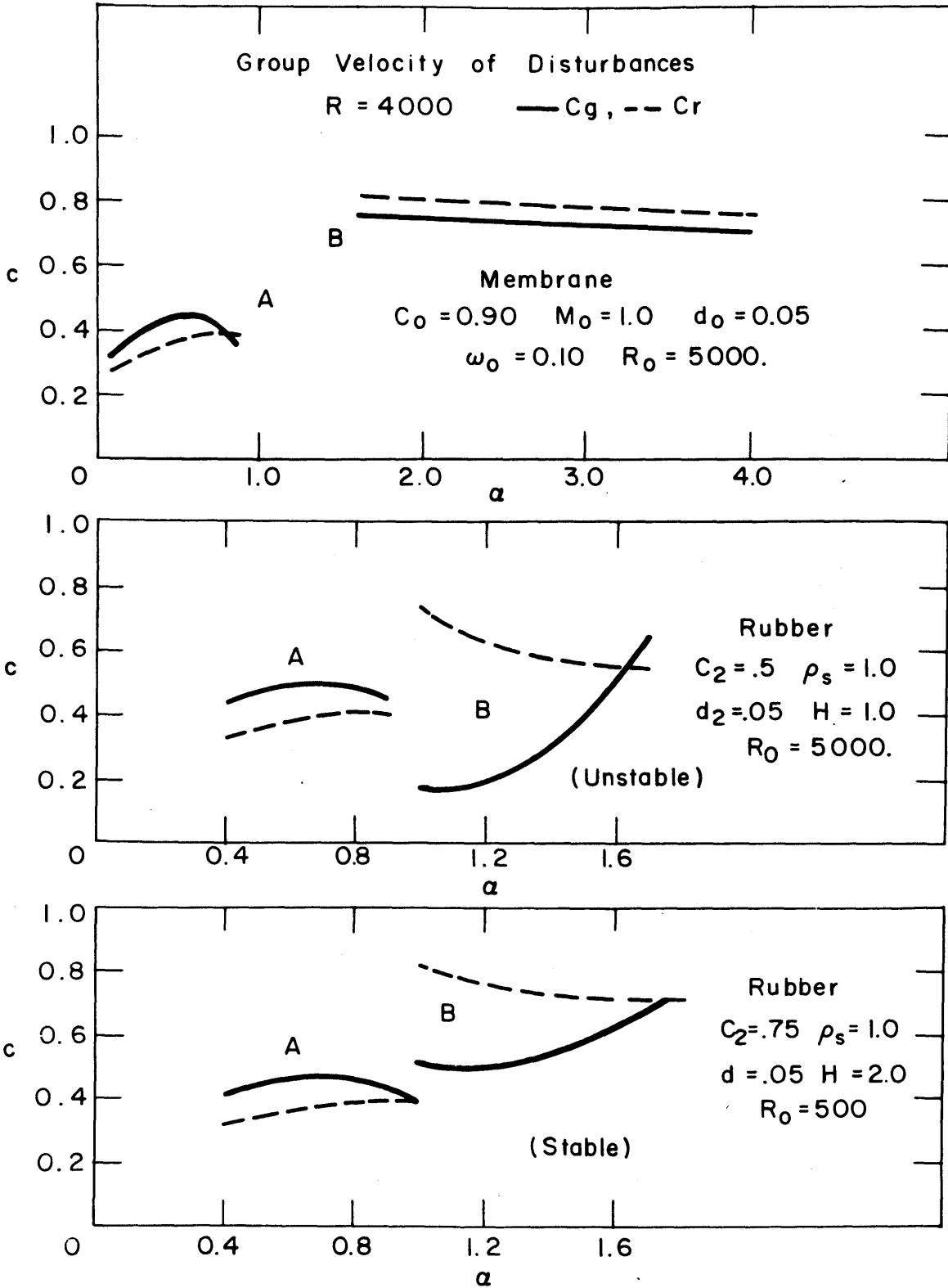


Figure 27
140

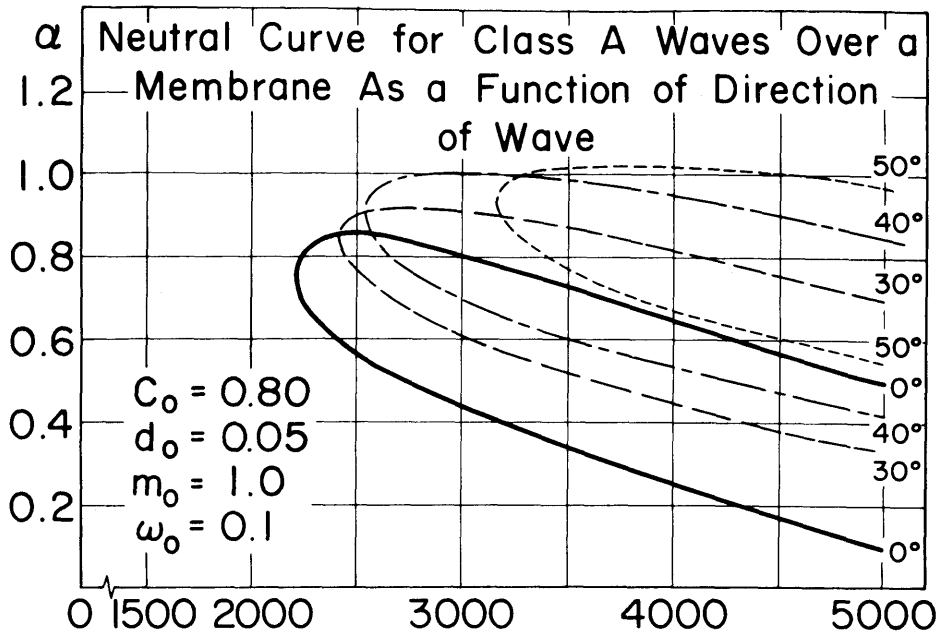


Figure 28

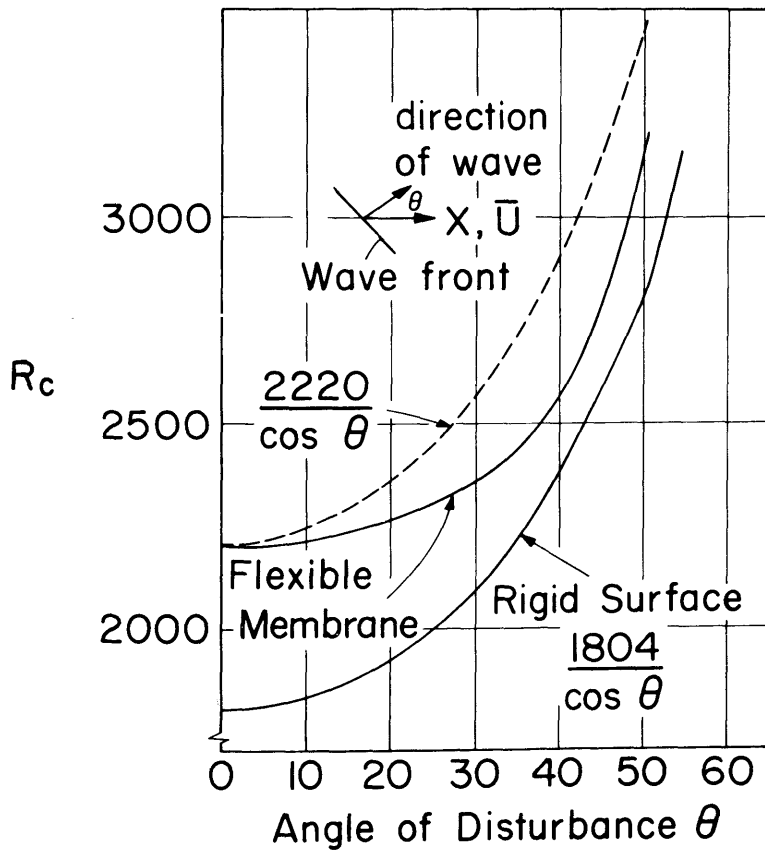


Figure 29. Critical Reynolds Number for Oblique Disturbances

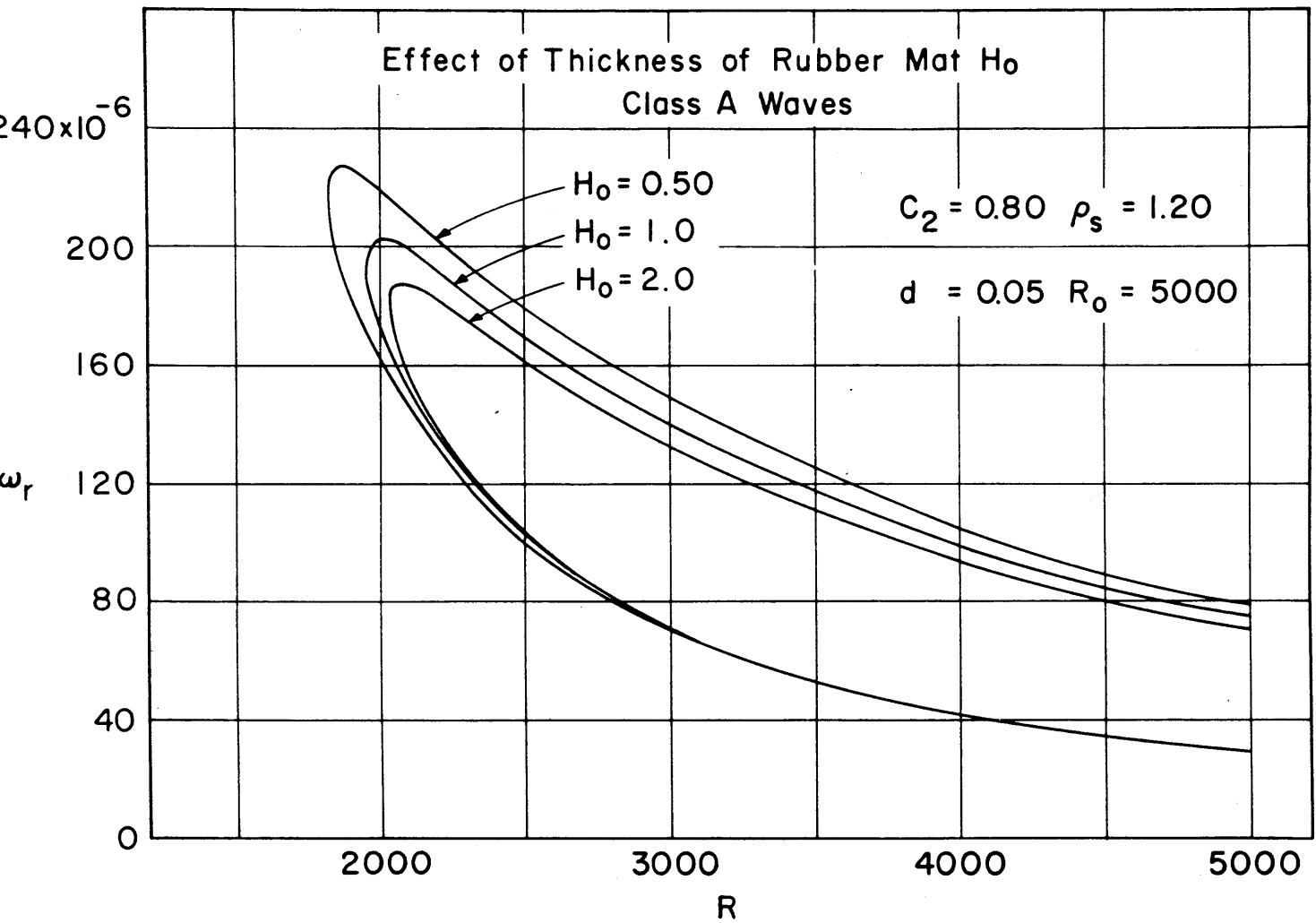


Figure 30

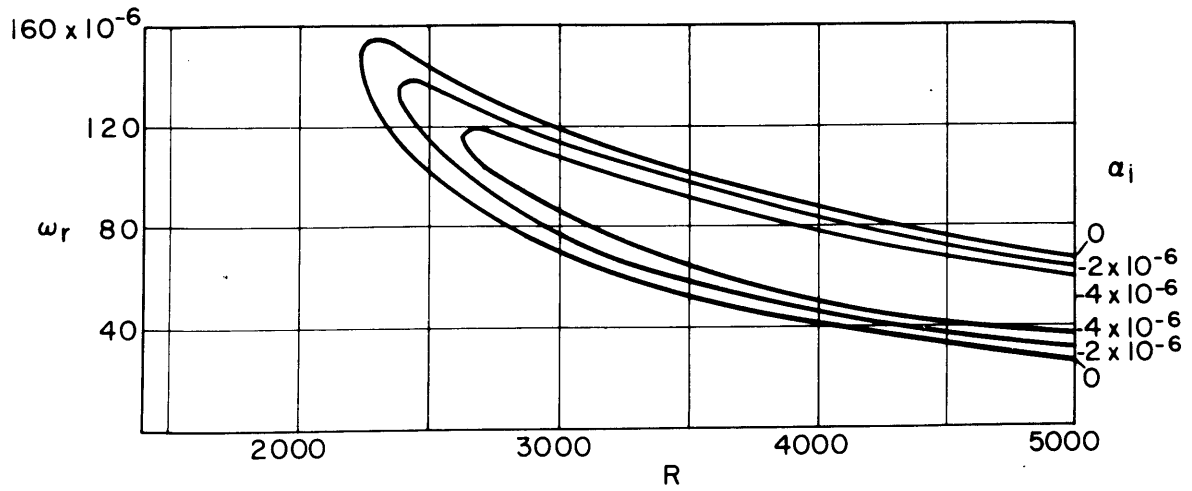
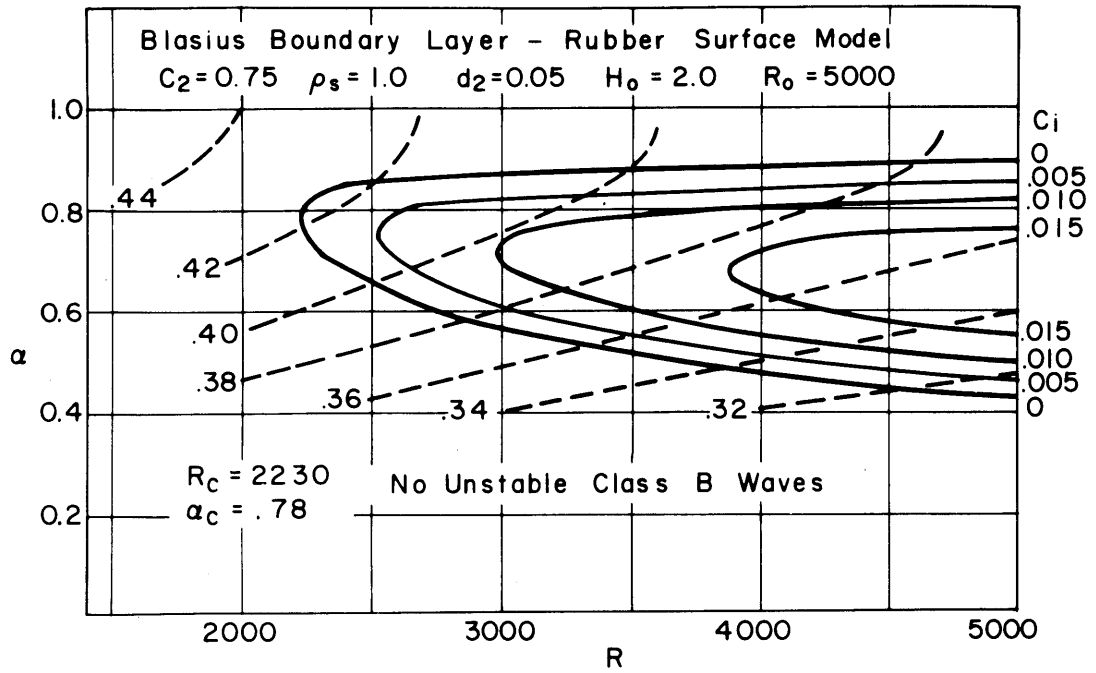


Figure 31. Eigenvalues for a Rubber Surface

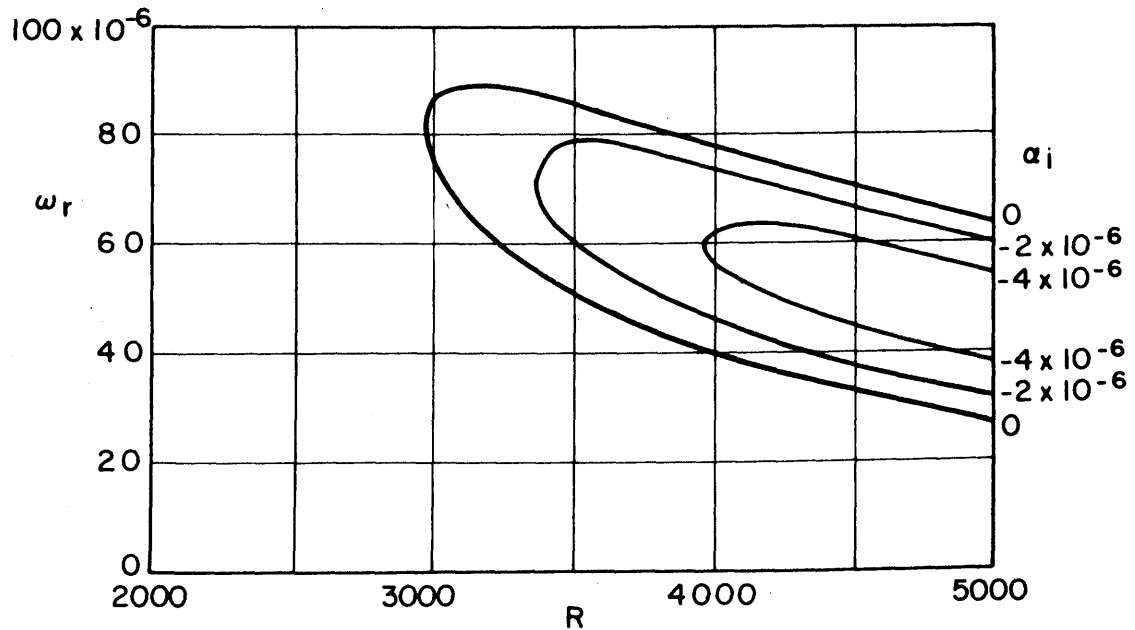
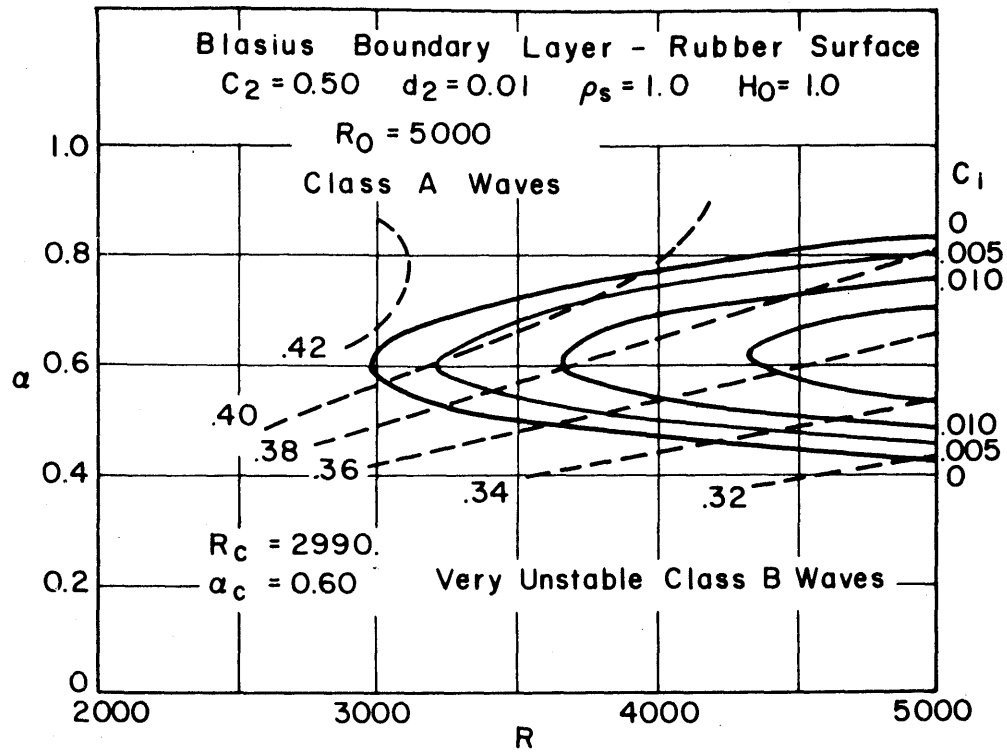


Figure 32. Eigenvalues for a Rubber Surface

BLASIUS BOUNDARY LAYER - RUBBER SURFACE

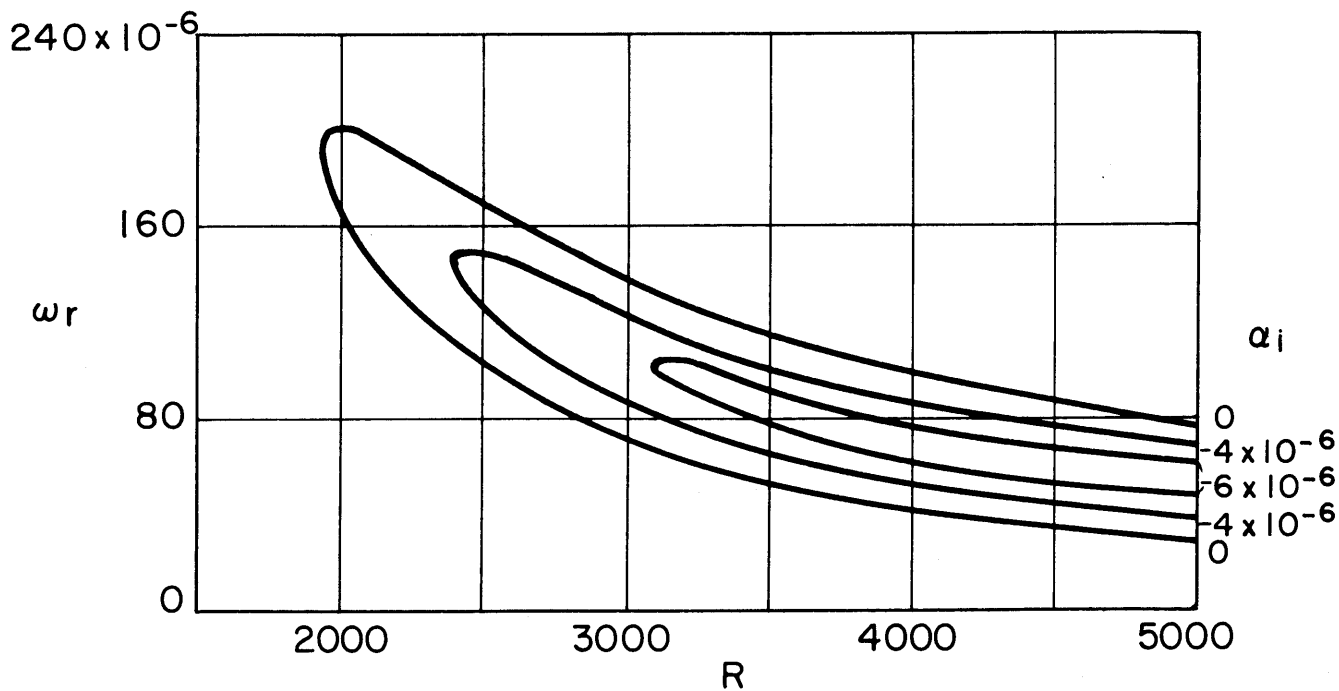
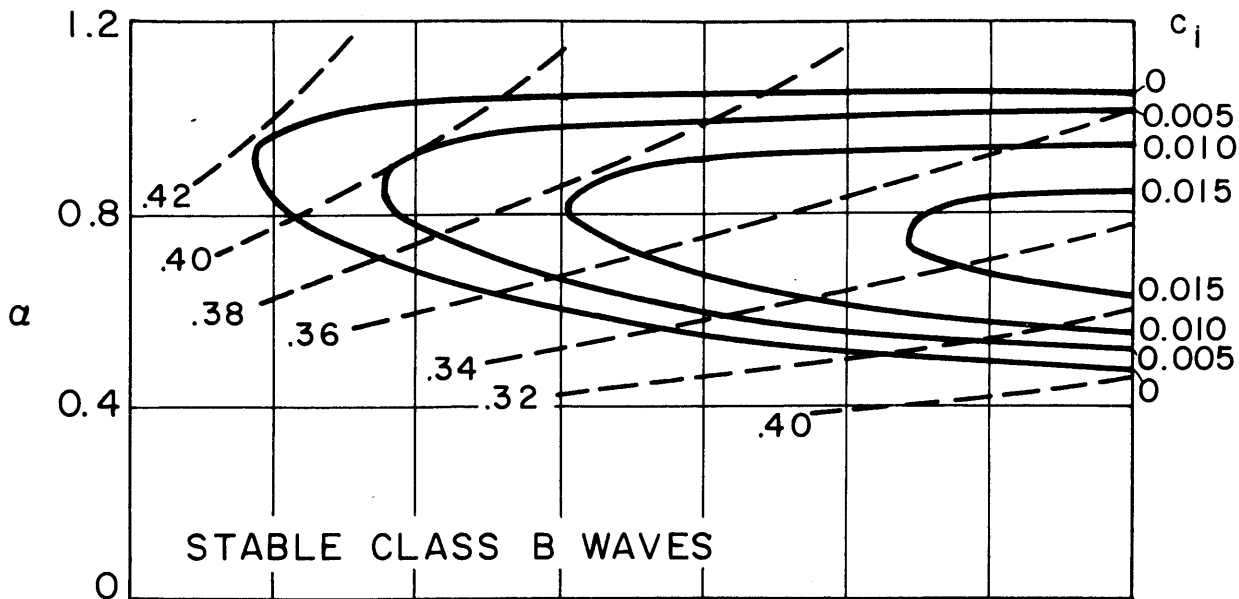


Figure 33. Eigenvalues for Rubber Surface
 $c_2 = 0.80$ $\rho_s = 1.2$ $d_2 = 0.05$
 $H_0 = 1.0$ $R_0 = 5000$

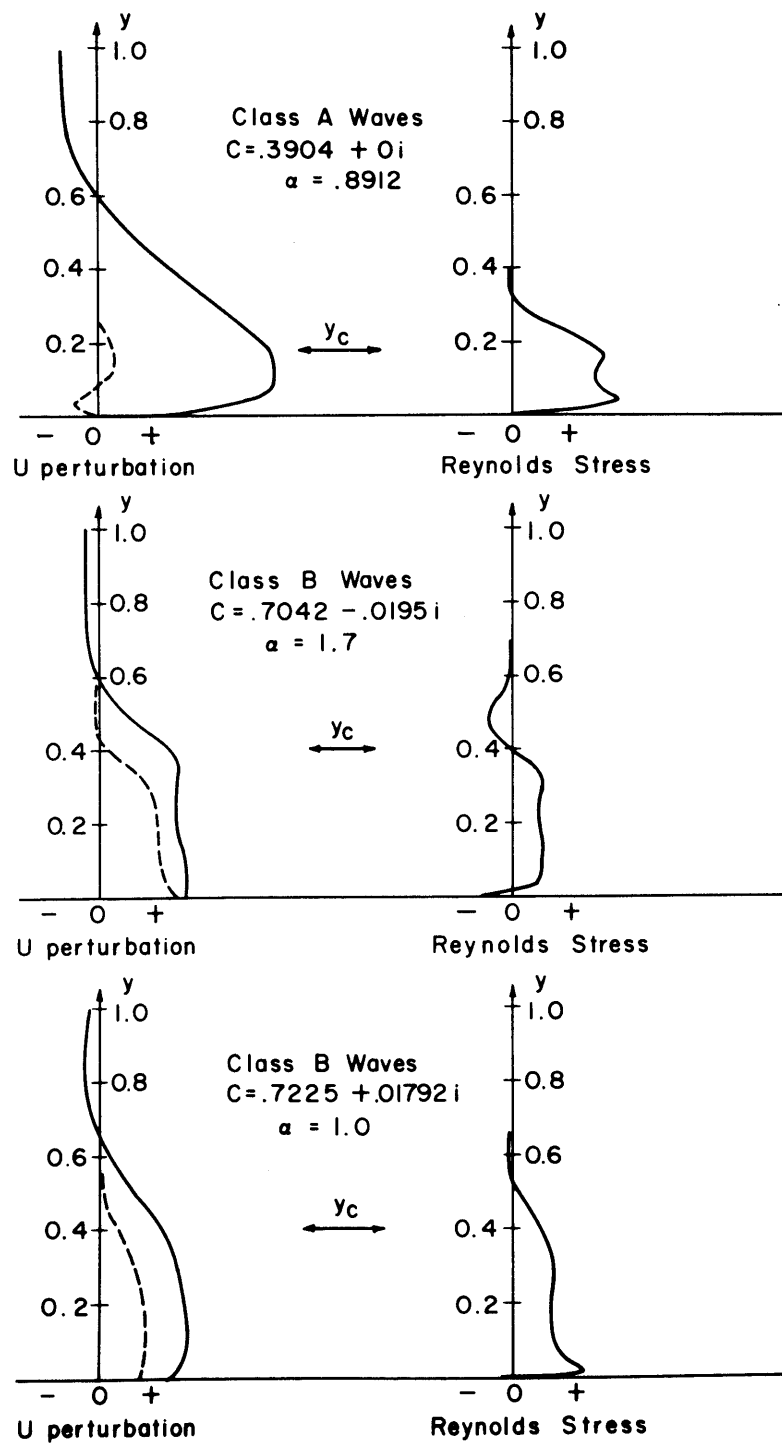


Figure 34. Disturbance Amplitude Distribution - Rubber Surface

(a)(b) $c_o = 0.75$ $d_2 = 0.05$ $H_o = 2.0$

(c) $c_o = 0.50$ $d_2 = 0.01$ $H_o = 1.0$

$\rho_s = 1.0$ $R_o = 5000$

--- 90° out of phase

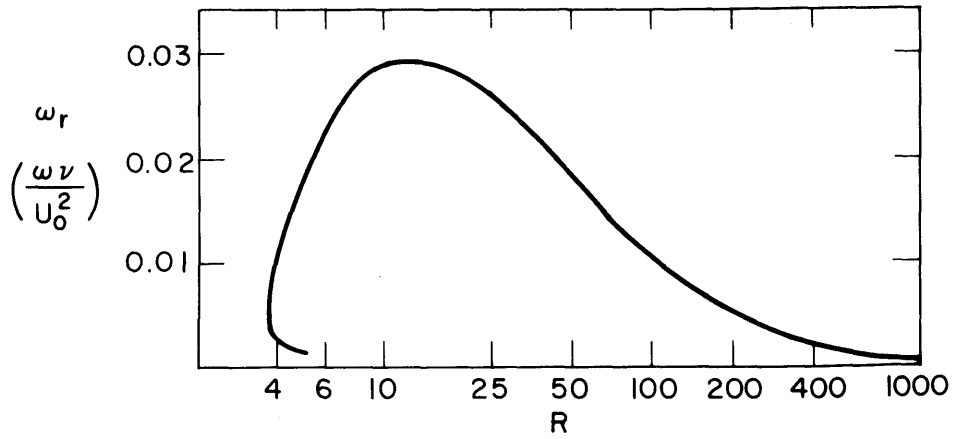
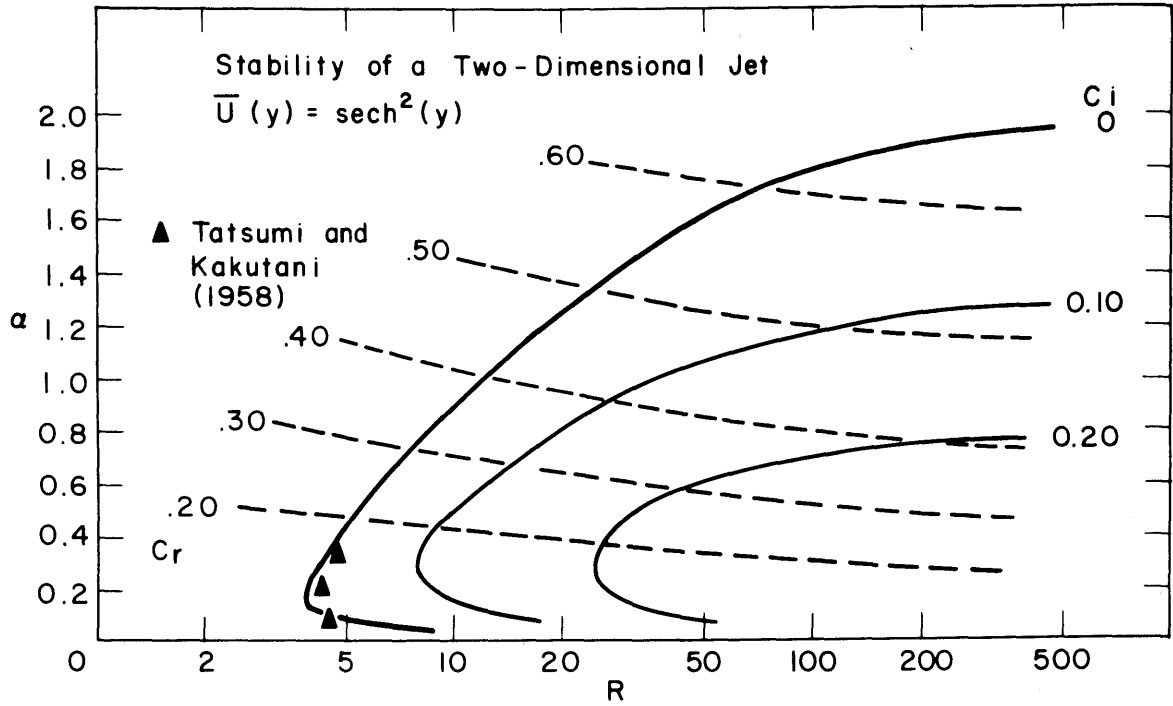


Figure 35

APPENDIX A

Asymptotic Solution of the Orr-Sommerfeld Equation

To solve the Orr-Sommerfeld equation (A.1)

$$\phi^{iv} - 2\alpha^2 \phi'' + \alpha^4 \phi - i\alpha R \{ (\bar{U} - c)(\phi'' - \alpha^2 \phi) - \bar{U}'' \phi \} = 0 \quad (\text{A.1})$$

one looks first for an expansion of the form

$$\phi(y) = \phi^{(0)} + \frac{1}{\alpha R} \phi^{(1)} + \dots \quad (\text{A.2})$$

where $\phi^{(0)}$ satisfies the "inviscid" equation

$$(\bar{U}(y) - c)(\phi^{(0)''} - \alpha^2 \phi^{(0)}) - \bar{U}''(y)\phi^{(0)} = 0 \quad (\text{A.3})$$

As described by Lin (1955), solutions of (A.3) can easily be obtained as convergent series in α^2

$$\phi^{(0)}(y) = (\bar{U}(y) - c) \sum_{n=0}^{\infty} \alpha^{2n} g_n(y) \quad (\text{A.4})$$

Inserting (A.4) into (A.3) one finds the set of equations

$$\begin{aligned} (\bar{U} - c)^2 g_0'' + 2\bar{U}'(\bar{U} - c)g_0' &= 0 \\ (\bar{U} - c)^2 g_{n+1}'' + 2\bar{U}'(\bar{U} - c)g_{n+1}' &= (\bar{U} - c)^2 g_n \end{aligned} \quad (\text{A.5})$$

which yields two sets of solutions

$$g_{0a} = 1 \qquad g_{0b} = \int_0^y (\bar{U}-c)^{-2} dy$$

and

$$g_{n+1}(y) = \int_0^y (\bar{U}-c)^{-2} dy \int_0^y (\bar{U}-c)^2 g_n dy \qquad (A.6)$$

giving two independent solutions

$$\phi_a^{(0)}(y; \alpha, \epsilon) ; \phi_b^{(0)}(y; \alpha, \epsilon)$$

as series in α^2 .

Let the combination of $\phi_a^{(0)}$ and $\phi_b^{(0)}$ that vanishes at ∞ be ϕ_1 . It is seen that ϕ_1 is well behaved except near $y = y_c$ where

$$\bar{U}(y_c) = c \qquad (A.7)$$

for real values of c . Lin discusses the correct technique for bypassing this singular point by considering c to have a small positive imaginary part.

It must be noted, however, that in the region near y_c , this solution ϕ_1 will not be a good approximation to the solution of the full equation. In order to examine the region around the critical point more closely, one must perform a stretching of coordinates around the critical point

$$\eta = (y - y_c) / \epsilon \qquad (A.8)$$

and expand ϕ in the series

$$\phi(y) = \phi_{(0)}(\eta) + \epsilon \phi_{(1)}(\eta) + \dots \qquad (A.9)$$

With this substitution, the Orr-Sommerfeld equation becomes

$$\frac{1}{\epsilon^4} \phi^{IV} - \frac{2\alpha^2}{\epsilon^2} \phi'' + \alpha^4 \phi + i\alpha R \left\{ \epsilon \bar{U}'_c \eta \left(\frac{1}{\epsilon^2} \phi'' - \alpha^2 \phi \right) - \bar{U}'' \phi \right\} = 0 \quad (\text{A.10})$$

$$' = \frac{d}{d\eta}$$

where it is noted

$$\bar{U}(y) - c \simeq \bar{U}'_c (y - y_c) = \epsilon \bar{U}'_c \eta \quad (\text{A.11})$$

If $\epsilon \sim (\bar{U}'_c \alpha R)^{-1/3}$, the leading terms in this equation are

$$\phi_{(0)}^{IV} + i\eta \phi_{(0)}'' = 0 \quad (\text{A.12})$$

The solution to this equation that dies at $+\infty$ is called

ϕ_3

$$\phi_3(y) = \int_{-\infty}^{\eta} \int_{-\infty}^{\xi} H_{1/3}^{(1)} \left(\frac{2}{3} [i\zeta]^{3/2} \right) \zeta^{1/2} d\zeta d\xi \quad (\text{A.13})$$

$$\eta = (\alpha R \bar{U}'_c)^{1/3} (y - y_c)$$

Tollmien gave an improved solution, uniformly valid for all y , of similar form (see Lin (1955))

$$\phi_3(y) = \left(\frac{\eta}{\bar{U} - c} \right)^{5/4} \int_{-\infty}^{\eta} \int_{-\infty}^{\xi} H_{1/3}^{(1)} \left(\frac{2}{3} [i\zeta]^{3/2} \right) \zeta^{1/2} d\zeta d\xi \quad (\text{A.14})$$

$$\eta = (\alpha R)^{1/3} \left[\frac{3}{2} \int_{y_c}^y (\bar{U}(\xi) - c)^{1/2} d\xi \right]^{2/3}$$

where the arguments go through as before only with more care in the definition of η and in the interpretation of (A.11).

Both ϕ_1 and ϕ_3 are solutions of the Orr-Sommerfeld equation that decay as $y \rightarrow \infty$, correct to order $(\alpha R)^{-1/3}$. They must be combined to satisfy the conditions of compatibility at $y = 0$.

$$\bar{\Phi} = \phi_1 + A \phi_3 \quad (\text{A.15})$$

so that

$$\frac{\bar{U}'_w}{c} \bar{\Phi}_w + \bar{\Phi}'_w = Y_{12}(\alpha, c) \hat{p}_w \quad (\text{A.16})$$

where

$$\hat{p}_w = \alpha^2 \int_0^\infty (\bar{U} - c - \frac{i\alpha}{R}) \bar{\Phi} dy - \frac{i\alpha}{R} \bar{\Phi}'_w \quad (\text{A.17})$$

$$\hat{p}_w \simeq \alpha^2 \int_0^\infty (\bar{U} - c) \bar{\Phi} dy + O(\alpha R^{-1}) \simeq c \phi'_{1w} + \bar{U}'_w \phi_{1w} + O(\alpha R)^{-1/3} \quad (\text{A.18})$$

(A.18) is derived from a partial integration of (A.3) discarding higher order terms.

Thus one finds that the combination

$$\bar{\Phi} = \phi_1 - (1 - c Y_{12}) \frac{(\bar{U}'_w \phi_{1w} + c \phi'_{1w})}{(\bar{U}'_w \phi_{3w} + c \phi'_{3w})} \phi_3 \quad (\text{A.19})$$

will satisfy (A.16). Define

$$\frac{\bar{U}_w'}{c} \frac{\phi_{3w}}{\phi_{3w}'} = -(1+\lambda)F(z) \quad (\text{A.20})$$

in which

$$\lambda = \frac{\bar{U}_w'}{c^{3/2}} \left[\frac{3}{2} \int_0^{\gamma_c} (c - \bar{U})^{1/2} dy \right] - 1 \quad (\text{A.21})$$

$$z = (\alpha R)^{1/3} \left[\frac{3}{2} \int_0^{\gamma_c} (c - \bar{U})^{1/2} dy \right]^{2/3} \quad (\text{A.22})$$

$$F(z) = - \frac{\int_{-\infty}^{-z} \int_{-\infty}^{\eta} \zeta^{1/2} H_{1/3}^{(1)} \left(\frac{2}{3} [i\zeta]^{3/2} \right) d\zeta d\eta}{z \int_{-\infty}^{-z} \zeta^{1/2} H_{1/3}^{(1)} \left(\frac{2}{3} [i\zeta]^{3/2} \right) d\zeta} \quad (\text{A.23})$$

then

$$\Phi_w = \phi_{1w} + (1 - c Y_{12}) \frac{(\phi_{1w} + \frac{c}{\bar{U}_w} \phi_{1w}') (1 + \lambda) F(z)}{1 - (1 + \lambda) F(z)} \quad (\text{A.24})$$

By the definition of boundary-layer admittance

$$Y_0 = \frac{i\alpha \Phi_w}{\hat{p}_w} = \frac{i\alpha \Phi_w}{\bar{U}_w' \phi_{1w} + c \phi_{1w}'}$$

$$Y_0 = \frac{i\alpha}{\bar{U}'_w} \left\{ \left(1 + \frac{c\phi'_{1w}}{\bar{U}'_w} \right)^{-1} + \frac{(1-cY_{12})(1+\lambda)F(z)}{1-(1+\lambda)F(z)} \right\} \quad (\text{A.25})$$

Introducing

$$u+iv = \left[1 + \frac{\bar{U}'_w \phi'_{1w}}{c\phi'_{1w}} \right]^{-1} \quad (\text{A.26})$$

one can write

$$Y_0(\alpha, c; R) = -\frac{i\alpha}{\bar{U}'_w} \left[u+iv + \frac{(1-c)Y_{12}(1+\lambda)F(z)}{1-(1+\lambda)F(z)} \right] \quad (\text{A.27})$$

Finally, defining

$$\mathcal{F}(z) = [1-F(z)]^{-1} \quad (\text{A.28})$$

(A.27) is reduced to

$$Y_0(\alpha, c; R) = -\frac{i\alpha}{\bar{U}'_w} \left[u+iv - \frac{\mathcal{F} - cY_{12}(1+\lambda)(\mathcal{F}-1)}{1+\lambda(1-\mathcal{F})} \right] \quad (\text{A.29})$$

As discussed by Landahl (1962), λ is less than 0.05 for $c \leq 0.7$, and z differs from $(\alpha R)^{1/3} c \bar{U}_w'^{-2/3}$ by less than 3 per cent for $c \leq 0.7$; one may neglect λ in (A.29) to get the simplified equation (A.30):

$$Y_0(\alpha, c; R) = - \frac{i\alpha}{\bar{U}_w'} [u + iv + (cY_{12} - 1)\mathcal{F} - cY_{12}] \quad (\text{A.30})$$

Setting the admittance of the boundary layer to the normal admittance of the surface, one gets

$$\Delta Y = Y_{11} - Y_0 = \frac{\bar{U}_w' Y_{11}}{i\alpha} + [u + iv + (cY_{12} - 1)\mathcal{F} - cY_{12}] = 0$$

or

$$\mathcal{F}(z) = [u + iv - \frac{i\bar{U}_w'}{\alpha} Y_{11} - cY_{12}] / (1 - cY_{12}) \quad (\text{A.31})$$

$$z = c \bar{U}_w'^{-2/3} (\alpha R)^{1/3}$$

The right-hand side of (A.31) is a function of (α, c) alone. For higher values of c , one may retain the correction terms $\lambda(c)$ to get

$$\mathcal{F}(z) = G(\alpha, c) = \frac{(1+\lambda)[u + iv - \frac{i\bar{U}_w'}{\alpha} Y_{11}] - (1+\lambda)cY_{12}}{1 + \lambda[u + iv - \frac{i\bar{U}_w'}{\alpha} Y_{11}] - (1+\lambda)cY_{12}} \quad (\text{A.32})$$

A simple technique for the solution of (A.32) is given by Landahl (1962). One can plot the function $\mathcal{F}(z)$ on an Argand diagram (\mathcal{F}_i vs \mathcal{F}_r) with Z a parameter along the curve. Since the right-hand side is a function of (α, c) alone, one can plot it for constant α letting (real) c be a

parameter on these curves. Intersections with $\mathcal{F}(z)$ are determined for a given α , z and c by interpolation. This is sufficient to determine the Reynolds number R and describe the neutral curve. A similar technique is described by Schlichting (1955).

A table of $\mathcal{F}(z)$ is provided by Miles (1959). Lin (1955) provides formulas

$$v = -\pi \bar{U}_w' c \left(\frac{\bar{U}_c''}{\bar{U}_c'^3} \right) (1 + O(c^3)) \quad (\text{A.33})$$

$$u = \frac{v}{\pi} \ln c + O(c) + \frac{\bar{U}_w' c}{\alpha^2} \left(\int_0^1 (\bar{U} - c)^2 dy \right)^{-1}$$

or

$$u = \frac{\bar{U}_w' c}{\alpha (1-c)^2} + O(1) \quad (\text{A.34})$$

for small c , α .

These ideas can be used to give estimates on the size of eigenvalues to be expected, but are insufficient for accurate computation unless more accurate representations for u , v are used.

APPENDIX B

Numerical Techniques

The numerical integration of the Orr-Sommerfeld equation is a difficult task because of the rapid growth of the "viscous" solution. Several numerical schemes for performing this integration have been attempted and all have been successful when sufficient care is taken to control parasitic errors.

A very accurate technique, which is a modification of a numerical scheme proposed by W. E. Milne and N. Obrechhoff as given by Hildebrand (1956), uses a one-step formula

$$\varphi(y-h) = \varphi(y) - \frac{h}{2} [\varphi'(y) + \varphi'(y-h)] \quad (\text{B.1})$$

$$-\frac{h^2}{10} [\varphi''(y-h) - \varphi''(y)] - \frac{h^3}{120} [\varphi'''(y-h) + \varphi'''(y)] + \mathcal{E}$$

where

$$\mathcal{E} = -\frac{h^7}{100800} \varphi^{vii}(\eta) \quad (y-h < \eta < y) \quad (\text{B.2})$$

Equation (B.1) is valid for sufficient iteration between the derivatives at $y-h$ to permit convergence to within acceptable tolerances. Equation (B.1) is written for $\varphi, \varphi', \varphi'', \varphi'''$ with $\varphi^{iv}, \varphi^v, \varphi^{vi}$ related to the lower derivatives. This is best illustrated by the following definitions.

$$S_1 = \varphi(y) - h\varphi'(y) + \frac{h^2}{2}\varphi''(y) - \frac{h^3}{6}\varphi'''(y)$$

$$S_2 = \varphi'(y) - h\varphi''(y) + \frac{h^2}{2}\varphi'''(y)$$

$$S_3 = \varphi''(y) - h\varphi'''(y)$$

$$S_4 = \varphi'''(y)$$

$$S_5 = F(\varphi, \varphi'', y) = G(\varphi, y)$$

$$S_6 = \frac{dF}{dy}(\varphi, \varphi'', y) = G(\varphi', y) + G'(\varphi, y)$$

$$S_7 = \frac{d^2F}{dy^2}(\varphi, \varphi'', y) = G(\varphi'', y) + 2G'(\varphi', y) + G''(\varphi, y)$$

(B.3)

Using (B.3) in four sets of (B.1), one finds

$$\varphi(y-h) = S_1 + \frac{h^4}{1200}(7T_5 + 43S_5) + \frac{h^5}{2400}(5T_6 - 11S_6) + \frac{h^6}{3600}(T_7 + S_7)$$

$$\varphi'(y-h) = S_2 - \frac{h^3}{30}(T_5 + 4S_5) + \frac{h^4}{1200}(-13T_6 + 23S_6) - \frac{h^5}{800}(T_7 + S_7)$$

$$\varphi''(y-h) = S_3 - \frac{h^2}{20}(3T_5 + 7S_5) + \frac{h^3}{120}(5T_6 - 7S_6) + \frac{h^4}{240}(T_7 + S_7) \quad (\text{B.4})$$

$$\varphi'''(y-h) = S_4 - h(T_5 + S_5) - \frac{h^2}{10}(T_6 - S_6) - \frac{h^3}{120}(T_7 + S_7)$$

where in (B.4)

$$T_5 = G(\varphi, y-h)$$

$$T_6 = G(\varphi', y-h) + G'(\varphi, y-h) \quad (B.5)$$

$$T_7 = G(\varphi'', y-h) + 2G'(\varphi', y-h) + G''(\varphi, y-h)$$

The results of $\varphi \dots \varphi''''$ are tested for convergence on successive iterations. If convergence is not obtained to the desired accuracy, new values for $T_5 \dots T_7$ are used and (B.9) is recomputed. The calculation of $S_1 \dots S_6$ gives excellent first estimates for the new values at $(y-h)$, so no predictor formula is used.

However, the computation proceeds rather slowly, partly due to its iterative nature, and partly because of the large number of multiplications involved. Furthermore, knowledge of G' and G'' required the added derivatives \bar{U}' , \bar{U}'''' , \bar{U}^{iv} of the velocity profile, which information is generally not available.

In spite of these objections, the results of the integration showed excellent agreement with other methods of solutions of the Orr-Sommerfeld equation, validating the basic hypothesis. Furthermore, the efficiency of the purification scheme as verified by using a technique where the numerical integration was, for all practical purposes, exact.

The accuracy of the integration scheme was such that the results of the integration were changed by less than 0.01 per cent by a changing step size by a factor of 10. It was found that 50 integration steps gave the most rapid com-

putation time, and successful integrations were performed with as few as 12 steps. However, for fewer than 50 steps, any direct savings in the number of computations was negated by added iterations to convergence. In these tests, convergence to four digits in the third derivative was the only iteration check required. Typical computation time was ten seconds on the IBM 7090 digital computer.

The next successful integration scheme used (and the form used in the final version) was a standard Runge-Kutta integration for fourth order equations as presented by Collatz (1951). The accuracy of this scheme was checked by comparing the integrations with the former scheme, other authors, and varying step size. The scheme used is shown in Table B.1.

at y

$$V_{00} = \varphi(y)$$

$$V_{10} = -h \varphi'(y)$$

$$V_{20} = h^2/2 \varphi''(y)$$

$$V_{30} = -h^3/6 \varphi'''(y)$$

$$k_1 = h^4/24 F(V_{00}, 2V_{20}/h^2, y)$$

at $y-h/2$

$$V_{01} = V_{00} + \frac{1}{2} V_{10} + \frac{1}{4} V_{20} + \frac{1}{8} V_{30} + \frac{1}{16} k_1$$

$$V_{11} = V_{10} + V_{20} + \frac{3}{4} V_{30} + \frac{1}{2} k_2$$

$$V_{21} = V_{20} + \frac{3}{2} V_{30} + \frac{3}{2} k_1$$

$$V_{31} = V_{30} + 2k_1$$

$$k_2 = h^4/24 F(V_{01}, 2V_{21}/h^2, y-h/2)$$

at $y-h$

$$V_{02} = V_{00} + V_{10} + V_{20} + V_{30} + k_2$$

$$V_{12} = V_{10} + 2V_{20} + 3V_{30} + 4k_2$$

$$V_{22} = V_{20} + 3V_{30} + 6k_2$$

$$V_{32} = V_{30} + 4k_2$$

$$k_3 = h^4/24 F(V_{02}, 2V_{22}/h^2, y-h)$$

$$k = 1/5(8k_1 + 8k_2 - k_3)$$

$$k' = 1/5(9k_1 + 12k_2 - k_3)$$

$$k'' = 2k_1 + 4k_2$$

$$k''' = 2/3(k_1 + 4k_2 + k_3)$$

$$\varphi(y-h) = V_{00} + V_{10} + V_{20} + V_{30} + k$$

$$\varphi'(y-h) = -\frac{1}{h}(V_{10} + 2V_{20} + 3V_{30} + k')$$

$$\varphi''(y-h) = \frac{2}{h^2}(V_{20} + 3V_{30} + k'')$$

$$\varphi'''(y-h) = -\frac{6}{h^3}(V_{30} + k''')$$

Table B.1

Computations of the effect of the placement of the outer edge of the boundary layer were made by Powers, et. al. (1963). They computed results by varying $\delta \sqrt{U_0/\nu} x$ for the Blasius profile selecting values of 5, 6, 10. The results for $\delta \sqrt{U_0/\nu} x = 6$ were indistinguishable from those for 10, and the smaller number was selected for these calculations.

The Runge-Kutta scheme used has sufficient accuracy for $\alpha R \leq 10^4$ with the selected step size of 0.016 (64 integration steps). The time for integration averages to 31/60 of a second on the IBM 7094, 47/60 on the IBM 7090. The integration routine is programmed in 7090/94 FORTRAN II using a FORTRAN complex arithmetic package. Additional savings would result by programming in an assembler language such as FAP, or by writing out all of the complex operations.

APPENDIX C

Computer Programs

C.1 Use of the Computer Programs

The calculation of the eigenvalues of the Orr-Sommerfeld equation is performed by a series of computer programs written in the IBM FORTRAN and FAP computer languages. A description of these programs and sample listings of the more important subroutines is given in following sections. From these descriptions, interested users can supply their desired velocity profiles, compliant boundary models, and eigenvalue criterions, either from the described programs or from their own (compatible) programs.

Input to these programs is in the form of five standard IBM punched cards (detailed in Table C.1 below) which specify the parameters of the boundary, the wave number and Reynolds-number range to be investigated, initial estimates for the eigenvalues, and the desired tolerance.

Output from the programs is a buffered printout of the eigenvalues calculated at the desired wave numbers and Reynolds numbers, and includes computations of additional useful values such as the complex frequency, the group velocity, and the spatial amplification rates. In addition, a series of auxiliary programs have been written to interpolate the calculated eigenvalues to assist in the plotting of the stability loci.

These subroutines print identification labels on the output to specify the velocity profile, type of boundary and its parameters, and the eigenvalue criterion used. Provision is also made to accept a 5-digit sequence number to aid in identifying the output, and the date and time of the

run. All of the results are presented in a clearly readable and labeled form, so no difficulty should be experienced in their interpretation.

Data Card Number	Column	Information	Format*
1	1-80	Surface Parameters (up to 8) (See Table C.2)	8F10.4
2	1-80	Wave numbers (up to 8)	8F10.4
3	1-80	Reynolds numbers (up to 8)	8F10.4
4	1-20	First estimate of c_r, c_i at R_1, α_1 (1,1)	2F10.4
	21-40	Second estimate of c_r, c_i at (1,1)	2F10.4
	41-60	Estimate of increment of c_r, c_i at R_1, α_2 from (1,1)	2F10.4
	61-80	Estimate of increment of c_r, c_i at R_2, α_1 from (1,1)	2F10.4
5	1	Number of α 's on Card 2	I1
	2	Number of R's on Card 3	I1
	3-7	Identification number (less than 32628)	I5
	8-15	Tolerance for eigenvalue criterion (order of 0.005)	E8.1

Table C.1. Format of Input Cards for Computer Programs

Note: Additional data may be supplied for additional cases repeating the format of Cards 1 - 5.

* IBM FORTRAN II format specification

Type of Surface	Variable	Column
Membrane	c_0	1-10
	m_0	11-20
	d_0	21-30
	not used	31-40
	ω_0	41-50
	not used	51-70
	R_0	71-80
Rubber Surface	c_2	1-10
	ρ_5	11-20
	d_2	21-30
	H_0	31-40
	not used	41-70
	R_0	71-80
Shear Flows	k - Note 1	1-10
	s - Note 2	11-20
	Note 3	21-30
	not used	31-80

Table C.2. Details of First Input Data Card

Note 1: For profiles that are $f(ky)$ - results are presented for $f(y)$

Note 2: If non-zero, ϕ_3 integration starts at $e^{-(\alpha R)^s}$ but argument of the exponential must be < 80

Note 3: If non-zero, results of every estimate are printed

C.2 Description of Computer Programs

All of the following programs are written for compatibility with the IBM FORTRAN II Monitor System (FMS). The instructions are in general compatible with the IBM 709/7090/7094 computers with specific exceptions as noted below. A short description of the function of each program follows, with the more important options detailed. Sample listings are presented in the following section.

- (MAIN) Executive program labeled SEEKn. This program reads the input data, allocates storage for the eigenvalues, and directs the calculation of the eigenvalues. There is provision for complete recovery of all buffered results if overflow occurs in the integration routine, if convergence is not obtained for a specific eigenvalue within a prescribed number of estimates (30), or if insufficient time remains to complete another calculation. (MAIN) provides for labeling and printout of all of the eigenvalues, and calls the interpolation subroutines. The available options of main are:
- SEEK7 - The current result option with the above features, FORTRAN II coded.
 - SEEK5 - MAD coded program to test compatibility of the two programming systems. (obsolete)
 - SEEK9 - For use with shear flows. This program provides the feature listed in Note 1 of Table C.2.
- UNTRAP (FPT) This routine is a FAP coded modification of the MIT version of IBM (FPT), the floating point trap routine. The UNTRAP option permits recovery and printout in case an overflow condition is detected in a floating point calculation. If UNTRAP is not called, the execution of the routine halts further calculation and returns control back to the monitor. The argument of untrap is a statement label in MAD or FAP, or a variable previously appearing in a FORTRAN II ASSIGN statement.
- ADMIT The numerical integration routine is called ADMIT, and its options are labeled ADMITn. This performs the numerical integration of the Orr-Sommerfeld equation, getting the velocity profile from subroutine PROFIL. It features the purification scheme, and outputs the real and

imaginary parts of the boundary-layer admittance.
The arguments of ADMIT are $(R, \alpha, c_r, c_i, Y_{or}, Y_{oi})$

ADMIT1 - A FORTRAN coded routine that uses a modified Milne-Obrechhoff integration scheme to integrate through the boundary layer in 51 steps. This routine makes extensive use of FORTRAN II complex arithmetic subroutines.

ADMIT2 - Same as above except (1) FAP coded, (2) Uses MACRO FAP operation, and (3) Blasius profile is built in.

ADMIT8 - A Runge-Kutta integration scheme of 63 steps is used. Handles arbitrary flexible surfaces by calling SURFX to provide transverse admittance. Execution time 31/60 sec on IBM 7094.

ADMIT7 - Similar to ADMIT8 except uses 64 steps to integrate for sinuous disturbances of jets and shear flows.

ADMIT9 - Similar to ADMIT8 except saves results of the numerical integrations in a buffer for use in constructing eigenfunctions.

PROFIL
IDAD
OUTER
WALL

These are the multiple entry points to one FAP coded subroutine that provides the varied functions of (1) storing the velocity profile for the ADMIT routine by using the arguments shown in the listing. (2) IDAD is an identification entry that printout the type of integration routine, velocity profile, and the time and date of the run by calling GETTM. (3) OUTER provides the option for using profiles that asymptotically do not reach the normalizing value \bar{U}_0 , and (4) WALL provides the slope of the velocity profile at the wall. The available options of this routine are

BLASBL - The Blasius boundary layer for ADMIT8-9.

FS-.05 - The Falkner-Skan similarity profile for an adverse pressure gradient flow for ADMIT8-9.

KLEB - A profile measured experimentally by Klebanoff, Tidstrom, and Sargent (1961) for ADMIT8-9.

SECHn - Jet profile of the form $\text{sech}^2(ny)$ for ADMIT7

TANHn - Shear flow of the form $\tanh(ny)$ for ADMIT7

PROF1 - Blasius boundary layer for ADMIT1

COMBIN This routine is a two entry point FAP subroutine that
IDCOMB provides the eigenvalue criterion that is used by
 (MAIN). It accepts arguments of the form (α , c_r , c_i ,
 Y_{or} , Y_{oi}) calls the surface normal admittance
 routine SURFY, and returns an appropriate combination
 of Y_o and Y_{11} in place of Y_o . IDCOMB identifies the
 combination used at object time. The options of this
 routine that have been used are

COMBIN1 $Y_o - Y_{11}$

COMBIN2 $(Y_o - Y_{11}) / | Y_{11} |$

COMBIN3 $Y_o / Y_{11} - 1$

COMBIN4 Y_o

COMBIN5 $Y_o^{-1} - Y_{11}^{-1}$

EIGEN This subroutine is a FORTRAN coded program to determine
 the next estimate for the eigenvalue. Its arguments
 are found in the listings. Its options are

EIGEN1 - A linear estimation formula

EIGEN2 - Uses all previous estimates of the eigenvalue
 to compute the next try by a Lagrangian ex-
 trapolation formula of the inverse eigenvalue
 criterion.

EIGEN3 - Similar to EIGEN2 except that if convergence
 is not attained after 6 attempts, the estimates
 are put in order (best guess last) and the
 smallest four values are used for subsequent
 calculations.

EIGEN4 - A direct calculation of the next guess using
 the smallest three previous guesses and a
 quadratic formula. This routine does not
 work well due to the multivalued solution it
 provides.

SURFX This is a three entry point FAP coded routine that gives
SURFY the tangential and normal admittances, and identifies
IDSURF the type of surface model used and its parameters.

SOLID - Rigid surface admittance (i.e., zero)

SURF1 - Provides calling sequence for FORTRAN coded routine SURF2 according to the following list

$$\text{SURFX}(\alpha, c_r, c_i, Y_{12r}, Y_{12i}) = \text{SURF2}(\alpha, c_r, c_i, Y_{12r}, Y_{12i}, 1)$$

$$\text{SURFY}(\alpha, c_r, c_i, Y_{11r}, Y_{11i}) = \text{SURF2}(\alpha, c_r, c_i, Y_{11r}, Y_{11i}, 2)$$

$$\text{IDSURF} = \text{SURF2}(0, 0, 0, 0, 0, 3)$$

For any given α and c , SURFX must be called before SURFY for correct results.

The options of SURF2 are

WATER1 - inviscid liquid with no surface tension

MEMBR2 - spring supported membrane surface

MEMBR3 - "tailored" membrane surface

RUBBR2 - rubber surface model

EXTRAP A FAP coded subroutine that provides the first two estimates of the next eigenvalue. The logic for the prediction is in (MAIN).

SMOOTH A FAP coded program that provides FORTRAN calling sequences for SMOOT. This program is called by (MAIN) to smooth and differentiate the phase speed to determine the group velocity. It will only work given at least 7 values of α in the input list.

SMOOT Modified version of IBM SHARE subroutine CL SMD3 (SHARE listing #331)

ORDER This short FORTRAN coded subroutine rearranges the eigenvalues stored in the Buffers of (MAIN) in the correct sequence needed by POINTS

POINTS This routine provides calling sequences for a series of FAP coded subroutines that interpolate the eigenvalues and print out the results of the interpolation in a form suitable for plotting. These are a very specialized series of subroutines, useful only in conjunction with the storage and calling sequence shown in (MAIN). They include several novel programming features, but can be used only on the IBM 7094 computer, for they use instructions peculiar to that

machine. All routines are programmed in 7094 MACRO-FAP. The other routines in this package are called MINMAX, LOADER, ODD, SAVE, POUT.

Listing of these programs are very long and will not be included in this report. Storage requirements are 928 lower core locations plus approximately 14500 locations in COMMON for buffers.

There is a series of other routines called that are either used for debugging purposes or peculiar to the MIT version of the FMS system. Acceptable dummies for these routines are shown below written in the FAP language.

	FAP		
	COUNT	17	
	ENTRY	RSCLCK	
	ENTRY	STOPCL	
	ENTRY	TIMLFT	
	ENTRY	GETTM	
	ENTRY	DUMPIT	
	ENTRY	FTNPM	
	ENTRY	UNTRAP	Note 1
RSCLCK	TRA	1,4	
STOPCL	TRA	2,4	
GETTM	TRA	3,4	
TIMLFT	CLA	= 3000B17	
	STO*	1,4	
	TRA	2,4	
DUMPIT	EQU	RSCLCK	
FTNPM	EQU	STOPCL	
UNTRAP	EQU	STOPCL	Note 1
	END		

Note 1: only if standard IBM (FPT) is used.

C.3 Listing of the Important Computer Programs

While it is recognized that it is very difficult to follow the programming techniques of another, the following listings are provided as examples of the programming performed. All of the subsequent programs are reproductions of decks that have been successfully compiled and run. Only samples of the most important programs are presented in this section, since it is felt that a complete listing of all options would not be of general interest.

```

*      LIST8
*      LABEL
CSEEK7  ROOT SEEKER PROGRAM
C
      DIMENSION C(60),Y(60),AMP(30),A(8),R(8),CR(8,8),CI(8,8),OMR(8,8),
1      OMI(8,8),AM(8,8),KT(8,8),BR(8),BI(8),ARG(8)
      DIMENSION CG(8,8),AI(8,8)
      DIMENSION ERASE(2)
      EQUIVALENCE (ERASE(1),C(1))
      COMMON ARG,ARE
C      UNTRAP INSURES PRINTOUT IN CASE OF OVERFLOW IN ADMIT
      ASSIGN 298 TO LP
      CALL UNTRAP(LP)
C      ERASE CLEARS OUT ALL STORAGE LOCATIONS BEFORE YOU START
999    DO 601 I=1,694
601    ERASE(I)=0.
C
C      INPUT OF DATA ** 8- ARG'S TO COMMON FOR SURFACES
C      8 ALPHA'S AND R'S, 8 VALUES OF C TO HELP FIND NEXT EV'S
C      JM IS NUMBER OF ALPHAS, KM NUMBER OF R'S ICASE LABELS OUTPUT
C      ETA IS TOLERANCE
1      READ 1,(ARG(I),I=1,8),(A(I),I=1,8),(R(I),I=1,8), C1R,C1I,C2R,
1      C2I,CRWA,CIWA,CRWR,CIWR, JM,KM,ICASE,ETA
1      FORMAT(4(8F10.4/),2I1,I5,E8.1)
C
C      SET UP INITIAL ESTIMATES ON EIGENVALUES
      C(1)=C1R
      C(31)=C1I
      C(2)=C2R
      C(32)=C2I
C      START OF LOOP OVER ALL ALPHAS AND ALL R'S
      DO 292 K=1,KM
      DO 291 J=1,JM
      CALL RSCLCK
      I=1
      ARE=R(K)
      ALPHA=A(J)
C      101 AND DOWN FINDS Y(ALPHA,C,R) TO WORK WITH
101    SEAR=C(I)
      SEAI=C(I+30)
      CALL ADMIT(ARE,ALPHA,SEAR,SEAI,YEAR,YEAI)
      CALL COMBIN (ALPHA,SEAR,SEAI,YEAR,YEAI)
      AMP(I)=SQRTF(YEAR**2+YEAI**2)
      Y(I)=YEAR
      Y(I+30)=YEAI
C      IF AMP(Y) IS WITHIN TOLERANCE, C IS AN EIGENVALUE
      IF (AMP(I)-ETA)200,200,102
C      NEED AT LEAST TWO ESTIMATES BEFORE AUTO-PREDICTOR CAN BE USED
102    IF(I-2)103,104,104
103    I=2
      GO TO 101
C      SUBROUTINE EIGEN COMPUTES THE NEXT ESTIMATE FOR C
104    CALL EIGEN (C,Y,AMP,I)
      I=I+1

```

```

C     ONLY STORAGE FOR 30 TRIES
      IF(I-30)101,299,298
C     CONTROL GOES TO 200 IF A EV IS FOUND
200  AM(K,J)=AMP(I)
      CR(K,J)=SEAR
      CI(K,J)=SEAI
      OMR(K,J)=ALPHA*SEAR/ARE
      OMI(K,J)=ALPHA*SEAI/ARE
201  CALL STOPCL (JT)
      KT(K,J)=JT
      CALL TIMLFT(LT)
C     TEST TO SEE IF ENOUGH TIME IS LEFT FOR ANOTHER CASE
      IF(JT-LT+1500)290,297,297
C     FROM NOW TILL 292 -- TRY TO PREDICT FIRST ESTIMATES FOR NEXT PT
290  IF(J-1)500,400,401
400  C(1)=CR(K,J)
      C(31)=CI(K,J)
      GO TO 403
401  DO 402  L=1,J
      BR(L)=CR(K,L)
402  BI(L)=CI(K,L)
      C(1) =EXTRAP(BR,A,A(J+1),J)
      C(31)=EXTRAP(BI,A,A(J+1),J)
403  IF(K-2)405,406,407
405  C(2) =C(1)+CRWA
      C(32)=C(31)+CIWA
      GO TO 291
406  C(2)=CR(1,J+1)
      C(32)=CI(1,J+1)
      GO TO 291
407  DO 408  L=1,K
      BR(L)=CR(L,J+1)
408  BI(L)=CI(L,J+1)
      C(2) =EXTRAP(BR,R,R(K),K-1)
      C(32)=EXTRAP(BI,R,R(K),K-1)
291  CONTINUE
      IF(JM-7)414,415,415
415  DO 416  L=1,JM
416  BR(L)=CR(K,L)
C     SMOOTH TAKES THE DERIVITIVE D(CR)/D(ALPHA) TO GET THE GROUP
C     VELOCITY AND ALPHA-I
      CALL SMOOTH(A,BR,JM,1,2,0)
      DO 413  L=1,JM
      CG(K,L)=CR(K,L)+A(L)*BR(L)
413  AI(K,L)=-OMI(K,L)/CG(K,L)
414  IF(K-1)500,409,410
409  C(1)=CR(K,1)
      C(31)=CI(K,1)
      GO TO 412
410  DO 411  L=1,K
      BR(L)=CR(L,1)
411  BI(L)=CI(L,1)
      C(1) =EXTRAP(BR,R,R(K+1),K)
      C(31)=EXTRAP(BI,R,R(K+1),K)
412  C(2)=C(1)+CRWR
      C(32)=C(31)+CIWR
292  CONTINUE

```



```

C      PRINTOUT OF THE RESULTS
300    CALL IDAD
      CALL IDCOMB
      CALL IDSURF
      PRINT 6, ICASE
      PRINT 4, ((R(L),A(M),CR(L,M),CI(L,M),OMR(L,M),OMI(L,M),CG(L,M),
1      AI(L,M),AM(L,M),KT(L,M),M=1,JM),L=1,KM)
C      SUBROUTINE ORDER REARRANGES THE ARRAY FOR SUB. POINTS
      CALL ORDER (R,A,CR,CI,OMR,OMI,CG,AI,JM,KM)
      DO 600 LL=1,6
      IF (LL-4)602,600,602
602    CALL POINTS(CR,CI,OMR,OMI,CG,AI,R,KM,A,JM,LL)
600    CONTINUE
500    GO TO 999
C      BACK TO START TO TRY ANOTHER CASE
297    PRINT 8
      GO TO 300
298    PRINT 9
      GO TO 300
299    PRINT 10
      GO TO 300
C      OUTPUT FORMAT STATEMENTS
4      FORMAT(OPF10.1,2F12.4,F13.6,1P5E13.3,I10)
6      FORMAT(6H- R9X5HALPHA8X2HCR9X2HCI11X3HOMR8X3HOMI12X2HCG12X2HAI
111X4HAMPY10X4HTIME /120X4HCASE I5)
8      FORMAT (16H-**OUT OF TIME**)
9      FORMAT (22H-**OVERFLOW IN ADMIT**)
10     FORMAT (34H-**NO CONVERGENCE AFTER 30 TRIES**)
      END

*      LIST8
*      LABEL
CMEMBR2  MEMBRANE ROUTINE
SUBROUTINE SURF2 (A,CR,CI,YR,YI,I)
I      DIMENSION C(1),Y(1),B(1)
      COMMON COR,EMO,DE,ALO,OMO,B,RO,R
      GO TO (100,200,300),I
100     YR=0.
      YI=0.
      RETURN
200     IF(RO)202,201,202
201     RO=R
202     RATIO=RO/R
      C(1)=CR
      C(2)=CI
      CO=COR**2
      D=DE*RATIO/A
      OM=OM*OM*RATIO*RATIO/A**2
      EM=EMO
      IF(A-ALO)203,204,204
203     EM=EMO*(A/ALO)**2
I204    Y=(0.,1.)*C/(EM*(CO-C*C-(0.,1.)*C*D+OM))
      YI=-Y(2) /RATIO
      YR=-Y(1) /RATIO
      RETURN
300     PRINT 301,COR,EMO,ALO,DE,OMO,RO
      RETURN
301     FORMAT(18HOMEMBRANE WITH CO=F7.4,4H, M=F7.4,10H AT ALPHA=F7.4,9H,
1AND DE=1PE8.1,6H, OMO=OPF7.4,8H, AT RO=F8.1,12H MASS VARIES)
      END

```

```

*      LIST8
*      LABEL
CADMIT8  RUNGE-KUTTA, COMPLEX ARITH. VERSION OF ADMITTANCE ROUTINE
        SUBROUTINE ADMIT (R,ALPHA,CR,CI,YR,YI)
C
I      DIMENSION S(4,2),V0(3,2),V1(3,2),V2(3,2),V3(3,2),BETA(1),GK1(2),
1      GK2(2),GK3(2),GK4(2),D1(1),D2(1),CEE(1),X(1),W3(1),Z(4),C10(1),
2      C11(1),C12(1),C20(1),C21(1),C22(1),Y(1)
C
        H1=-0.16E-01
        H2=H1*H1/2.
        H3=H1*H2/3.
        H4=H1*H3/4.
        HH=H4/H2
        SM=1.E-15
        H1S=H1*SM
        H2S=H2*SM
        H3S=H3*SM
        A=ALPHA
        A2=A*A
        A4=A2*A2
        AA=2.*A2
        AR=A*R
        HAR=HH*AR
        AAR=A2*AR
        HAAR=H4*AAR
        HHAR=HAR*H2
        CEE(1)=CR
        CEE(2)=CI
        C10=(AA+AR*CEE(2))*HH
        C11=C10
        C12=C10
        COI=-HAR*CEE(1)
        C20=-H4*(A4+AAR*CEE(2))
        C21=C20
        C22=C20
        COJ=HAAR*CR
C
C      START OF INITIAL CONDITIONS
C
        CALL OUTER(U0)
        BETA(1)=A2+AR*CEE(2)
        BETA(2)=AR*(U0-CEE(1))
I      BBETA=-SQRTF(BETA)
I      V0(1,1)=SM
I      V0(1,2)=SM
I      V1(1,1)=-A*H1S
I      V2(1,1)=A2*H2S
I      V3(1,1)=-A*A2*H3S
I      V1(1,2)=BBETA*H1S
I      V2(1,2)=BETA*H2S
I      V3(1,2)=BBETA*BETA*H3S
C
C      END OF INITIAL CONDITIONS--NUMERICAL INTEGRATION FOLLOWS
C
DO 111  I=1,125,2

```

```

CALL PROFIL (U0,U1,U2,D2U0,D2U1,D2U2,I)
C10(2)=COI+HAR*U0
C11(2)=COI+HAR*U1
C12(2)=COI+HAR*U2
C20(2)=COJ-HHAR*D2U0-HAAR*U0
C21(2)=COJ-HHAR*D2U1-HAAR*U1
C22(2)=COJ-HHAR*D2U2-HAAR*U2
DO 108 J=1,2
I GK1(J)=C10*V2(1,J)+C20*V0(1,J)
DO 105 K=J,4,2
V0(2,K)=V0(1,K)+.5*V1(1,K)+.25*V2(1,K)+.125*V3(1,K)+.0625*GK1(K)
V1(2,K)=V1(1,K)+V2(1,K)+.75*V3(1,K)+.5*GK1(K)
V2(2,K)=V2(1,K)+1.5*V3(1,K)+1.5*GK1(K)
105 V3(2,K)=V3(1,K)+2.*GK1(K)
I GK2(J)=C11*V2(2,J)+C21*V0(2,J)
DO 107 K=J,4,2
V0(3,K)=V0(1,K)+V1(1,K)+V2(1,K)+V3(1,K)+GK2(K)
V1(3,K)=V1(1,K)+2.*V2(1,K)+3.*V3(1,K)+4.*GK2(K)
V2(3,K)=V2(1,K)+3.*V3(1,K)+6.*GK2(K)
107 V3(3,K)=V3(1,K)+4.*GK2(K)
I GK3(J)=C12*V2(3,J)+C22*V0(3,J)
DO 108 K=J,4,2
HK5=2.*GK2(K)
HK1=0.53333333*GK1(K)+0.26666667*HK5-0.06666667*GK3(K)
HK2=1.8*GK1(K)+1.2*HK5-0.2*GK3(K)
HK3=2.*(GK1(K)+HK5)
HK4=0.66666667*(GK1(K)+GK3(K))+1.33333333*HK5
V0(1,K)=V0(3,K)-GK2(K)+HK1
V1(1,K)=V1(3,K)-4.*GK2(K)+HK2
V2(1,K)=V2(1,K)+3.*V3(1,K)+HK3
108 V3(1,K)=V3(1,K)+HK4
C
C
C END OF NUMERICAL INTEGRATIONS -- PURIFICATION FOLLOWS
D1=U2-CEE(1)
D1(2)=-CEE(2)
D2=-A2*D1-D2U2
D2(2)=-A2*D1(2)
D1=D1/H2
D1(2)=D1(2)/H2
I TOP=D1*V2(1,1)+D2*V0(1,1)
I BOT=D1*V2(1,2)+D2*V0(1,2)
I P=-TOP/BOT
I V0(1,1)=V0(1,1)+P*V0(1,2)
I V1(1,1)=V1(1,1)+P*V1(1,2)
I V2(1,1)=V2(1,1)+P*V2(1,2)
I 111 V3(1,1)=V3(1,1)+P*V3(1,2)
C
C
C COMPUTATION OF CORRECT COMBINATION OF SOLUTIONS
DO 112 K=1,4
S(1,K)=V0(1,K)
S(2,K)=V1(1,K)/H1
S(3,K)=V2(1,K)/H2
112 S(4,K)=V3(1,K)/H3

```

```

      • CALL WALL (DUW)
I      W1=CEE*S(2,1)+DUW*S(1,1)
I      X1=CEE*S(2,2)+DUW*S(1,2)
      CALL SURFX (A,CEE(1),CEE(2),X(1),X(2))
I 120  W2=(1.,0.)-CEE*X
I      W3=(0.,1.)*CEE*X/AR
I      W4=S(4,1)-A2*S(2,1)
I      X4=S(4,2)-A2*S(2,2)
I      W5=W1*W2+W3*W4
I      X5=X1*W2+W3*X4
I      BA=-W5/X5
      DO 126 K=1,4
I 126  Z(K)=S(K,1)+BA*S(K,2)
I 114  Y=-A*AR*Z(1)/(Z(4)-A2*Z(2)+(0.,1.)*AR*(CEE*Z(2)+DUW*Z(1)))
      YR=Y(1)
      YI=Y(2)
      RETURN
      END

```

```

*      LIST8
*      LABEL
CEIGEN2 MULTI-POINT EIGENVALUE ESTIMATE
      SUBROUTINE EIGEN (C,Y,AMP,I)
I      DIMENSION C(30),Y(30),AMP(15)
I      SUM=(0.,0.)
      DO 4 K=1,I
I      TERM=(1.,0.)
      DO 3 J=1,I
      IF(J-K)2,3,2
I 2    TERM=-TERM*Y(J)/(Y(K)-Y(J))
      3 CONTINUE
I 4    SUM=SUM+C(K)*TERM
I      C(I+1)=SUM
      RETURN
      END

```

```

*      FAP
COUNT 110
*      SUBROUTINE PROFIL (U,U1,U2,D2U,D2U1,D2U2,I)
ENTRY  PROFIL
ENTRY  IDAD
ENTRY  WALL
LBL    BLASBL
PROFIL SXD  *-2,4
      SXA  RET,1
      CLA* 7,4
      PDC  ,1
      CLA  U+1,1
      STO* 3,4
      CLA  D2U+1,1
      STO* 6,4
      CLA  U,1
      STO* 2,4
      CLA  D2U,1
      STO* 5,4
      CLA  U-1,1
      STO* 1,4
      CLA  D2U-1,1
      STO* 4,4
RET    AXT  ,1
      TRA  8,4
IDAD   SXD  PROFIL-2,4
      TSX  $GETTM,4
      PZE  DATE
      PZE  TIME
      TSX  $(SPH),4
      PZE  FMT,1
      AXT  END-START,4
      LDQ  END,4
      STR
      TIX  *-2,4,1
      TSX  $(FIL),4
      LXD  PROFIL-2,4
      TRA  1,4
WALL   SXD  PROFIL-2,4
      CLA  =2.
      STO* 1,4
      TRA  2,4
      TITLE
FMT    BCI  2,((20A6))
START  BCI  ,1RUNGE-KUTTA INTEGRATION SCHEME * H=0.016 ** BLASIVS PROFILE
      BCI  3, * DATE OF RUN IS
DATE   PZE
      BCI  3, AND THE TIME IS
TIME   BCI  2,
END    EQU  *
U      OCT  201400000000,200777375702,200777337372,200777275636
      OCT  200777230424,200777157260,200777101665,200777017535
      OCT  200776730330,200776633470,200776530617,200776417325
      OCT  200776276761,200776146700,200776006377,200775635142
      REM  ADDITIONAL CARDS UP TO NUMBER 64
PROFL
PROFL
PROFL
PROFL

```

```

*      FAP
      COUNT      52
*      SUBROUTINE COMBIN3 (ALPHA,CR,CI,YR,YI)
      ENTRY      COMBIN
      ENTRY      IDCOMB
      LBL        COMBIN3,PLEASE
COMBIN  SXD      *-2,4
      CLA        1,4
      STA        SUB+1
      CLA        2,4
      STA        SUB+2
      CLA        3,4
      STA        SUB+3
SUB     TSX      $SURFY,4
      PZE        **
      PZE        **
      PZE        **
      PZE        A
      PZE        A+1
      TXI        *+2,0,1
      PZE        COMBIN-2,,66
      LXD        COMBIN-2,4
      CLA        2
      STO        BIN
      CAL        $(IFDP)
      SLW        2
      CLA*       4,4
      STO        TOP
      CLA*       5,4
      STO        TOP-1
      STR        A
      PZE        A+1
      CLA        TOP-2
      FSB        =1.
      STO*       4,4
      LDQ        TOP-3
      STQ*       5,4
      CLA        BIN
      STO        2
      TRA        6,4
BIN     PZE        0,0,0
IDCOMB  SXD      COMBIN-2,4
      TSX        $(SPH),4
      PZE        FMT,,1
      TSX        $(FIL),4
      LXD        COMBIN-2,4
      TRA        1,4
FMT     BCI        8,(42H0COMBIN3 COMPUTES Y0/Y11 -1.0 FOR CLASS B. )
A       BSS        2
      COMMON     -206
TOP     COMMON     4
      END

```

```

*      FAP
      COUNT      33
*      CALLING SEQUENCE FOR FORTRAN PROGRAM SURFACE
      ENTRY      SURFX
      ENTRY      SURFY
      ENTRY      IDSURF
      LBL        SURF1
SURFX  SXD        *-2,4
      CLA        =1B17
      STO        I
      TRA        *+4
SURFY  SXD        SURFX-2,4
      CLA        =2B17
      STO        I
      CLA        1,4
      STA        SUB+1
      CLA        2,4
      STA        SUB+2
      CLA        3,4
      STA        SUB+3
SUB    CALL       SURF2,,,,,I+1,I+2,I
      LXD        SURFX-2,4
      CLA        I+1
      STO*       4,4
      CLA        I+2
      STO*       5,4
      TRA        6,4
I      BSS        3
IDSURF SXD        SURFX-2,4
      CLA        =3B17
      STO        I
      CALL       SURF2,,,,,,I
      LXD        SURFX-2,4
      TRA        1,4
      END

```

```

*      FAP
      COUNT      50
*      FUNCTION EXTRAP(X,Y,YO,I)
      ENTRY      EXTRAP
      LBL        EXTRAP
EXTRAP SXD      *-2,4
      SXA        RET,1
      SXA        RET+1,2
      CLA        1,4
      STA        I+2
      CLA        2,4
      STA        CALC
      STA        CALC+1
      STA        CALC+4
      CLA        3,4
      STA        CALC+3
      CLA*       4,4
      SUB        =1B17
      STD        I
      STD        RET-1
      STZ        SUM
      AXT        0,1
OUT    CLA        =1.
      STO        TERM
      AXT        0,2
IN     SXD        COMP,1
      PXD        ,2
      CAS        COMP
      TRA        CALC
      TRA        *+9
CALC  CLA        **,1
      FSB        **,2
      STO        HOLD
      CLA        **
      FSB        **,2
      FDP        HOLD
      FMP        TERM
      STO        TERM
      TXI        *+1,2,1
I     TXL        IN,2,**
      LDQ        TERM
      FMP        **,1
      FAD        SUM
      STO        SUM
      TXI        *+1,1,1
      TXL        OUT,1,**
RET   AXT        **,1
      AXT        **,2
      TRA        5,4
COMP  PZE
HOLD  PZE
TERM  PZE
SUM   PZE
      END

```


BIOGRAPHY

Richard E. Kaplan was born in Philadelphia, Pa. on July 4, 1938. He was educated in the public schools of Upper Darby (Pa.) Township and graduated from the Upper Darby Senior High School in June 1956.

He entered Massachusetts Institute of Technology as a freshman in September 1956 and enrolled in the Department of Aeronautics and Astronautics. In 1958, he was selected for the departmental honors course and received the Bachelor and Master of Science degrees in June 1961. His Master's thesis was entitled "Fluid Oscillation in Cylindrical Shells."

He was a National Merit Scholar and a National Science Foundation Fellow during this period.

He enrolled in the doctoral program of the Department of Aeronautics and Astronautics in September 1961 and held positions of teaching assistant and research assistant, besides being a member of the research staff of the Aeroelastic and Structures Research Laboratory.

He is a member of Tau Beta Pi, Sigma Gamma Tau, and Sigma Xi, and is a recipient of the Karl Taylor Compton prize. He has published a paper with Professor Leon Trilling entitled, "On Undamped Waves in an Infinitely Long Plasma Jet," AFOSR-TN-59-695.

Mr. Kaplan has been appointed Assistant Professor in the School of Engineering at the University of Southern California for the academic year 1964-65 and will teach in the Graduate Department of Aerospace Studies.